Design and Develop Lignin-based Recyclable Copolymers for Hydrophobic Coatings

A Dissertation Presented for the

Doctor of Philosophy

Degree

The University of Tennessee, Knoxville

Di Xie

May 2024

Copyright © 2024 by Di Xie
All rights reserved.

ACKNOWLEDGEMENTS

I extend my deepest gratitude to those who provide any support and encouragement during my PhD study at The University of Tennessee, Knoxville (UTK), which have been greatly instrumental for my completion of doctoral dissertation.

First of all, I am profoundly grateful to my advisor, Dr. Mi Li, for his financial support, guidance, and professional advice through the journey. His commitment to academic excellence and scholarly standards has been tremendously helpful for my completion of the degree. I also want to greatly appreciate my committee members, Drs. Arthur Ragauskas, Yunqiao Pu, and Sheng-I Yang, for their invaluable resources and access to Oak Ridge National Laboratory (ORNL), expertise, constructive feedback, and dedication to helping to refine my research during this journey.

Secondly, I want to express my gratitude to the professors and colleagues who never hesitated to train me new skills and provided assistances including Drs. Wei Wang, David Harper, Xianzhi Meng, Kendhl Seabright, Yunxuan Wang, Luna Liang, and Shuyang Zhang. Another group of people I owe a gratitude is my peers, including Kailong Zhang, Mohammad Alipanahrostami, and Zhongjin Zhou, for the sources of support and intellectual exchange.

Thirdly, I would like to appreciate Center of Renewable Carbon at UTK, Joint Institution of Biological Sciences, Bioscience Division at ORNL, School of Natural Resources at UTK, and all the personnels working there for the research sources, the office site, the collaborative atmosphere, and any other warm-hearted support that is too many to list here.

Last but not least, I would like to express my sincerest appreciation to my families who always give me endless support and freedom to pursue my career goals. I could not remember how many times they encouraged me to face the challenges bravely, solve problems proactively, and think positively… Special thanks to my friends who helped me improve my English and stood by me during this demanding endeavor.

This dissertation was finished combined with collective efforts, supports and comments offered by the individuals mentioned above. I am truly grateful for the time and effort each one has input in shaping this scholarly contribution.

ABSTRACT

Due to the abundance, renewability, biodegradability, overall hydrophobicity, good compatibility with cellulose, and anti-UV/oxidant abilities, lignin has great application potentials in hydrophobic coatings on cellulose-based substrates. However, lignin's structural heterogeneity and rigidity challenge its value-added utilization. Herein, Kraft lignin (KL), from paper mills, is fractionated into more homogeneous fractions (FL), nanosized into lignin micro-nanospheres (LMNS), chemically modified and copolymerized with other constituents to fabricate hydrophobic coating materials with improved coating performances.

To investigate structure-property relationships of lignin-based copolymers, solvent fractionation is conducted to obtain FLs with different molecular weight (MW) and hydroxyl (OH) contents to prepare copolymers by integrating with ε-caprolactone (ε-CL), oleylamine (OAm), and bis(3-aminopropyl)-terminated-poly(dimethyl siloxane) (PDMS), respectively. Results show that 1) KL and FLs are successfully copolymerized with ε-CL *via* ring-opening polymerization (ROP) to form lignin-grafted PCL copolymers (lignin-*g*-PCL), where high-MW FL favors the ROP of ε-CL. 2) LA-modified KL (MKL) and FL (MFL) are successfully copolymerized with OAm and PDMS to form lignin-OAm grafted and lignin-PDMS crosslinked polyimines, respectively, *via* Schiff-base reactions, where low-MW FL favors the copolymerization with amines. 3) The lignin-OAm polyimines can be self-repaired and reprocessed, while lignin-PDMS polyimines can be repaired with assistance. 4) Lignin incorporation improves the hydrophobicity, thermal stability, and UV-blocking abilities of synthesized lignin-based copolymers, benefiting the further applications.

The prepared copolymers are coated on cellulose-based substrates including paper, wood, and fabric for surface hydrophobization. Results show that: 1) Lignin-*g*-PCL coated filter paper separates hexane-, petroleum ether-, and chloroform-water mixtures with outstanding separation efficiencies up to 99% and excellent reusability. 2) Lignin-PDMS polyimines exhibit good coating hydrophobicity, adhesion, and removability on printing paper. The hydrophobicity is further enhanced by LMNS surface roughening. 3) Robust superhydrophobicity is achieved on the cross-section of the wood block (WB-C) with water

contact angle up to 173° and roll-off angle low to 5°, which is mechanically, chemically, and water stable. 4) The polyimines-LMNS coatings improve the stiffness and tensile strength of the paper and improve the stiffness and ductility of the fabric.

These studies are expected to provide new insight into lignin-based polymerization and lignin valorization for hydrophobic coatings.

TABLE OF CONTENTS

INTRODUCTION 1
CHAPTER I 7
LITERATURE REVIEW 7
1.1. Lignin and lignin structural heterogeneity 8
1.2. Lignin-based copolymers 10
1.2.1. Lignin-based copolymers with natural polymers 10
1.2.2. Lignin-based copolymers with synthetic bio-derived polymers 11
1.2.3. Lignin-based recyclable copolymers 12
1.3. Lignin hydrophobization 14
1.3.1. Lignin esterification 14
1.3.2. Lignin silylation 16
1.4. Lignin nanosizing 17
1.5. Lignin for hydrophobic and superhydrophobic coatings 19
CHAPTER II 23
EFFECT OF LIGNIN STRUCTURE ON THE PHYSICOCHEMICAL PROPERTIES OF LIGNIN-G-PCL AND ITS APPLICATION FOR WATER/OIL SEPARATION 23
2.1. Abstract 25
2.2. Introduction 26
2.3. Materials and Methods 28
2.3.1. Materials 28
2.3.2. Lignin fractionation 29
2.3.3. Synthesis of lignin-g-PCLs 29
2.3.4. Characterization of lignin-g-PCLs and lignin-g-PCL films 30
2.3.5. Enzymatic biodegradation of lignin-g-PCL films 32
2.3.6. Water/Oil separation with lignin-g-PCLs coated filter paper 32
2.4. Results and discussion 33
2.4.1. Lignin fractionation 33
2.4.2. Structural characterization of lignin-g-PCLs 36
2.4.3. Physicochemical properties of lignin-g-PCLs 41

2.4.4. Biodegradability of lignin-g-PCLs 47
2.4.5. Application of CFP with lignin-g-PCL for oil/water separation 49
2.5. Conclusions 54
CHAPTER III 56
SYNTHESIS OF BIO-BASED REPAIRABLE POLYIMINES 1 WITH TAILORED PROPERTIES BY LIGNIN FRACTIONATION 56
3.1. Abstract 58
3.2. Introduction 59
3.3. Materials and Methods 61
3.3.1. Materials 61
3.3.2. Lignin fractionation and modification 62
3.3.3. Synthesis of lignin-based polyimines 63
3.3.4. Characterization of lignin, modified lignin, and lignin-based polyimines 63
3.3.5. Repairability of synthesized polyimines 66
3.4. Results and discussion 67
3.4.1. Lignin fractionation and modification 67
3.4.2. Synthesis and characterization of polyimines 68
3.4.3. Physicochemical properties of polyimines 73
3.4.4. Reprocessing ability and repairability of polyimines 81
3.5. Conclusions 87
CHAPTER IV 88
APPLICATION OF LIGNIN-PDMS POLYIMINES FOR REMOVABLE HYDROPHOBIC COATINGS 88
4.1. Abstract 89
4.2. Introduction 90
4.3. Materials and Methods 90
4.3.1. Preparation of coating agents 91
4.3.2. Preparation of hydrophobic coatings 91
4.3.3. Characterizations of fabricated coatings 91
4.4. Results and discussion 93

4.4.1. Coating performances of polyimines 93
4.4.2. Chemical degradation of polyimines 95
4.4.3. Coating removability of polyimines 95
4.5. Conclusions 98
CHAPTER V 100
ROBUST SUPERHYDROPHOBIC COATINGS WITH LIGNIN-PDMS POLYIMINE CROSSLINKING NETWORK AND LIGNIN MICRO-NANOSPHERES 100
5.1. Abstract 102
5.2. Introduction 103
5.3. Materials and Methods 105
5.3.1 Materials 105
5.3.2. Preparation of LMNS 105
5.3.3. Preparation of coating agents 106
5.3.4. Preparation of superhydrophobic coatings 106
5.3.5. Characterizations of LMNS and superhydrophobic coatings 107
5.4. Results and discussion 110
5.4.1. LMNS formation 110
5.4.2. Enhancement of coating hydrophobicity 110
5.4.3. Enhancement of coating durability 115
5.4.4. Characterization of coatings 119
5.5. Conclusions 126
CHAPTER VI 128
SUMMARY AND OUTLOOK 128
6.1. Summary 129
6.2. Outlook 130
LIST OF REFERENCES 132
APPENDIX 155
Appendix A – Supporting information for Chapter II Effect of Lignin Structure on the Physicochemical Properties of Lignin-grafted-poly(ε-caprolactone) and its Application for Water/Oil Separation 155

Appendix B – Supporting information for Chapter III Synthesis of Bio-based Repairable Polyimines with Tailed Properties by Lignin Fractionation 159
Appendix C – Supporting information for Chapter V Robust Superhydrophobic Coatings with Polyimine Crosslinking Network and Lignin Micro-nanospheres 165
VITA 169

LIST OF TABLES

Table 2-1 Weight-average (M_w), number-average (M_n) molecular weight, and molar-mass dispersity ($Đ_M$) of lignin and lignin-*g*-PCLs measured by GPC, and the average length of PCL arms measured by ^{1}H NMR 35

Table 2-2 Quantification of hydroxyl groups in lignin and lignin-*g*-PCLs determined by ^{31}P NMR..... 37

Table 2-3 Crystallization (T_c) and melting (T_m) temperatures, crystallinity degree (X_c), temperature at the onset of thermal degradation (T_{onset}) and temperature at maximum mass loss (T_{max}) of KL, PCL and lignin-*g*-PCLs 44

Table 2-4 The minimum, median and maximum values of g_d and g_{sp} as well as hydrophilicity index ($\gamma_{sp}/(\gamma_{sp}+\gamma_d)$) and specific surface area of KL and lignin-*g*-PCLs 46

Table 3-1 Weight-average (M_w), number-average (M_n) molecular weight and molar mass dispersity ($Đ_M$) of lignin, modified lignin and lignin-based polyimines 69

Table 3-2 Solvent stability and gel fraction of synthesized lignin-based polyimines 74

Table 3-3 Glass transition temperature (T_g), temperatures at the onset of thermal degradation (T_{onset}) and maximum mass loss (T_{max}), residual carbon content (C_r), and calculated average activation energy (E_a) of lignin, modified lignin, and lignin-based polyimines..... 76

Table 3-4 The minimum, median and maximum values of γ_d and γ_{sp} as well as hydrophilicity index ($\gamma_{sp}/(\gamma_{sp}+\gamma_d)$) and specific surface area of lignin, modified lignin and lignin-based polyimines 80

Table 4-1 Coating properties of lignin-PDMS polyimines on paper and glass before and after removal 99

Table 5-1 Decreasing percentage (%) of WCA of coated woody substrates after 100-cycle tape peeling and 1.5-h waterdrop impact..... 118

Table 5-2 Normalized atomic concentration (%) of surface elements on coated and neat cellulosic substrates 122

Table 5-3 Young's modulus, maximum tensile strength, and tensile strain at maximum tensile stress (Extension) of neat and coated substrates..... 124

Table 5-4 Temperatures at the onset of thermal degradation (T_{onset}) and maximum mass loss (T_{max}), residual carbon content (C_r) of neat and coated substrates 125
Table 5-5 The minimum, median and maximum values of γ_d and γ_{sp} as well as hydrophilicity index ($\gamma_{sp}/(\gamma_{sp}+\gamma_d)$) and WCA of CW, CW-c1, and NW 127
Table 7-1 Young's modulus, tensile strength and impact strength of neat PCL and lignin-*g*-PCL films..... 155
Table 8-1 Quantification of hydroxyl groups in lignin and modified lignin determined by ^{31}P NMR..... 164
Table 9-1 ANOVA analysis of WCA of different coating products and their controls 1 166
Table 9-2 ANOVA analysis of WCA of different coating products and their controls 2 167
Table 9-3 ANOVA analysis of WCA of different coated wood block section products and their controls 167
Table 9-4 ANOVA analysis of WCA of different coated 2D products and their controls 167
Table 9-5 ANOVA analysis of WCA of different coated wood block sections before and after knife scratch..... 168
Table 9-6 ANOVA analysis of WCA of different coated 2D substrates before and after knife scratch 168
Table 9-7 The minimum, median and maximum values of γ_d and γ_{sp} as well as hydrophilicity index ($\gamma_{sp}/(\gamma_{sp}+\gamma_d)$) and specific surface area of KL and LMNS..... 168

LIST OF FIGURES

Figure 1-1 Schematic representation of typical oligomeric structures of acetone-soluble fraction of softwood Kraft lignin 9
Figure 1-2 Imine exchange (a) and imine metathesis (b) of dynamic imine bonds..... 15
Figure 1-3 Esterification of lignin by 12-C dodecanoyl chloride, 16-C stearoyl chloride[58] (a), and esterification of hydroxyethyl lignin by 18-C oleic acid (b)..... 18
Figure 2-1 ^{31}P NMR spectra of lignin fractions (left) and lignin-*g*-PCLs (right). a: aliphatic OH, b: C_5 substituted OH, c: guaiacyl OH, d: *p*-hydroxyphenyl OH, e: carboxylic OH 35
Figure 2-2 Relation of lignin M_w with OH content (A) and phenolic OH content (B). *r*: Pearson correlation coefficient; *P*: P value; R^2: coefficient of determination; *: statistical significance 37
Figure 2-3 Relation of copolymer M_w with PCL size (A), relation of lignin M_w with copolymer M_w and PCL size (B), relation of lignin M_w with OH decreasing percentage (C), and copolymer M_w with OH content in their corresponding lignin fraction (D). *r*: Pearson correlation coefficient; *P*: P value; R^2: coefficient of determination; *: statistical significance 39
Figure 2-4 FTIR-ATR spectra of KL, PCL, and lignin-*g*-PCLs..... 42
Figure 2 5 DSC heating (A), DSC cooling (B), TGA (C), and DTG (D) curves of KL and lignin-*g*-PCLs. The inserted figure is the heating curve of F_{ins}-PCL tested by DSC.44
Figure 2-6 Dispersive (A) and specific (B) surface energy of KL, PCL, and lignin-*g*-PCLs 46
Figure 2-7 Tensile strength (A), impact strength (B), and UV-vis spectra (C) of PCL and lignin-*g*-PCL films 48
Figure 2-8 Lipase hydrolysis of neat PCL and lignin-*g*-PCL films..... 50
Figure 2-9 SEM images of FP (A) and CFP-C (B) under a scale bar of 1,000; Separation efficiencies at the first cycle, cycles with separation efficiencies over 92% (C) and separation efficiencies of CFP-C under 15 cycles (D) for separating chloroform-, petroleum ether- and hexane-water mixtures..... 52
Figure 3-1 Proposed mechanisms of lignin modification and polyimine synthesis 70

Figure 3-2 FTIR spectra of lignin-based polyimines 72
Figure 3-3 ^{13}C NMR spectra of lignin-based polyimines with DMSO-d_6 as a solvent 72
Figure 3-4 DSC (a), TGA (b), and DTG (c) curves of lignin, modified lignin, and lignin-based polyimines 76
Figure 3-5 Stress-relaxation curves (a-d) and the Arrhenius equation plots (a'-d') of MKL-O (a, a'), MFL-O (b, b'), MKL-P (c, c'), and MFL-P (d, d'). The dashed line refers to the 1/e (~ 0.37) of the initial modulus. 78
Figure 3-6 Dispersive (a) and specific (b) surface energy and WCA (c) of lignin, modified lignin, and synthesized lignin-based polyimines 80
Figure 4-1 The procedures to prepare polyimine coatings on paper and glass slides..... 92
Figure 4-2 WCA of CP coated with MKL-P (a) and MFL-P (c), and CG coated with MKL-P (b) and MFL-P (d) 94
Figure 4-3 Coating adhesion of lignin-PDMS polyimines on paper 96
Figure 4-4 UV-blocking ability of paper and glass coated with and without lignin-PDMS polyimines 96
Figure 4-5 Chemical degradation of lignin-PDMS polyimines 97
Figure 4-6 Removability of lignin-PDMS polyimine coatings..... 97
Figure 5-1 Schematic diagram of the preparation of coatings on wood, paper, fabric, and glass slides. MKL: modified kraft lignin; PDMS: polydimethylsiloxane; THF: tetrahydrofuran; LMNS: lignin micro-nanospheres..... 108
Figure 5-2 FTIR spectra (a) and particle size distribution (b) of KL and LMNS; SEM image of LMNS (c)..... 112
Figure 5-3 WCA of the products and controls of WB-C, WB-T, WB-R, CW, CP, CF, and CG (a); WCA of WB-C, WB-T, WB-R, CW, CP, CF, and CG products before and after knife scratch (b); WCA of WB-C, WB-T, WB-T, and CW products, and WB-C-control 1 (WB-C-c1) after immersing under liquids with different pH values (1, 6, 9, 13) for 12 h at RT (c); WCA of WB-C, WB-T, WB-T, and CW products after different tape-peeling cycles (d); WCA of WB-C, WB-T, WB-T, and CW products under different waterdrop impact time (e); WCA of WB-C, WB-T, WB-T, and CW products after immersing under water at RT for different time (f); CA of WB-C using liquids

with different pH values (g), and different daily liquids (h); self-cleaning silica dust on WB-C. The inserted graph in Figure 5-3b refers to WB-R. The inserted graphs in Figures 5-3d – 5-3f refer to WB-C product. 112
Figure 5-4 SEM images of the products (upper row), control 2 (middle row), and neat substrates (lower row) of WB-C, WB-T, WB-R, CW, CP, and CF 116
Figure 5-5 FTIR (a), EDS (b), UV transmittance (c), and stress-strain curve (d) of neat and coated cellulosic substrates. NW: neat wood, NP: neat paper, NF: neat fabric, CW: coated wood, CP: coated paper, CF: coated fabric 121
Figure 5-6 TGA (a), DTG (b) curves of neat and coated cellulosic substrates. NW: neat wood, NP: neat paper, NF: neat fabric, CW: coated wood, CP: coated paper, CF: coated fabric. 124
Figure 5-7 Dispersive (a) and specific (b) surface energy of CW, CW-c1, and NW. CW: coated wood product, CW-c1: coated wood control 1, NW: neat wood 124
Figure 7-1 Fractionation procedure of kraft lignin 155
Figure 7-2 ^{1}H NMR spectra of lignin-*g*-PCLs. Signal assignment is displayed as top left image referred by literature[91]; e_1 (2.30 ppm), e_2 (1.64 ppm) and e_3 (1.38 ppm) represent -CH_2- in different positions of PCL chains, e_4 (4.05 ppm) represents repeating -CH_2O- units in PCL chains, and e_4' (3.65 ppm) represents end -CH_2OH- group in PCL chains..... 156
Figure 7-3 FTIR spectra of FP, CFP-P and CFP-C. Signals assignments are referred by literatures.[45, 197]..... 156
Figure 7-4 SEM images of FP (bottom) and CFP-C (upper) under scale bars of 105 (left) and 300 (right)..... 157
Figure 7-5 WCA of neat PCL, lignin-*g*-PCL films (A), CFP-C coated by different concentrations (0.2, 0.4, 0.6, 0.8 and 1.0 mg/mL) of F1-PCL/acetone solutions (B) 158
Figure 7-6 Separation efficiencies of FP coated with KL-PCL, F_{ins}-PCL, F1-PCL, F2-PCL, and F3-PCL for separating chloroform-, petroleum ether- and hexane-water mixtures under the first cycle..... 158

Figure 8-1 Solvent fractionation of KL into FL..... 159
Figure 8-2 FTIR spectra of lignin and modified lignin..... 159
Figure 8-3 ^{1}H NMR spectra of lignin and modified lignin..... 160
Figure 8-4 ^{13}C NMR spectra of lignin and modified lignin..... 160
Figure 8-5 ^{31}P NMR spectra of lignin and modified lignin. (a) aliphatic OH, (b) C5-substituted OH, (c) guaiacyl OH, (d) p-hydroxyphenyl OH, and (e) carboxylic OH. 161
Figure 8-6 Solid-state NMR spectra of MKL-P and MFL-P..... 161
Figure 8-7 GPC curves of PDMS, lignin, modified lignin (left) and polyimines (right) 162
Figure 8-8 Stress-relaxation curves and the Arrhenius equation plots of MKL (a and a') and MFL (b and b')..... 162
Figure 8-9 Reprocess ability test for lignin-OAm polyimine films..... 163
Figure 8-10 Self-healing ability test for lignin-OAm polyimine films..... 163
Figure 8-11 Images of lignin-PDMS polyimine films before (left) and after (right) repair 164
Figure 9-1 Tape-peeling test of control 1 (a), control 2 (b), and WB-T (c)..... 165
Figure 9-2 Waterdrop impact test of control 1 (a), control 2 (b), and WB-T (c)..... 165
Figure 9-3 WCA of WB-T after being immersed under water for different time 165
Figure 9-4 SEM images of CG and CG-c2; CG: coated glass product, CG-c2: coated glass control 2 166
Figure 9-5 FTIR spectra of NW and CW (a), NP, NF, CP, and CF (b)..... ….166

LIST OF ABBREVIATIONS

3D	Three-dimensional
G	Guaiacyl
S	Syringyl
H	*p*-Hydroxyphenyl
KL	Kraft lignin
MWL	Milled wood lignin
EHL	Enzymatic hydrolysis lignin
MW	Molecular weight
DCM	Dichloromethane
THF	Tetrahydrofuran
DCPN	Dynamic covalent polymer networks
UV	Ultraviolet
LMNS	Lignin micro-nanoshperes
FL or F_x	Fractionated lignin
OH	Hydroxyls
M_w	Weight-average molecular weight
M_n	Number-average molecular weight
$Đ_M$	Molar-mass dispersity
Da	Delta
PLA	Polylactic acid
PVA	Poly(vinyl alcohol)
PHBH	Poly(3-hydroxybutyrate-co-3-hydroxyhexanoate)
PCL	Poly(ε-caprolactone)
PBS	Poly(butylene succinate)
ROP	Ring opening polymerization
CL	ε-caprolactone monomers
T_m	Melting temperature
F_x-*g*-PCL	Lignin-grafted-poly(ε-caprolactone) copolymers
PEG	Poly(ethylene glycol)

WCA	Water contact angle
-SiR_3	Silyl groups
TDMSCl	Tert-butyldimethylsilyl chloride
DVDZ	Divinyl Tetramethyldisilazane
TSPI	3-(Triethoxysilyl) propyl isocyanate
PDMS-OH	Monocarbinol-terminated polydimethylsiloxane
HDIT	Hexamethylene diisocyanate trimer
LNS	Lignin nanospheres
GVL	γ-valerolactone
DMSO	Dimethyl sulfoxide
DMSO-d_6	Deuterated DMSO
CL/OH	ε-CL-to-lignin OH molar ratio
RT	Room temperature
DI	Deionized
FP	Filter paper
CFP	Coating filter paper
$SnOct_2$	Stannous octanoate
TMDP	2-chloro-4,4,5,5-tetramethyl-1,3,2-dioxaphospholane
$CHCl_3$	Chloroform
$CDCl_3$	Deuterated chloroform
NHND	N-hydroxy-5-norbene-2,3-dicarboxylic acid imide
SiO_2	Silicon dioxide
GPC	Gel permeation chromatographic
FTIR	Fourier transform infrared
NMR	Nuclear Magnetic Resonance
DSC	Differential scanning calorimetric analysis
TGA	Thermal gravimetric analysis
DTG	Differential thermal gravimetric analysis
X_c	Crystallinity degree
T_g	Glass transition temperature

T_{max}	Temperature at the maximum mass loss
T_{onset}	Onset temperature of thermal degradation
C_r	Residual carbon content
E_a	Calculated average activation energy
iGC	Inverse gas chromatography
SEA	Surface energy analyzer
CFP-B	Blank control of coated filter paper
CFP-P	Coated filter paper with neat PCL
CFP-C	Coated filter paper with lignin-*g*-PCL copolymers
r	Pearson correlation coefficient
R^2	Coefficient of determination
P	P value
γ_{sp}	Specific surface energy
γ_d	Dispersive surface energy
$\gamma_{sp}/(\gamma_{sp}+\gamma_d)$	Hydrophilicity index
OAm	Oleylamine
PDMS	Bis(3-aminopropyl)-terminated-polydimethylsiloxane
MKL	Modified Kraft lignin
MFL	Modified fractionated lignin
MKL-P	Polyimines synthesized by MKL and PDMS
MFL-P	Polyimines synthesized by MFL and PDMS
MKL-O	Polyimines synthesized by MKL and OAm
MFL-O	Polyimines synthesized by MFL and OAm
LA	Levulinic acid
DCC	Dicyclohexylcarbodiimide
DAP	4-dimethylaminopyridine
CP	Coated paper
CG	Coated glass
CP-MKL-P	Coated paper with MKL-P
CP-MFL-P	Coated paper with MFL-P

CG-MKL-P	Coated glass with MKL-P
CG-MFL-P	Coated glass with MFL-P
CP-MKL-P-R	Coated paper with MKL-P after removal
CP-MFL-P-R	Coated paper with MFL-P after removal
CG-MKL-P-R	Coated glass with MKL-P after removal
CG-MFL-P-R	Coated glass with MFL-P after removal
WB	Wood block
WC	Wood chip
CW	Coated wood chip
CW-c1	Control 1 of coated wood chip
CW-c2	Control 2 of coated wood chip
NW	Neat wood chip
NP	Neat paper
CF	Coated fabric
NF	Neat fabric
NG	Neat glass
WB-C	Coated cross-section of WB
WB-T	Coated tangential sections of WB
WB-R	Coated radical sections of WB
2D	Two dimensional
ROA	Roll-off angle
CA	Contact angle
SEM	Scanning electron microscopy
EDS	Energy dispersive X-ray spectroscopy
DLS	Dynamic laser scattering
ANOVA	Analysis of variance

INTRODUCTION

As an important component within the broad range of renewable natural resources, biomass derives from living organisms such as wood, agricultural crops, and organic waste, which can be used for various purposes like feedstocks to manufacture bioproducts and biochemicals, or as energy source through combustion, gasification, fermentation or upgrading to produce heat, electricity, or bioenergy. Plant biomass is a crucial component of the earth's ecosystems because plants can be harvested sustainably without permanently depleting the resource. Plant biomass is composed of various organic and inorganic components, mainly including cellulose, lignin, hemicellulose, protein, lipid, ash, and extractives. The relative proportions of these components can vary widely among different plant species and tissues.

Lignin, as the second most abundant biomass after cellulose and the most abundant phenolic biomass, is a three-dimensional (3D) complex amorphous polymer network primarily composed of guaiacyl (G), syringyl (S), and *p*-hydroxyphenyl (H) subunits.[1] Lignin is primary present as a binder between cellulose, hemicellulose, and other components in the secondly layer of plant cell walls, especially in woody plants. Lignin is biosynthesized by the polymerization of three phenylpropane precursors including coniferyl, sinapyl, and *p*-coumaryl alcohols in plants. The special aromatic structures of lignin provide structural integrity, strength, rigidity, and protection of plants. Lignin is typically catalogued as technical (industrial) lignin (e.g. Kraft lignin (KL), lignosulfonate, alkaline/soda lignin, organosolv lignin) and native (isolated) lignin (e.g. milled wood lignin (MWL), cellulosic enzymatic hydrolysis lignin (EHL), dioxane lignin) depending on the isolation method employed.[2-4]

KL is the main byproduct industrial Kraft pulping process from pulp and paper mills with an annual production of ~ 10 million tons globally.[5] KL is often considered a high-value lignin due to its relatively low level of chemical modifications during the pulping process. Majority of KL is underused in mills by direct combustion to generate heat, while only less than 5% of KL is used for value-added industrial products.[6] The difficulties of utilizing KL are attributed to, but not limited to, the complex and heterogeneity structures,

poor compatibility with other polymers, lack of cost-efficient value-added application pathways, dark color, smelly odor, etc.

The heterogeneous structure of lignin, such as molecular weight (MW) (from a few thousands to tens of thousands delta (Da)) and functional group types (such as aliphatic OH, phenolic OH, carboxylic, methoxy, etc.), usually causes nonuniform properties including reactivities, thermal stability, compatibility, solubility, and dispersity.[7] Typically, aliphatic OH content, glass transition temperature (T_g), and thermal stability increase, while phenolic OH and methoxy contents, solubility, and dispersibility decrease with the augment of lignin MW.[8-11] The feedstock heterogeneity could be imparted to the lignin-derived products, leading to disparate performances.[12] Therefore, it is of great importance to investigate the influence of lignin structure on the structures and properties of synthesized polymers, so as to build up the structure-property relationship, explore the synthesis mechanisms, and design the optimal synthesis molecules.

Although prevailing in high abundance, low cost, good biodegradability, etc., lignin remains one of the challenging renewable polymers to be utilized in a large scale in industries owning to the poor dispersity (in many common solvents and other polymer matrixes) and compatibility (with other polymers), solubility, flexibility, etc.[13] Chemical modification of lignin is usually needed to overcome these limitations.[14] For example, Huang et al. reported that the solubility of esterified lignin in organic solvents including acetone, dichloromethane (DCM), tetrahydrofuran (THF) and acetonitrile is greatly improved.[15] For another example, Shorey et al. reported that the dispersity of silylated lignin in rubber composites is effectively enhanced.[14] Overall, necessary modifications of lignin might be beneficial to the valorization of lignin.

Between the two main polymer catalogs, thermoplastics are easy to be reprocessed and reshaped under heat and/or pressure; however, it brings issues like aging and performance reduction. Generally, thermosets feature better water-resistant and mechanical properties due to the highly crosslinked networks; however, traditional thermosets are difficult to degrade and re-heal because of the irreversible covalent bonds. Therefore, the investigation of biodegradable and sustainable novel thermoplastics and

thermosets is highly required. For a purpose of circular economy, develop chemically recyclable polymers, such as dynamic covalent polymer networks (DCPN), has attracted increasing attentions as the DCPN can be reprocessed or repaired under certain conditions. Integrating bio-derived feedstocks, such as lignin, in DCPN complies to the future trend of sustainability, whereas remains a challenge.[16]

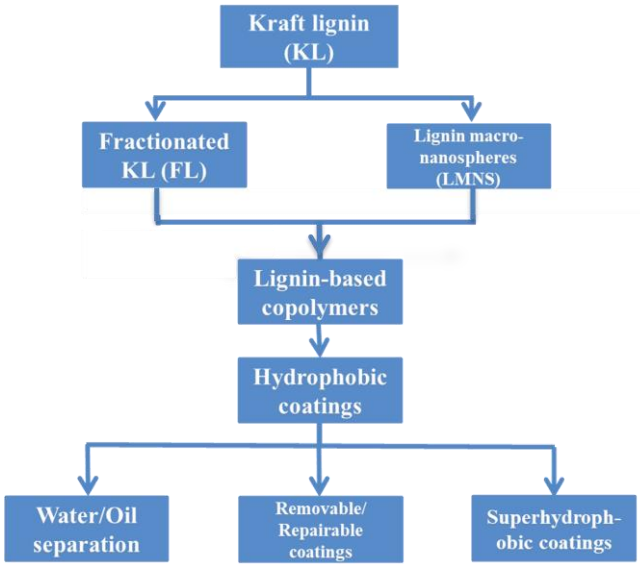
Lignin is naturally hydrophobic and water-stable for acting as a natural binder of plants. It possesses certain structural characteristics such as phenylpropane units, aromatic rings, ethers, C-C linkages, high molecular weight, etc. that make lignin less polar and less prone to interact with water molecules.[17] Given its overall hydrophobic nature, lignin has been widely used to fabricate hydrophobic materials such as coatings,[18-20] bioplastics,[21] adhesives,[22] insulation and packaging materials,[23, 24] etc.

As to the application of lignin for hydrophobic coatings, although it enables the sustainability, it cannot be denied that it usually sacrifices the coating performances such as protective effect, hydrophobicity, and coating duration. In spite of the excellent thermal stability and anti-ultraviolet (UV) ability of lignin brought by its polyphenolic structures, there are still a few issues need to be addressed: 1) the hydrophilic groups like OH and COOH in lignin would restrict the water repellency of lignin-based coatings; 2) the heterogeneity of lignin structures could lead to non-uniform coating performances of lignin-based coatings; 3) the rigidity, brittleness, and poor film-forming ability of lignin and lignin-based polymers would be detrimental to the coating performances like uniformity and mechanical strength. 4) the coating removability and repairability that enable the flexible usage environment and contribute to the industrial and earth sustainability remain to be developed.

Therefore, the current study aims to 1) investigating how the lignin structural heterogeneity affects the structures and physicochemical properties of synthesized lignin-based polymers; 2) develop and design chemical recyclable lignin-based polymers through dynamic (imine) covalent bonds; 3) obtain durable, removable, repairable hydrophobic/superhydrophobic lignin-based coatings by salinization with soft and low-surface-energy polydimethylsiloxane with good film-forming ability, and by surface

roughening *via* introducing the hierarchical nano-microstructures of lignin micro-nanospheres (LMNS).

The current study mainly focuses on the synthesis, characterization, and application of lignin-based (recyclable) copolymers and their applications for hydrophobic coatings (Scheme 1). Firstly, to investigate the effects of lignin structural heterogeneity, KL is fractionated into more homogeneous fractions (FLs) with diverse MW and OH content by solvent fractionation. Then, KL and FLs are synthesized with other chemicals to form lignin-based copolymers. Lignin modification could be needed before the synthesis. The structures and properties of synthesized copolymers are characterized to build up structure-property relationships of the copolymers. Secondly, the synthesized copolymers are applied for hydrophobic coatings by dip coating. To apply the coatings, copolymers are coated on filter paper for water/oil separation. To explore the recyclability of the synthesized copolymers, the removability and repairability of the coatings are investigated. To further enhance the surface hydrophobicity and coating robustness, LMNS is expected to chemically synthesize with low-surface-energy poly(dimethyl siloxane) and construct a macro-nano hierarchical structures synergistically.



Scheme 1 Proposed technical roadmap of the current dissertation

CHAPTER I
LITERATURE REVIEW

1.1. Lignin and lignin structural heterogeneity

Lignin, an abundant, renewable and biodegradable three-dimensional polymeric macromolecule in plant cell walls, is primarily composed of guaiacyl (G), syringyl (S), and *p*-hydroxyphenyl (H) subunits.[1] Lignin is typically cataloged as industrial lignin and native lignin based on the isolation processes.[2-4] KL yielded by the acidification of black liquor from the sulfate pulping process had a worldwide production of approximately 130 million tons in 2015.[25, 26] It provides a cheap and readily available source to develop value-added composites, blends, and chemicals[26, 27], at a really small share, in addition to the major low-value usage for energy generation at pulping mills.[25, 28] Furthermore, KL possesses rich phenolic hydroxyls (OHs) because the β-aryl ether bonds are largely cleaved during the pulping process, providing more versatility for chemical modifications.[29, 30] Figure 1-1 shows a schematic structures of acetone-soluble fraction of Kraft lignin from softwood.

Lignin is well known to have heterogeneous structures due to the variety of the plant sources, cooking or isolation methods, which leads to the various structural characteristics such as MW (*e.g.* the weight-average MW (M_w) of KL from Norwegian spruce and Eucalyptus grandis is reported to be 6,650 Da and 1980 Da, respectively[12]), intermolecular linkages (β-O-4', β-β', β-5', etc.), functional groups (OHs, carbonyls, methoxies, etc.) and corresponding discrepant physicochemical properties such as solubility, dispersity, biocompatibility, mechanical, surface, and thermal performances, bioactivity, etc.[12, 31, 32] The feedstock heterogeneity could be imparted to the lignin-derived products, leading to disparate performances. For instance, one KL fraction from eucalyptus with a M_w of 5,678 Da could enhance the ultimate tensile strength of chitosan films due to the increased phenolic OH content; however, KL fraction with 2,422 Da and 2.17 mmol/g caused an inverse effect due to the discrepant blending homogeneity with chitosan.[33] Another study showed that the ethanol-soluble KL fraction from bamboo displayed a benign antimicrobial activity against Gram-positive and -negative bacteria lacks similar antimicrobial activity due to a lower phenolic content and poor water

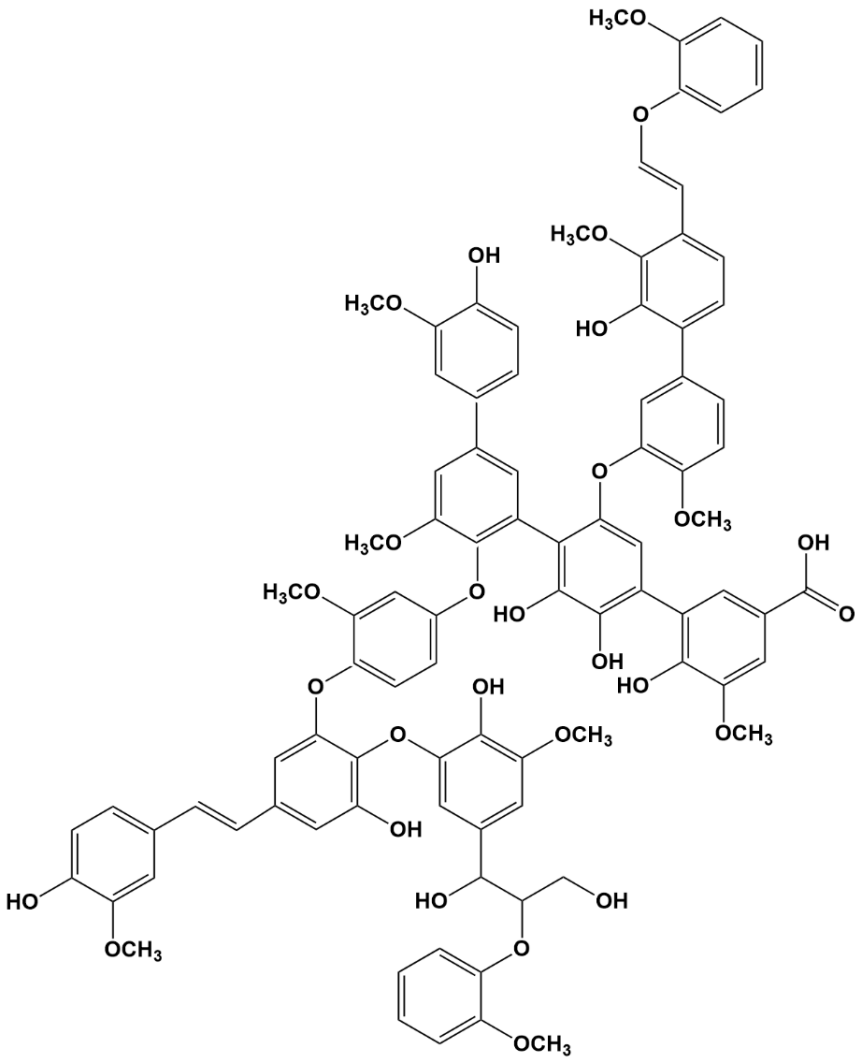


Figure 1-1 Schematic representation of typical oligomeric structures of acetone-soluble fraction of softwood Kraft lignin[34]

solubility.[35] Moreover, high-M_w KL fractions from *Pinus caribaea* esterified with succinic anhydride showed stronger ability to disperse bentonite in water than their unfractionated counterparts by stopping bentonite from flocculation/aggregation *via* larger steric hinderance.[36] Therefore, refining KL into more homogeneous feedstock fractions is important to afford comparable and stable product performances.

1.2. Lignin-based copolymers

1.2.1. Lignin-based copolymers with natural polymers

Due to the increasingly serious environmental concerns, abundant natural biomass, such as cellulose, starch, chitosan, protein, lipid, *etc*. from plants and animals, become a precious treasure as alternative feedstocks in manufacturing industry because of their high abundance, low cost, good biodegradability, and other featured properties.[37] Inspired by the primary texture of wood structure, lignin was incorporated with cellulose sheet by successive infiltration and hot pressing to obtain a reinforced sheet *via* lignin-cellulose hydrogen bonding and lignin self-bonding. The lignin-cellulose sheet exhibited excellent tensile strength of 200 MPa which was greatly stronger than most of commercially petroleum-based plastics, similar flexibility with cellulose paper, as well as comparable water stability with plastics.[38] In addition, a lignin-protein polymer network was synthesized by the crosslinking of carbonyl, amino and hydroxyls. The polymer displayed that lignin improved the tensile strength and water resistance of protein films.[39] Apart from elevated mechanical properties and water resistance, lignin brought extra UV absorbance ability, antioxidant and antimicrobial activities for lignin-cellulose or lignin-chitosan composites.[33, 40, 41]

However, natural polymers like cellulose and starch are hydrophilic and water sensitive due to the rich amount of OH groups, which will negatively affect the mechanical and wet stability so as to limit their applications. In addition, although lignin was proven to confer additional properties especially mechanical strength for natural polymers, the strengthening effect is greatly impacted by lignin structures and types. Taking the lignin-

chitosan polymerized film as an example, only one KL fraction with a M_w of 5,678 g/mol and a low S/G ratio can improve the ultimate tensile strength, while other KL fractions with different M_w and structural characteristics, or organosolv lignin cannot.[33] Therefore, this fully natural composite system has strict requirements for lignin characteristics that are influenced by extraction processes, and plant origins, which will cause difficulty in large-scale industrial manufacturing. Furthermore, most fabrication processes are energy-consuming, and require additives. Overall, main challenges for lignin-natural polymer composites including limited wet stability and lignin structural heterogeneity remain to be resolved.

1.2.2. Lignin-based copolymers with synthetic bio-derived polymers

Bio-derived synthetic polymers such as polylactic acid (PLA), poly(vinyl alcohol) (PVA), poly(3-hydroxybutyrate-co-3-hydroxyhexanoate) (PHBH), poly (ε-caprolactone) (PCL), poly(butylene succinate) (PBS), etc. have drawn people's attention due to the good biodegradability and more stable performance than natural polymers.[42-45] Lignin was investigated to integrate with the catalog of synthetic bio-derived polymers through chemical polymerization. For example, Abdollahi *et al.* synthesized a lignin-grafted-PCL copolymer (lignin-*g*-PCL) with PCL chains grafted to lignin skeletons through ring opening polymerization (ROP) of ε-caprolactone monomers (CL). They discovered that thermally stable lignin core could increase the melting temperature (T_m) and crystallinity of PCL and the rigid lignin core generated little influences on the thermos-plasticity and easy processability of PCL.[45] Another study further investigated that the OHs in lignin nanoparticles could initiate the ROP of CL and lactide to form a lignin-PCL-PLA copolymer, and the synthesized copolymers could enhance the toughness, flexibility, and UV-shielding ability of PLA.[23]

To overcome the limitations such as poor dispersibility, compatibility, solubility, etc. of lignin, chemical modifications of lignin provide solutions due to the rich reactive sites such as OHs, methoxy, carbonyls, in lignin. For instance, lignin esterified with succinic anhydride could increase the interfacial compatibility between lignin and PLA.[43] Besides,

lignin modified with maleic anhydride could be well dispersed in PHBH matrix. [42] They found out that lignin addition improved the mechanical properties and thermal stability of PLA and PHBH and brought great UV-shielding ability, enhanced thermal stability and photostability, antioxidant, anti-inflammatory and antimicrobial activities.

However, there are still many challenges to synthesize lignin with these bio-derived polymers. Firstly, most of the time, lignin would intensify the brittleness and/or reduce the transparency of these polymers. Secondly, lignin heterogeneity in M_w, structure, origin, extraction process and modification methods would result in the application impediment with synthetic biopolymers. Thirdly, the poor compatibility between lignin and these bioderived synthetic polymer impedes the synthesis and further utilization even if modifying strategies can help to relieve the barriers. These aspects undoubtfully are burdens on a broader application of lignin-synthetic biocomposites.

1.2.3. Lignin-based recyclable copolymers

To promote a green, sustainable and circular economy, researchers are dedicated to developing chemically recyclable polymers using bio-derived polymers as a partial replacement that could be potentially applied in manufacturing industries.[46] To realize the chemical recycling, dynamic covalent exchange, polymerization and depolymerization, and condensation-reverse reaction are feasible strategies. Dynamic covalent exchange occurs in DCPN that can be chemically recycled, re-healed, and re-shaped *via* topological transformation.[47] The construction of DCPN can be achieved *via* multiple mechanisms such as transimination, transesterification, transalkylation, etc.[48] Self-healing DCPN usually are reprocessable under triggering (such as heat, pressure, light, solvent, etc.) *via* network rearrangement with minimal performance sacrifice.

Lignin, as a cheap and sustainable aromatic polyol, has been widely investigated to develop novel bio-based DCPN by synthesizing with multiple polymers such as polyurethane[46], poly(ethylene glycol) (PEG)-epoxy[49], polyolefin[50], etc. For instance, a mechanically-strong lignin-based DCPN was synthesized by lignin and petroleum-derived polyols *via* non-covalent (hydrogen bonds and metallic coordination bonds) and covalent

(carbamate) bonds, which could be reprocessed and re-healed under near-infrared light and maintain the 98% of the mechanical strength.[51,52] Another example is that a thermoset was catalytically synthesized with lignin and PEG-epoxy *via* dynamic transesterification with adequate coating hardness and adhesion performances, which could be removed by mild alkaline and repaired with the assistance of glycol.[49]

The reversible condensation between amines and ketone/aldehydes is one of the most common reactions to construct robust molecules by the formation of covalent imine bonds in organic chemistry.[53] The imine bonds can break and reform simultaneously under heat, pressure, excessive free amines, catalysts, or solvent *via* imine metathesis and exchange reactions (Figure 1-2).[16, 47, 53, 54] In terms of the bio-based DCPN developed by dynamic imine bonds, vanillin is widely investigated as a feedstock[54, 55] due to the 1) aldehyde group that allows the imine condensation and 2) existence as a monomer that favors the polymer recyclability. However, to obtain vanillin-based polyimines with highly crosslinked networks with favorable thermomechanical properties, vanillin is required to be modified to enrich the aldehydes, and afterward to crosslink with expensive multiamines.[54-56] In this case, the imine bond crosslinking density, MW, thermomechanical and other performances of vanillin-based polyimines would be restrained since the aldehyde concentration is limited. In a previous report, a lignin-based polyimine thermoset was successfully synthesized and reprocessed under hot press *via* dynamic imine chemistries with a minimally detrimental effect on mechanical strength.[16] The re-processibility highly depends on the dynamic imine exchange and metathesis, which are closely influenced by the temperature, stress, polymer compositions and structures, molecular chain flexibility and rigidity, etc.[15, 16]

Lignin structural heterogeneity could also affect the structures and properties of synthesized DCPN. Recently, a prior study reported that the lignin-based polyurethane DCPN synthesized by low-MW lignin with rich hydroxyl groups exhibited higher crosslinking density, mechanical strength, and anti-aging ability.[46]

These studies give us insight that lignin is feasible and promising for constructing high-performance re-processable and re-healable DCPN with minimal performance

sacrifice. However, those DCNPs demand external stimuli of non-degradable metallic catalysts to activate the dynamic reactions. Therefore, catalyst-free synthesis and activation of lignin-based DCNP are highly required because the absence of a catalyst eliminates the need for hazardous and expensive materials, simplifying the synthesis procedure, and reducing environmental impact.

1.3.Lignin hydrophobization

Lignin is naturally amphipathic due to the hydrophobic aromatic and aliphatic groups, as well as the hydrophilic OHs; it is also water- and thermo-stable for acting as a natural binder of plants and high carbon content, respectively; what's more, it possesses excellent anti-UV/antioxidant activities due to the rich phenolic structures.[57] More importantly, the rich functional groups, especially OH groups, allow lignin to be structurally modified to improve the hydrophobicity. All these features indicate lignin a good candidate for constructing biobased hydrophobic materials.[20]

To apply lignin for hydrophobic materials, hydrophobic modification of lignin is typically required. The reported methods include lignin esterification with long-chain alkyls[58], lignin silylation[14], lignin nanosizing[59], lignin (catalytic) pyrolysis[60, 61], etc. The first three methods used in the current dissertation are reviewed below.

1.3.1. Lignin esterification

Lignin esterification takes advantage of the newly formed ester bonds and other grafted non-polar groups such as long-chain alkyls from the esterification agents to increase the hydrophobicity of modified lignin.

For example, Singam *et al.* esterified lignin with propionic acid, and then coated esterified lignin, blended with cellulose acetate, on paper sheets to achieve a hydrophobic coating with water contact angle (WCA) over 130°.[62] In another study, Gordobil *et al*. esterified organosolv lignin with a long aliphatic chain (12-C) of dodecanoyl chloride (Figure 1-3a) to obtain a hydrophobic agent with improved thermal, water, and oil stability

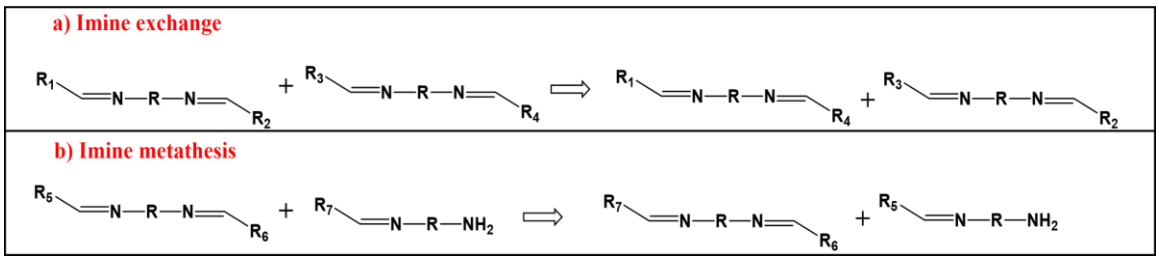


Figure 1-2 Imine exchange (a) and imine metathesis (b) of dynamic imine bonds.[54]

to be applied to hydrophobic wooden products (WCA ≈ 140°).[63] Besides, Meng *et al*. also esterified de-alkaline lignin with a long aliphatic chain (16-C) of stearoyl chloride (Figure 1-3a) to prepare lignin-based petaloid nanoflakes for superhydrophobic surfaces.[58] Furthermore, Hua et al., esterified hydroxyethyl lignin with oleic acid catalyzed by sulfuric acid (Figure 1-3b). The esterified lignin is soluble in toluene and THF, and is coated on multiple substrates including glass, paper, and wood, with elevated WCA above 120°.[64]

However, the lignin esterification demands catalysts and highly reactive and moisture-sensitive esterifying agents such as acyl chloride which typically is toxic and requires anhydrous conditions. Additionally, the hydrophobicity of modified lignin-based esters closely relates to the selection of esterifying agents and lignin, which causes uncertainty and more workload to screen feedstocks. Lastly, the hydrophobicity is limited if lignin is exclusively chemically esterified without the intervene of microstructures. Therefore, lignin esterification often serves as a pre-step that needs further hydrophobization treatments for the fabrication of hydrophobic materials.

1.3.2. Lignin silylation

Lignin silylation is to introduce low-surface-energy silyl groups (-SiR_3) to lignin to enhance the hydrophobicity. The widely used silyating agents are tert-butyldimethylsilyl chloride (TDMSCl)[65], divinyl tetramethyldisilazane (DVDZ)[66], 3-(triethoxysilyl) propyl isocyanate (TSPI)[14], and so forth.

For instance, KL was modified by a silylating agent TSPI containing silane groups through the reaction between the OHs and isocyanate groups, which greatly improved the hydrophobicity, rubber compatibility, rubber dispersibility of lignin.[14] In another study, OH in soda lignin was silylated by TDMSCl, showing an obvious hydrophobicity with a WCA over 100° and complete solubility in low-polarity solvents including acetone, ethyl acetate, and diethyl ether.[65] Another instance is that the OH in KL was silylated by DVDZ with ~ 30% substitution of OH in KL, which enhanced the molecular flexibility, adhesion, reactivity, and processability of KL with polyacrylonitrile. Although authors did not investigate the surface properties, we speculate that the silylated KL possess good

hydrophobicity to be applied for hydrophobic membrane and film materials due to the introduction of SiC and SiOC bonds.[66]

Sometimes, a crosslinker is used to introduce low-surface-energy silicone to lignin, which provides an alternative method to lignin silylation. For example, Chen *et al*. prepared lignin-based polyurethanes through the covalent immobilization of monocarbinol-terminated polydimethylsiloxane (PDMS-OH) to lignin with the help of a crosslinker hexamethylene diisocyanate trimer (HDIT), which shows applicability to fabricate hydrophobic coatings with good water repellency (WCA up to 105 °).[67]

Lignin silylation is an effective pathway to greatly improve the hydrophobicity of lignin, however, corrosive, toxic, and hazardous chloride-containing or isocyanate-containing silylating agents or crosslinker are typically used. Therefore, a greener and safer silylation method is highly required. To add to this, it is still difficult to realize super-hydrophobicity due to the lack of rough surface microstructures.

1.4. Lignin nanosizing

Lignin nanosizing have been well acknowledged as a promising routine allowing the value-added applications of industrial waste lignin that is typically discharged to the river or burned to generate heat for mills.[59] Lignin nanospheres (LNS), different from inorganic nanospheres, such as silica oxides, metal oxides, etc., have favorable features including sustainability, biodegradability, low cost, renewability, anti-UV/oxidant/microbial activities, richness in surface functional groups, together with high specific surface area and well-defined surface properties.[59, 68, 69] Benefiting from these characteristics, LNS have been utilized as functional fillers in polymers for (super)hydrophobic, anti-bacterial/UV, drug delivery, absorbent materials, etc.[59, 70-73]

Multiple lignin nanosizing technologies including solvent exchange (self-assembly), pH shifting, interfacial polymerization, aerosol flow reactor, and mechanical treatments, etc. have been reported.[68, 69, 71, 74] Thereof, solvent exchange is the most commonly used method due to the simple operation, good spherical shape, high applicability, and other

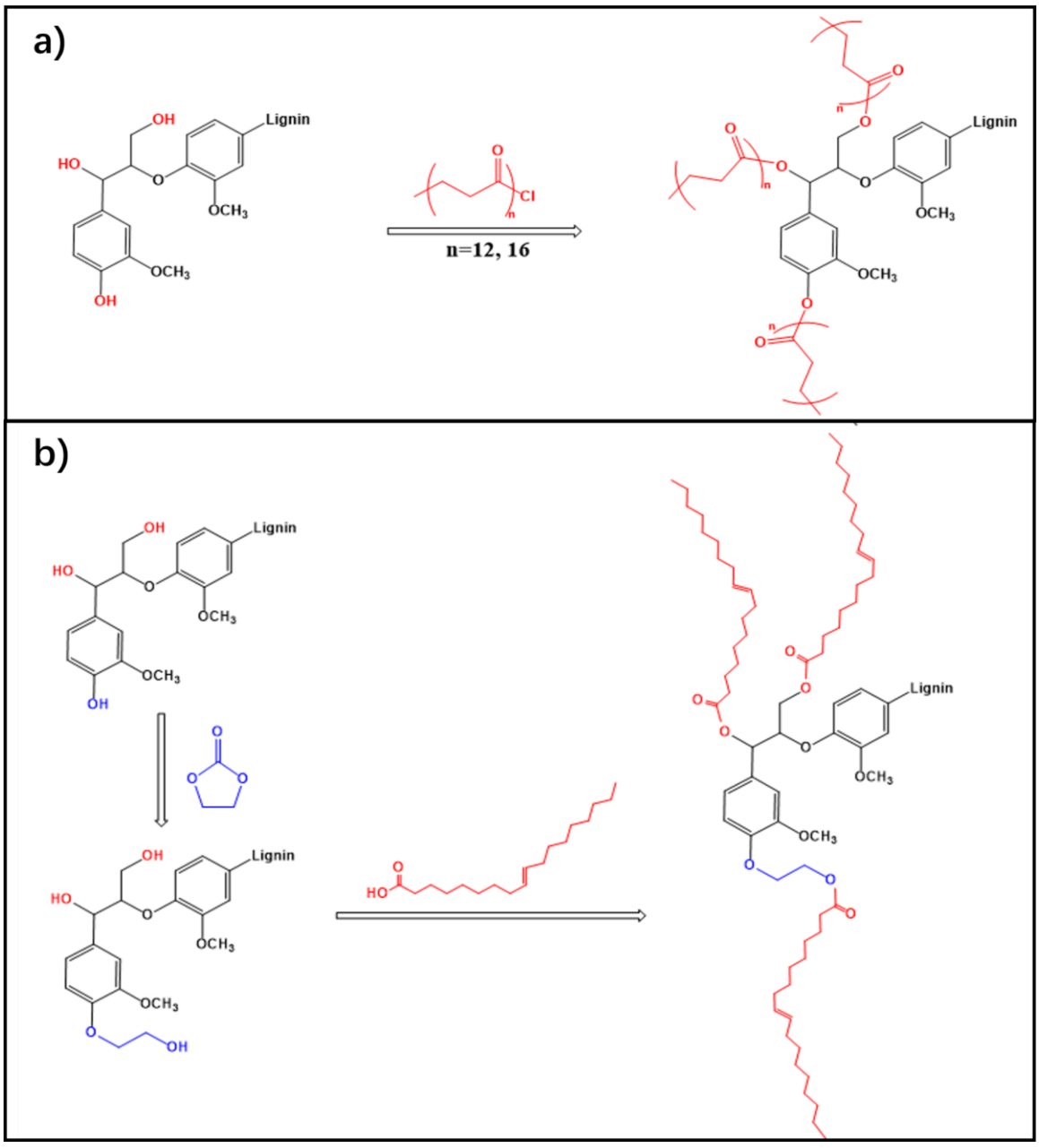


Figure 1-3 Esterification of lignin by 12-C dodecanoyl chloride[63], 16-C stearoyl chloride[58] (a), and esterification of hydroxyethyl lignin by 18-C oleic acid[64] (b)

advantages.[59, 68] In general, solvent exchange uses organic solvents to dissolve lignin molecules first, and then uses antisolvent, typically water, to precipitate LNS by the self-assembly of lignin molecules. Commonly used organic solvents are γ-valerolactone (GVL), THF, dimethyl sulfoxide (DMSO), ethylene glycol, DMSO, acetone, cetyltrimethylammonium bromide, etc.[68, 69, 71, 72, 74-76] THF and water is a testified effective solvent-antisolvent combination to prepare well-shaped LMNS. However, lignin modification (*e.g.,* acetylation)[76] to improve the lignin solubility and/or time-consuming dialysis process[68] to remove toxic solvents are typically required. It is worth noting that GVL is bio-derived, hypotoxic, renewable, and stable with high lignin solubility (the tested concentration of saturated EHL/pure GVL solution is 158.88 mg/mL[70]).

The internal interactions of LNS primarily are weak intermolecular forces such as hydrogen bonding, π–π interactions, and electrostatic and hydrophobic forces, leaving hydrophilic groups on the surfaces of LNS spheres. Due to the instability of LNS, scientists are investigating stabilization technologies to facilitate the utilization of LNS. For example, Wang et al, stabilized LNS by hydrothermal treatments *via* lignin self-condensation under high temperatures. The covalent-noncovalent forces stabilization reduces the average particle size and solubility in ethanol and THF, and improves the thermal stability of LNS that has application potentials in superhydrophobic coatings to replace nano-sized inorganic materials.[59] Based on these, their team prepared stabilized LMNS using a GVL/water exchange method followed by hydrothermal treatments for superhydrophobic coatings on wood. The size of prepared LMNS can be controlled by initial lignin concentration, amount of added water ratio, temperature, and sonication duration.[70]

1.5. Lignin for hydrophobic and superhydrophobic coatings

Hydrophobic coatings, usually coupled with water-resistant, anti-UV light, anti-corrosion, self-cleaning properties and so forth, have displayed various applications and application potentials in biomedical, packaging, automotive, marine and energy industries, etc.[77] Lignin, owning to its biodegradability, renewability and overall hydrophobicity, is

widely investigated to prepare hydrophobic coatings.[78] However, due to the OH and COOH groups, lignin is considered amphiphilic. The hydrophobicity needs to be further enhanced by hydrophobization or nanosizing treatments, which have been reviewed in Sections 1.3. and 1.4. above.

Additionally, lignin structures are rigid because of the rich aromatic rings, so the film-forming ability of lignin is poor. Therefore, incorporating polymers with soft chains is necessary to improve the molecular mobility of lignin, so as to be feasible for uniformed coating surfaces. For example, softwood KL was modified with ethylene carbonate to consume the phenolic OH and esterified with oleic acid to graft long alkyl (18-C) chains (Figure 1-3b), and then the esterified lignin was applied as hydrophobic coatings. The WCA is influenced by the coating methods and substrates, showing a highest WCA of 147°on spray coated wood.[64] For another example, pine alkaline lignin was used to synthesize with PDMS-OH with good film-forming ability to form polyurethanes coated on glass slides. The lignin-based polyurethane coatings show good translucency, omniphobicity, excellent water repellency (WCA up to 105 °), anti-fouling, and UV-block abilities.[67]

Also, considering the natural biocompatibility, lignin-based coatings usually have good coating performances on cellulose-based substrates such as wood and paper. For instance, Camillla *et al.*'s brought forward a fully bio-based protective coating using LNS, and cellulose nanofibrils and nanocrystals as greener alternatives for toxic varnishes to preserve the roughness and surface morphology of the substrates including wood, paper, and fabric, which is highly hydrophobicity (WCA up to 120°), anti-aging, UV-shielding, and easy to be removed.[79]

Last but not least, lignin could act as particulates and to enhance the coating hydrophobicity through surface roughening and as a hardener to enhance the coating adhesion. For example, Alexander et al., prepared colloidal LNS with good water dispersity for the fabrication of biobased, stable, and multifunctional coatings together with epoxies. The fabricated coatings have a WCA reaches up to 120°, and great resistance to solvent, stains, abrasions, heat, and light.[80]

Superhydrophobic coatings have coating surface with an apparent WCA greater than 150° and a ROA less than 10°, which can stay dry, self-clean, and avoid fouling.[81] Inspired by the superhydrophobic surface present in plants and insects, biomimetic materials attract great attention among scientists for advanced application potentials in biotechnology, construction, water/oil separation, medicine, and heat transfer.[81-84] With continuous efforts made by researchers, the Cassie-Baxter model attached the importance of surface texture to the wettability of porous surfaces[85], providing a well-established method to build up superhydrophobic surface, that is, the combination of low-surface-energy chemistry and micro- and/or nanoscale surface roughness to mimic natural superhydrophobic surface like lotus leaf, duck feather, etc.[61, 86]

LMNS is studied to be further enhance the hydrophobicity of coatings by roughen the surface through the construction of hierarchical microstructures *via* the macro-scale and nano-scale spheres, which proposes a novel pathway to utilize LMNS for superhydrophobic coatings.[70] For example, LMNS was prepared by self-assembly and hydrothermal treatment to coat on a silicon board with a superhydrophobic surface (WCA up to 151.9°).[59] As mentioned in Section 1.4., LMNS was used fabricate superhydrophobic wood coating surfaces with a WCA up to 164.4° and a sliding angle low to 5°. Besides, the coated wood exhibits excellent mechanical resistance to knife scratch, tape peeling and waterdrop impact, as well as chemical resistance to organic solvents including THF, ethanol, and acetone, multiple daily liquids including tea, milk, juice, and saline, and strong acid (pH = 1), as well as great photothermal effect to be applied for deicing and antibacterial materials.[70]

Based on these pioneering studies, LMNS is hypothesized to have significant potentials to be employed for superhydrophobic coatings on cellulose-based substrates, such as wood, paper, and fabric, due to 1) surface roughening through deposition or chemical etching of LMNS, 2) the construction of hierarchical microstructures by the macro-scale and nano-scale spheres, 3) the improved biocompatibility and adhesion with hydrophilic groups like OH and COOH on the surface of cellulose-based substrates due to its hydrophobic core and hydrophilic surface formed by the self-assembly of lignin

molecules in solvent-antisolvent preparation process, 4) possible availability of surface hydrophobic functionalization by long-chain alkyls and other non-polar molecules or functional groups.

CHAPTER II

EFFECT OF LIGNIN STRUCTURE ON THE PHYSICOCHEMICAL PROPERTIES OF LIGNIN-G-PCL AND ITS APPLICATION FOR WATER/OIL SEPARATION

A version of this chapter was originally published as:

Xie D., Pu Y., Meng X., Bryant N. D., Zhang K., Wang W., Ragauskas A. J., Li M. (2022). Effect of Lignin Structure on the Physicochemical Properties of Lignin-grafted-poly(ε-caprolactone) and its Application for Water/Oil Separation. *ACS Sustainable Chemistry and Engineering*, 10, 50, 16882-16895.

Author contributions are listed as follows. DX: conceptualization, methodology, investigation, formal analysis, data curation, writing-original draft. YP: resources, data curation, writing-review & editing. XM: investigation, writing-review & editing. NB: investigation, writing-review & editing. KZ: investigation, writing-review & editing. WW: resources, writing-review & editing. AR: resources, writing-review & editing. ML: conceptualization, methodology, supervision, validation, writing-original draft, project administration, and funding acquisition.

2.1. Abstract

Lignin-grafted-poly(ε-caprolactone) copolymers (lignin-g-PCLs) have shown wide application potentials in coatings, biocomposites, and biomedical fields. However, the structural heterogeneity of lignin affecting the structures and properties of lignin-g-PCL has been scarcely investigated. Herein, KL is fractionated into four precursors, i.e., Fins, F1, F2, and F3, with declining weight-average molecular weights (Mw) and increased OH contents. Lignin-g-PCLs (F_x-PCL) are synthesized with fractionated lignins and ε-caprolactone (ε-CL) via ring-opening polymerization, and subsequentially characterized by GPC, FTIR, 1H and 31P NMR, DSC, TGA, and iGC. Mechanical properties, UV-barrier ability and enzymatic biodegradability of synthesized copolymers are evaluated. Results show that lignin with higher molecular weight and aliphatic OH favors copolymerization, leading to lignin-g-PCLs with longer PCL arms. Moreover, lignin incorporation improves the thermal stability, hydrophobicity, and UV-blocking ability, but reduces the lipase hydrolysability of copolymers. We also demonstrate that lignin-g-PCL coated filter paper could successfully separates chloroform-, petroleum ether-, and hexane-water mixtures with separation efficiency up to 99.2%. The separation efficiencies remain above 90% even after 15 cycles. The structure differences of copolymers derived from fractionation showed minimal influence on the separate efficiency. This work provides new insights into lignin-based copolymerization and the value-added versatility of lignin.

2.2. Introduction

KL yielded by the acidification of black liquor from the sulphate pulping process provides a cheap and readily available source to develop value-added composites, blends, and chemicals[26, 27] in addition to the major low-value usage for energy generation at pulping mills[25, 28]. Furthermore, KL possesses rich phenolic OHs because the β-aryl ether bonds are cleaved during pulping process, providing more versatility for chemical modifications.[29, 30] However, the heterogeneous structure of KL, such as molecular weight (MW) and functional group (amount and types), usually causes nonuniform properties including reactivities, thermal stability, compatibility, solubility, and dispersity: Typically, aliphatic OH content, glass transition temperature, and thermal stability increase, while phenolic OH and methoxy contents, solubility, and dispersibility decrease with the augment of lignin MW.[8-11] The feedstock heterogeneity could be imparted to the lignin-derived products, leading to disparate performances. For instance, one KL fraction from eucalyptus with weight-average molecular weight (M_w) of 5,678 Da and phenolic OH content of 1.42 mmol/g could enhance the ultimate tensile strength of chitosan films, however, KL fraction with 2,422 Da and 2.17 mmol/g caused an inverse effect.[33] Another study showed that the ethanol-soluble KL fraction from bamboo displayed a benign antimicrobial activity against Gram-positive and -negative bacteria growth due to higher phenolic content and better water solubility; whereas the ethanol-insoluble KL lacks similar antimicrobial activity due to a lower phenolic content and poor water solubility.[35] Moreover, high-M_w KL fractions from *Pinus caribaea* esterified with succinic anhydride showed better dispersity than their unfractionated counterparts.[36] Therefore, refining KL into more homogeneous feedstock fractions is importance to afford comparable and stable product performance.

Poly(ε-caprolactone) (PCL), an aliphatic polyester, shows application potentials in plastic replacement, drug delivery, and tissue engineering.[87-89] Due to the biodegradability, good biocompatibility, easy processability, solubility in wide-range solvents, and miscibility with many other polymers, PCL has been widely investigated to copolymerize

with lignin via ring opening polymerization (ROP) of ε-caprolactone (ε-CL) to obtain lignin-*g*-PCLs that exhibit promising applications in coating[90], biocomposites[91], inflammation treatment[92], and tissue engineering[93]. Our prior work has found that (a) KL can be successfully copolymerized with ε-CL and (b) KL exhibited wider MW distribution than other technique lignin.[13] Therefore, it is feasible and necessary for us to investigate the effects of lignin structure on the physicochemical properties of lignin-*g*-PCLs. Lignin and PCL contribute synergistic impacts to the copolymers. Grafting PCL improves the dispersity, compatibility, and hydrophobicity of lignin, while lignin enhances anti-UV, antioxidation, anti-inflammation, osteo-conductivity, as well as cell-viability and -proliferation abilities of PCL.[13, 91-94] Lignin-*g*-PCL typifies a star-shaped molecular with a lignin core and PCL arms.[91, 95] Our prior work has demonstrated that technical lignin is reactive to copolymerize with ε-CL irrespective of their botanical sources and extraction methods,[13] but lignin content negatively affects the MW and thermal properties of the lignin-*g*-PCLs.[96] Moreover, the crystallinity degree (X_c) of the PCL segments in lignin-*g*-PCLs depends on the ε-CL-to-lignin OH (CL/OH) molar ratio to a great extent.[45, 91, 95] Nevertheless, reactivities of OHs differ among different OH types in terms of phenolic, aliphatic, carboxylic OHs, etc.,[31, 97] so simply applying CL/OH as a variant is insufficient to reveal the synthetic mechanism.

Different structural characteristics of lignin-*g*-PCLs lead to different physicochemical properties. The thermal properties of lignin-*g*-PCLs depend on the length of grafted PCL chains.[45] The lignin-*g*-PCLs become brittle when the PCL portion is semi-crystalline due to the phase separation between PCL and lignin, while they become flexible when the PCL portion is amorphous due to the interval molar mass among PCL chains.[95] Besides, the elongation at the break of lignin-*g*-PCLs is linked with both PCL chain length and the number of grafted PCL chains.[95] In addition, an elastomeric behaviour can be observed when the length of PCL chains is in a certain range (between 7-11).[95] Nevertheless, the effect of lignin structure including MW and OH content on the structures and properties of lignin-*g*-PCL has not been studied. According to the Hansen solubility parameter, boiling point, and heat of vaporization, sequential-solvent fractionation using the binary methanol-

acetone solvent system and aprotic hexane as antisolvent is an easy and effective approach to achieve structurally customized fractions of lignin (e.g., narrow-ranged MWs and varied OHs).[11] We postulated that using lignin fractions with more controlled structural features as feedstock for copolymerization will lead to distinguished features and properties of lignin-derived products, which will facilitate the valorization of lignin.[7]

In this work, to elucidate how the structure of lignin affects the synthetic lignin-*g*-PCLs, structurally heterogeneous KL was firstly fractionated using binary solvent and antisolvent sequential approach into different fractions with representative MWs and OH features. The lignin fractions were subsequently copolymerized with ε-CL to synthesize lignin-*g*-PCL via ROP. The structure and physicochemical properties of the synthesized lignin-*g*-PCLs were investigated to establish a "structure-property" relationship. The biodegradability of lignin-*g*-PCLs was also measured by lipase hydrolysis. Inspired by the naturally water-resistance function, lignin has been widely applied to fabricating hydrophobic filtration or absorption materials for water/oil separation.[86, 98-100] We finally applied lignin-*g*-PCLs to coating filter paper (FP) as a substrate for separating water and oil mixtures to explore new applications of lignin-*g*-PCLs. The present study is expected to provide a fundamental understanding of lignin copolymerization and advance lignin biorefinery and valorization.

2.3. Materials and Methods

2.3.1. Materials

Southern pine softwood KL, isolated via the LignoBoost process, was provided by Domtar Co. (SC. USA). PCL (M_w ~ 14,000 Da), ε-CL, stannous octanoate ($SnOct_2$), acetone, hexane, methanol, ethanol, chloroform ($CHCl_3$), acetic anhydride, THF, 2-chloro-4,4,5,5-tetramethyl-1,3,2-dioxaphospholane (TMDP, 95%), deuterated chloroform ($CDCl_3$, 99.8%), N-hydroxy-5-norbene-2,3-dicarboxylic acid imide (NHND), nonane, octane, heptane, acetonitrile, ethyl acetate, dichloromethane, petroleum ether, lipase (from *Pseudomonas fluorescens*), silicon dioxide (SiO_2) and silicone oil were purchased from

Sigma Aldrich (St. Louis, MO). Anhydrous pyridine was purchased from Spectrum Chemical (New Brunswick, NJ). All chemicals were used as received.

2.3.2. Lignin fractionation

KL was fractioned into four different fractions with different MWs according to a previous report[11] with some modifications (Figure 7-1). Briefly, 10 g KL was dissolved in 50 mL acetone-methanol cosolvent (7:3, v/v), and the suspension was centrifuged (10,000 rpm, 10 min, 4 ℃) to obtain and separate the insoluble fraction (F_{ins}) and supernatant. Next, 5 mL hexane was successively added to the supernatant followed by centrifugation to isolate the precipitate (F1) and the supernatant. The addition of hexane was repeated one more time to collect another precipitate (F2) and the soluble part was later concentrated to solid (F3) by rotary evaporation. The yields of F_{ins}, F1, F2, and F3 are 2.45%, 1.47%, 4.72%, and 73.31%, respectively. The four lignin fractions were further dried in a vacuum oven for the rest investigation in this study.

2.3.3. Synthesis of lignin-g-PCLs

KL and the four lignin fractions were respectively copolymerized with PCL by solvent-free ROP of ε-CL monomers based on our previous publication.[13] In brief, vacuum dried lignin samples, ε-CL (CL/OH molar ratio of 10, lignin OH content was measured by ^{31}P NMR), and 0.2 wt% catalyst $SnOct_2$ (based on ε-CL amount) reacted under stirring at 130 ℃ and N_2 atmosphere for 24 h. The crude product was then recovered by adding into cold methanol dropwise. Subsequently, it was thoroughly washed with cold methanol to remove ε-CL monomers and neat PCL. The product was air-dried for 24 h, followed by vacuum drying at 25 ℃ for 12 h to obtain lignin-*g*-PCL copolymers which were named KL-PCL, F_{ins}-PCL, F1-PCL, F2-PCL, and F3-PCL corresponding to the feedstocks KL, F_{ins}, F1, F2 and F3, respectively.

2.3.4. Characterization of lignin-g-PCLs and lignin-g-PCL films

Gel permeation chromatographic (GPC) was applied to determine the M_w and number-average molecular weight (M_n) of acetylated lignin and lignin-*g*-PCL copolymers. The molar-mass dispersity ($Đ_M$) is defined as the ratio of M_w to M_n. The acetylation was carried out in pyridine/acetic anhydride (1:1, v/v) based on previous work.[13] The acetylated lignin and lignin-*g*-PCL copolymers were dissolved in THF, and then filtered through a nylon filter with pore size of 0.45 μm for GPC analysis. Size-exclusion separation was performed on an Agilent 1200 HPLC system (Agilent Technologies, Inc., Santa Clara, CA, US) equipped with Waters Styragel columns (HR1, HR2, and HR6; Waters Corporation, Milford, MA, USA) and ultraviolet detector (wavelength: 270 nm). THF was used as the mobile phase at a flow rate of 0.5 mL/min, and polystyrene was used as a standard for calibration. The values were calculated by the averages of the duplicate sample with standard deviations.

Fourier transform infrared (FTIR) spectroscopic analyses of samples were performed by a FTIR spectrometer (Spectrum One FTIR system, PerkinElmer, Wellesley, MA) with a universal attenuated total reflection accessory. Wavenumbers ranged from 4,000 to 600 cm^{-1} for 32 scans with a resolution of 4 cm^{-1}. Nuclear Magnetic Resonance (NMR) spectral data were recorded with a Bruker Avance III HD 500 MHz spectrometer. 50 mg lignin-*g*-PCL copolymers were dissolved in 0.5 mL $CDCl_3$, and then transferred to a 5 mL NMR tube for ^1H NMR test. ^1H NMR pulse sequence was used on a BBO probe: spectra width 10 ppm in dimension with 64 scans, 16 transients and a 2 s pulse delay by employing a 1D-sequence "zg30" with a 30° flip angle at room temperature. The central $CDCl_3$ solvent peak at a chemical shift (δ) of 7.26 ppm was used for chemical shift calibration. ^1H NMR was used to characterize the structure of lignin-*g*-PCL, and calculate the average length of PCL arms (PCL size) grafted to lignin by the integration ratio of repeating $–CH_2O–$ units to $–CH_2OH–$ end group of PCL segment.[91] An inverse-gated decoupling pulse sequence (Waltz-16) was used for quantitative ^{31}P NMR experiments. The hydroxyl group were quantified according to the literature based on an internal standard of NHND.[101] The

acquired spectra were processed using a Bruker Topspin 3.5 software. Assignments of compositional subunits were referred to the reported literatures.[13, 91]

Differential scanning calorimetric (DSC) and thermal gravimetric analysis (TGA) were carried out using a Q-2000 differential scanning calorimeter (TA Instruments, USA) and Q-50 thermogravimetric analyzer (TA Instruments, USA), respectively. For DSC measurement, about 5 mg of each sample was hermetically sealed in an aluminum pan and then was subjected to a heating and cooling cycle twice, from 30 to 100 ℃, at a rate of 10 ℃/min under a nitrogen atmosphere. The second scanning DSC heating and cooling curves were used to determine melting (T_m) and crystallization (T_c) temperatures, and X_c.[13] For TGA measurement, around 5 mg of each sample was loaded into the ceramic crucibles for heating from 30 to 800 ℃ at a rate of 10 ℃/min under N_2. The onset temperature of thermal degradation (T_{onset}), and the temperature at the maximum mass loss (T_{max}) are determined by TGA and differential TGA (DTG) curves. Universal Analysis 2000 software was applied to analyze the data.

Inverse gas chromatography (iGC) experiments were conducted by an IGC surface energy analyzer (SEA) equipped with a flame ionization detector (Surface Measurements Systems (SMS), Ltd, Alperton, UK). Approximately 80 mg of dried sample were packed into an individual salinized glass column (length: 300 mm, inner diameter: 4 mm) using the SMS column packing accessory. Samples were injected by n-alkanes (nonane, octane, heptane, and hexane) and polar probe molecules (acetone, ethanol, acetonitrile, ethyl acetate, and dichloromethane) to determine the dispersive (γ_d) and specific (γ_{sp}) surface energies over surface coverage between 0.01 to 0.4 n/nm. Data were analyzed by advanced SEA analysis software (Advance Version 1.4.2.0).

PCL and lignin-*g*-PCL copolymer films were prepared using hot compression[91] under 0.1 MPa pressure at 60 ℃ to obtain films with a thickness of 2 mm. The films were cooled down at ambient environment prior to the measurement of mechanical, UV-blocking, and biodegradable properties. Mechanical properties were measured using an Instron 5943 universal tensile tester (Instron Co., USA) according to the standard ASTM 882-10.[102] With some modifications from a previous literature[103], coupons were prepared and cut from

the prepared films as a rectangle shape with 5 cm length and 1 cm width for mechanical property measurements. Each rectangular coupon was stretched with an initial grip separation and a crosshead speed of 50 mm/min at room temperature. The average values of five replicates are reported for each film.

The UV-protection ability of films was evaluated according to a literature method.[104] using UV-vis spectra as a function of light wavelength (ranges from 200 to 800 nm) against transmission recorded by an Evolution 60S UV-vis spectrometer (Thermo Fisher Scientific, USA).

2.3.5. Enzymatic biodegradation of lignin-g-PCL films

Enzymatic hydrolysis was used to assess the biodegradability of neat PCL and lignin-*g*-PCLs using a modified method.[105] In brief, lipase solution was prepared by dissolving amino lipase from *Pseudomonas fluorescens* in phosphate buffered solution (pH=8) to a concentration of 400 U/mL. Each specimen (10×10×0.2 mm^3) in triplicates were weighed, added to a 5 mL enzymatic solution, and placed in a shaker at 250 rpm under 45 ℃. Specimens were taken out, washed twice with DI water, air dried, weighed, and returned to the vials with 5 mL fresh lipase solution every 2 days for two weeks. The biodegradability was evaluated by the weight loss of samples as a function of time.

2.3.6. Water/Oil separation with lignin-g-PCLs coated filter paper

The CFP was prepared based on ref.[86] with minor modifications. FP was soaked in different concentrations (0.2, 0.4, 0.6, 0.8, and 1.0 mg/mL) of F1-PCL/acetone solutions for 12 h followed by solvent evaporation. Next, SiO_2 is dispersed well in silicone oil for the second impregnation for 2 h, and then stabilized under 40 ℃ for 6 h for further characterization. Neat PCL in acetone at a concentration of 1.0 mg/mL was also coated with the same procedure as a comparison. CFP-Blank (CFP-B) was prepared by coating only the SiO_2/silicone oil mixture. FPs were coated with different copolymers (*i.e.*, KL-PCL, F_{ins}-PCL, F1-PCL, F2-PCL, and F3-PCL) under the same concentration of 1 mg/mL to select the best one for further comparisons. FP coated with PCL and optimized F1-PCL

at a concentration of 1.0 mg/mL in acetone are named CFP-P and CFP-C, respectively. Water contact angle (WCA) and surface morphology of CFPs were measured using a contact angle goniometer (Ramé-Hart Instrument co., USA) and scanning electron microscope (Zeiss Aurga, Germany), respectively.

Water/Oil separation tests were conducted using a simple and convenient conical funnel set-up with CFP to separate water (dyed purple) from organic solvents (dyed orange) including petroleum ether, hexane, and chloroform [106]. The organic solvent/water mixtures were prepared by mixing 5 mL organic solvent and 5 mL water. The mixed liquid was added to the funnel and the separation process was ended when there was no droplet fell. The filtration efficiency (%) was calculated by the weight percentage of stopped water in the funnel over originally added water in mixed liquid at room temperature. To evaluate the reusability of CFP-C, filtration efficiencies of continuously used CFP-C during 15 cycles were recorded.

For statistical analysis, all data were processed using software including OriginPro 8.5 (OriginLab Corporation, Northampton, MA, USA) and Excel 2016 (Microsoft, Redmond, WA, USA)

2.4. Results and discussion

2.4.1. Lignin fractionation

The successive fractionation of KL (M_w=3,801±16 Da) using cosolvent of acetone-methanol (7:3, v/v) and antisolvent of hexane, resulted in four fractions with different M_w from high to low, namely F_{ins} (11,188±1011 Da), F1 (4,461±233 Da), F2 (3,086±295 Da), and F3 (1,691±100 Da) (Table 2-1). KL was well dissolved in acetone-methanol cosolvent due to their high hydrogen bonding capacities and the plasticizing effect of methanol owing to its small molecular size, which promotes the diffusion of organic cosolvent molecules into the compact lignin complexes.[11] When hexane was added, the difference between the Hansen solubility parameters of solvent and lignin increased remarkably, resulting in the precipitation of large lignin molecules. In contrast, lignin oligomers (low-M_w lignin) remain

soluble in the solvents because of their wider range of hydrogen bonding ability and Hansen solubility parameter than high-M_w counterparts until an extra amount of antisolvent is added.[107] Consequently, lignin fractions with declining M_w were sequential precipitated upon the amount of hexane addition in this work. Compared with the successive precipitation method using acetone followed by methanol,[108] F_{ins} in this work precipitated from the lignin solution dissolved by acetone-methanol co-solvent had a higher M_w (11,188 vs. 9,430 Da), suggesting that acetone-methanol cosolvent can dissolve more high-M_w lignin than single solvent. The F_{ins} had a wider $Đ_M$ than KL, which may be due to the presence of carbohydrates and/or lignin-carbohydrate complex of which the M_w are much different from lignin.[11, 12] On the contrary, the $Đ_M$ of the other three fractions, F1, F2, and F3, are in the range from 2 to 3 that are smaller than that of KL (Table 2-1), and are comparable with previously reported $Đ_M$ of 1.4-2.2[21] and 1.5-2.5[12], suggesting that the acetone-methanol cosolvent fractionation method used in this work effectively refines KL into more uniform fractions as the OH groups of lignin are important structural elements that serve as the initial sites for the ROP of ε-CL,[45] we have quantified the OH groups on the four lignin fractions using ^{31}P NMR spectroscopy. The aliphatic, phenolic (including C_5 substituted, guaiacyl, and *p*-hydroxyphenyl OHs), and the carboxylic OH were identified and well-resolved in the ^{31}P spectra (Figure 2-1).[101] The quantitative contents of the total, phenolic, aliphatic, and carboxylic OHs are 5.95±0.03, 3.56±0.02, 1.89±0.01 and 0.50±0.00 mmol/g in KL (Table 2-2), respectively, which are comparable with those reported studies on industrial softwood KLs.[11, 13] The high phenolic OH content is attributed to the cleavage of alkyl aryl ether bonds (such as β-O-4 and α-O-4) during pulping process, releasing more phenolic OH at the lignin aromatic rings.[8, 108]

Previous studies have shown that lignin aliphatic OH content increases while phenolic OH content decreases along with the increase of lignin M_w.[8, 11, 12] The correlation and regression analyses of the three representative lignin fractions (*i.e.,* F1, F2, and F3) in the current study are consistent with this relationship. In other words, lignin M_w has a positively linear correlation with the quantity of aliphatic OH (Pearson correlation coefficient (r) = 1.000, coefficient of determination (R^2) = 1.00, P value (P) = 0.189) and a negatively linear

Table 2-1 Weight-average (M_w), number-average (M_n) molecular weight, and molar-mass dispersity ($Đ_M$) of lignin and lignin-*g*-PCLs measured by GPC, and the average length of PCL arms measured by ^{1}H NMR

	M_w (Da)	M_n (Da)	$Đ_M$		M_w (Da)	M_n (Da)	$Đ_M$	PCL size
Lignin and lignin fractions				***Lignin-g-PCLs***				
KL	3801±16	1072±194	3.55±0.64	**KL-PCL**	44775±1100	19789±1084	2.21±0.07	32
F_{ins}	11188±1011	1983±39	5.64±1.21	**F_{ins}-PCL**	13472±190	4268±186	3.16±0.18	7
F1	4461±233	1556±12	2.87±0.89	**F1-PCL**	57143±1466	29262±120	1.95±0.04	40
F2	3086±295	1090±53	2.83±0.46	**F2-PCL**	38834±181	17240±96	2.25±0.00	25
F3	1691±100	779±44	2.17±0.31	**F3-PCL**	28686±248	12432±122	2.31±0.04	20

Note: The data are in a form of mean ± standard deviation

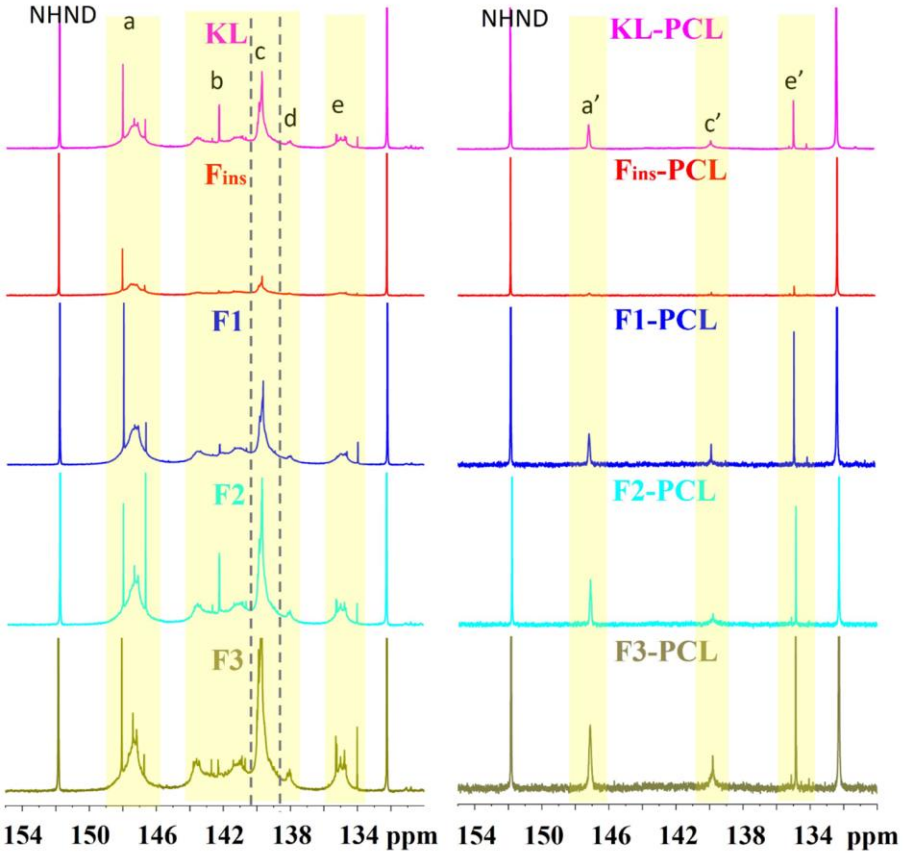


Figure 2-1 [31] P NMR spectra of lignin fractions (left) and lignin-*g*-PCLs (right). a: aliphatic OH, b: C_5 substituted OH, c: guaiacyl OH, d: *p*-hydroxyphenyl OH, e: carboxylic OH

correlation with the quantity of phenolic OH (r = -0.999, R^2 = 1.00, P = 0.031) (Figure 2-2A). Reasons why phenolic OH concentration increases with the reduction of lignin M_w could be that 1) β-O-4 linkages cleaves with the addition of hexane, forming new phenolic OHs.[11, 109] 2) phenolic OH itself is the chain end of the lignin oligomers[31], which means low-M_w lignin fraction has a high frequency of phenolic OH.[110] The elevation of phenolic OH content accordingly leads to an decreased proportion of aliphatic OHs. Also, it helps to explain why phenolic OH concentration is much lower in F_{ins} than in other lignin fractions (Table 2-2).

In sum, the obtained F1, F2, and F3 fractions are representative lignin fractions featuring declining M_W and aliphatic OH content but increased phenolic OH content. However, F_{ins} is not counted as a representative lignin fraction in this study because of its unusually high M_w, wide $Đ_M$, and low OH content, which will presumably hinder its ROP reaction due to the poor solubility and dispersibility, unfavorable homogeneity, and limited reactive sites. Besides, the poor solubility of F_{ins} in $CDCl_3$ led to an underestimated quantitation of OH content by ^{31}P NMR.

2.4.2. Structural characterization of lignin-g-PCLs

^{31}P NMR spectra confirmed the successful grafting copolymerization of lignin and

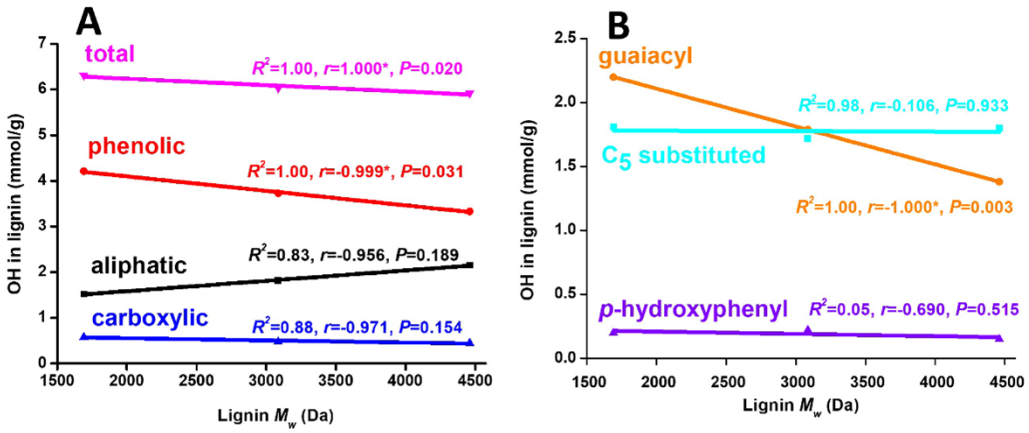
PCL due to the disappearance and substantially diminished phosphitylated OH peaks for the copolymers in comparison to the lignin feedstock in the current work. The ROP of ε-CL with aliphatic and phenolic OHs of lignin leads to the PCL segment ended with aliphatic OH at 145.4-150 ppm (a' in Figure 2-1); ε- CL reacting with carboxylic OHs leads to carboxylic OH at the end of the PCL segment shown by the peak at 133.6-136.0 ppm (e' in Figure 2-1). ROP of ε-CL itself can afford PCL linear homopolymer bearing both aliphatic OH and carboxylic OH in equivalent quantity. Firstly, lignin-*g*-PCLs exhibit fewer OH signals (a', c', and e') than their corresponding lignin fractions (a, b, c, d, and e) (Figure 2-1). The disappearance of both signal b assigned to C_5 substituted OH at 144.5-140.0 ppm and d assigned to *p*-hydroxyphenyl OH at 137.0-139.0 ppm after synthesis indicates they were replaced by PCL arms ended with aliphatic OHs. Secondly, compared

Table 2-2 Quantification of hydroxyl groups in lignin and lignin-*g*-PCLs determined by ^{31}P NMR

Types of OH (mmol/g)	Aliphatic	C_5 substituted	Guaiacyl	*P*-Hydroxy phenyl	Carboxylic	Total phenolic	Total
			Lignin				
KL	1.89±0.01	1.54±0.17	1.85±0.17	0.17±0.03	0.50±0.00	3.56±0.02	5.95±0.03
F_{ins}	0.66±0.00	0.27±0.01	0.36±0.02	0.01±0.00	0.01±0.00	0.63±0.01	1.30±0.01
F1	2.15±0.04	1.80±0.05	1.38±0.03	0.15±0.01	0.45±0.01	3.33±0.01	5.92±0.02
F2	1.82±0.01	1.72±0.02	1.72±0.02	0.22±0.02	0.48±0.01	3.73±0.00	6.03±0.03
F3	1.52±0.05	1.81±0.04	1.81±0.04	0.20±0.00	0.58±0.01	4.21±0.04	6.31±0.02
			Lignin-g-PCLs				
KL-PCL	0.33±0.01	UD	0.25±0.01	UD	0.21±0.01	0.25±0.01	0.79±0.00
F_{ins}-PCL	0.18±0.01	UD	0.11±0.00	UD	0.16±0.01	0.12±0.00	0.45±0.01
F1-PCL	0.46±0.01	UD	0.21±0.00	UD	0.33±0.01	0.21±0.00	1.00±0.00
F2-PCL	0.66±0.01	UD	0.33±0.00	UD	0.40±0.01	0.33±0.01	1.39±0.00
F3-PCL	0.77±0.01	UD	0.46±0.01	UD	0.57±0.02	0.45±0.01	1.80±0.00

Note: The data are in a form of mean ± standard deviation. UD: undetected

Figure 2-2 Relation of lignin M_w with OH content (A) and phenolic OH content (B). *r*:



Pearson correlation coefficient; *P*: P value; R^2: coefficient of determination; *: statistical significance

with corresponding lignin fractions, decreased aliphatic OH concentration in lignin-*g*-PCLs (Table 2-2) implies successful ROP occurrence because introducing PCL arms increases the product mass and thus reduces the concentration of aliphatic OH as the absolute total OH quantity is constant. Thirdly, barely diminished carboxylic OH content (Table 2-2) might be attributed to the end carboxylic OH introduced by PCL chains. Lastly, neat PCL possesses one aliphatic OH and one carboxylic OH located at each chain end.[13] If PCL was physically mixed with lignin OH, combined with M_w results that lignin portion is negligible compared with massive PCL portion, the products would still show a nearly equivalent quantity of aliphatic and carboxylic OH. However, the quantity of terminal aliphatic OH is higher than that of end carboxylic OH in lignin-*g*-PCLs (Table 2-2), validating the formation of covalent linkages between lignin and PCL.

The reactivity of OHs with ε-CL varies on the chemistry of OHs, e.g., aliphatic, phenolic, and carboxylic OHs. In this study, OH decreasing percentage is defined as the ratio of declined OH content after copolymerization to the original OH content in lignin, revealing the reaction degree of the OH. From the plots exhibiting the OH decreasing percentage of different types of OHs against the three fractions (Figure 2-3C), the magnitudes of decreasing percentages of all OH types increase as lignin M_w increases (Figure 2-3C), suggesting easier copolymerization between higher-M_w lignin and ε-CL. The aliphatic OH is positively correlated with the copolymer M_w with statistical significance (r = 0.997, R^2 = 0.99, and P= 0.045, Figure 2-3D), implying that aliphatic OH is the most reactive grafting site for PCL segments despite of the introduction of new aliphatic OH end to the copolymers. Our group have previously showed that the copolymerization reaction tends to occur preferentially at the aliphatic OHs rather than the phenolic OHs of lignin.[13] Another study by Najarro et al. showed a similar discovery that the PCL oligomers were mostly introduced to the aliphatic OHs in lignin, leaving the phenolic OH unmodified at a low CL/OH molar ratio (*i.e.*, 5/1) and completely reacted at a high ratio (*i.e.*, 25/1).[111] This was explained by the resistance of phenolic OHs were not activated to form the alkoxide, and in consequence, there was no activation of the OH or acyl C-O bonds with the monomer. We think this phenomenon can be explained by the higher nucleophilicity

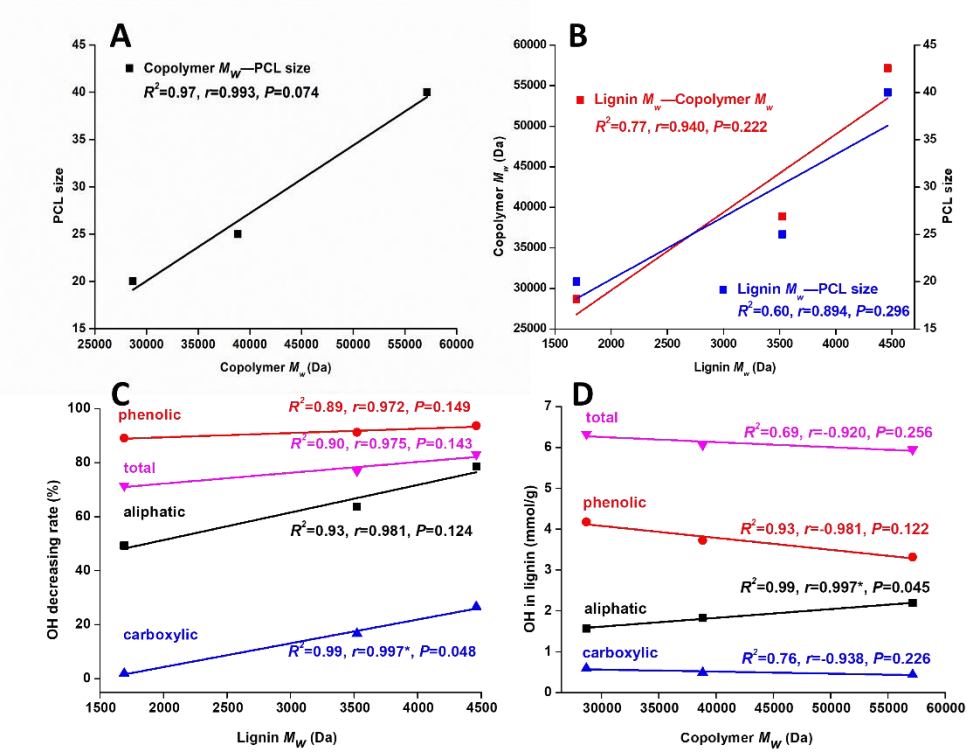


Figure 2-3 Relation of copolymer M_W with PCL size (A), relation of lignin M_W with copolymer M_W and PCL size (B), relation of lignin M_W with OH decreasing percentage (C), and copolymer M_W with OH content in their corresponding lignin fraction (D). r: Pearson correlation coefficient; P: P value; R^2: coefficient of determination; *: statistical significance

(stronger reactivity) and less steric hindrance effect of the aliphatic OHs towards ε-CL than phenolic OHs.[31, 112]

The MW of the synthesized lignin-*g*-PCLs is critical information to indicate (i) the reactivity of lignin fractions and (ii) structure of obtained copolymers. With respect to the M_w of synthetic copolymers, F_{ins}-PCL increases slightly from 11,188 Da to 13,472 Da, and the average length of PCL arms grafted to the copolymers is only 7 (Table 2-1). The limited degree of grafting copolymerization of F_{ins}-PCL is attributed to the limited number of OH grafting sites in F_{ins} (Table 2-2), as well as the poor solubility and dispersity of F_{ins} in ε-CL due to its high M_w, and 'xylan impurities' detected by ^{1}H NMR spectrum of F_{ins}-PCL at 4.32 ppm[113] (Figure 7-2). Besides, the M_w of the other three copolymers is significantly higher than that of their corresponding lignin fractions (Table 2-1), indicating that the M_w of copolymers is predominated by PCL segment instead of lignin core. The conclusion is also revealed by the positive correlation between copolymer M_w and the PCL size (r = 0.993, R^2 = 0.97, Figure 2-3A). In addition, both copolymer M_w and PCL size reveal a positive relationship with lignin M_w (r > 0.85, Figure 2-3B), implying that high-M_w lignin is beneficial to the formation of long-chain PCL arms and high-M_w lignin-*g*-PCLs. The reason might be that high-M_w lignin has more aliphatic OH with stronger reactivity with ε-CL. Overall, copolymer M_w highly depends on the aliphatic OH concentration that is positively related to M_w of lignin fractions.

The FTIR spectra confirmed that lignin-*g*-PCLs are featured with characteristic absorbance of both lignin and PCL, evidencing successful ROP of ε-CL grafted to lignin (Figure 2-4). The peaks at 1,596 cm^{-1} and 1,513 cm^{-1} are attributed to the aromatic skeleton vibration of lignin[114], indicating the presence of lignin constituent in the produced copolymers. The O—H stretching absorption bands located at 3,382 cm^{-1} and 3,432 cm^{-1} are found in the spectra of KL and copolymers respectively, showing a blue-shift in wavenumber after copolymerization which might be attributed to the intermolecular hydrogen bonding.[13, 45] The weaker band intensity of OH in copolymers than in KL spectra endorses the results that OH content reduces after ROP reaction, meaning the lignin is covalently linked with the PCL segment rather than physical blending, which agrees with

our ^{31}P NMR results. Thirdly, the remarkably stronger C—H stretching (2,950-2,830 cm^{-1}) and bending signals (1,460-1,360 cm^{-1} and 731 cm^{-1}) of methyl (CH_3) and methylene (CH_2) groups in copolymer spectra than those in KL spectrum are also detected, implying the presence of PCL constituent in the produced copolymers.[45] Lastly, the weak peak at 1,697 cm^{-1} and intensified peak at 1,721 cm^{-1} correspond to carbonyl groups in KL and copolymers spectra respectively,[13] and the signal strengthening and shift in copolymers could be explained by the formation of strong intermolecular hydrogen bonds with lignin OHs.[45, 96, 115]

2.4.3. Physicochemical properties of lignin-g-PCLs

The crystalline degree and thermal properties of the lignin-*g*-PCLs derived from different lignin fractions were determined and compared using DSC and TGA. Generally, the neat PCL has a X_c of 73.3%, T_m of 56 ℃ and T_c of 26 ℃ (Table 3).[45] In the present study, T_m of all copolymers decreases compared with that of neat PCL because the amorphous lignin backbone inhibits the crystallization and regular alignment of PCL polymer.[94] All copolymers except for F_{ins}-PCL present semi-crystalline structure with X_c between 30-45% and similar T_m at around 50 ℃ (Table 2-3). Thereinto, X_c of KL-PCL is obviously smaller than those of F1-PCL, F2-PCL, and F3-PCL, but larger than that of F_{ins}-PCL (Table 2-3), suggesting that fractionating KL to narrower-$Đ_M$ fractions is beneficial to the formation of crystallinity. Combined with the results from Figures 3B and 3C, as we hypothesized, the lignin MW heterogeneity appears to influence the copolymer structures. However, X_c of lignin-*g*-PCLs from the three representative lignin fractions, F1, F2, and F3, are similar, implying that lignin M_w causes insignificant effect on copolymer X_c. With respect to lignin-*g*-PCL synthesized from the non-representative lignin fraction, *i.e.*, F_{ins}-PCL, the lowest T_m of 44 ℃ and extremely low X_c of only 2.9% (inserted image in Figure 2-5A and Table 2-3) result from its existence of amorphous hemicellulose, low M_w, and short PCL size. In conclusion, we can assume F_{ins}-PCL is a three-dimensional amorphous network basically formed by hydrogen bonds between lignin and PCL, while F1-PCL, F2-PCL and F3-PCL are semi-crystalline copolymers composed of both crystalline and

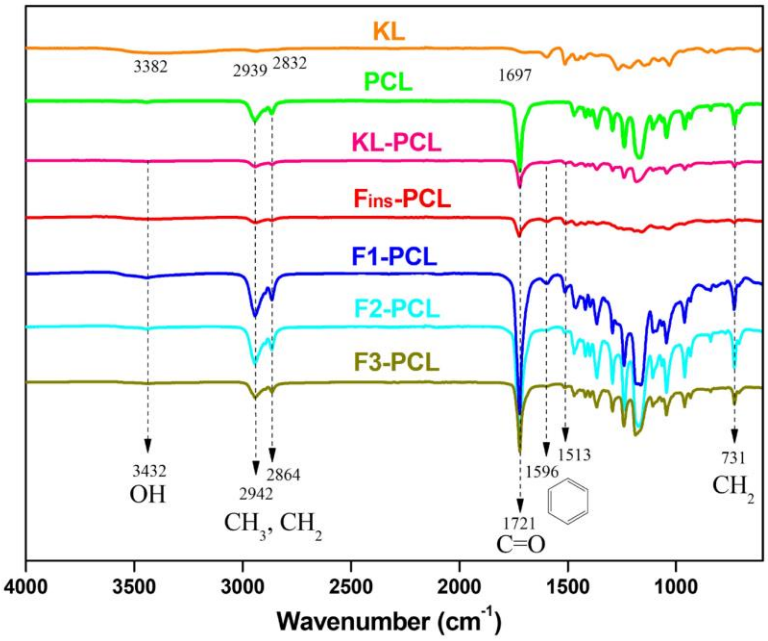


Figure 2-4 FTIR-ATR spectra of KL, PCL, and lignin-*g*-PCLs

amorphous structures.[95]

Lignin has been frequently used to improve the thermal stability of polymers through copolymerization, such as polyurethanes, poly(arylene ether sulfone), and poly(n-butyl acrylate-co-methyl methacrylate), via multiple mechanisms including introducing aromatic structures, increasing the copolymer M_w, and the formation of chain extended polymers at elevated temperatures.[26, 116-118] In this study, the thermal stability of lignin-*g*-PCLs also improved compared with neat PCL (T_{max}: ~400 °C *vs.* 373 °C, Figure 2-5D and Table 2-3), which is accordant with the result from a previous report.[91] This improved stability is likely attributed to that i) the integration of lignin moiety enhances the thermal stability of lignin-*g*-PCLs through introducing thermally stable aromatic rings and C-C bonds between lignin subunits that decompose at ~400 °C.[119] It can also be supported by the result that the T_{max} of KL (482 °C) is much higher than that of both copolymers (~ 400 °C) and neat PCL (373 °C) (Table 2-3). ii) The conversion of lignin OH groups to ester groups by grafting PCL arms on the lignin backbone has an additional stabilizing effect on the thermal stability of copolymers.[94, 115] Additionally, lignin-*g*-PCLs synthesized by the three representative lignin fractions displaying similar weight loss behaviors with T_{max} at around 400 °C (Figure 2-5D and Table 2-3) indicates that lignin M_w has a negligible influence on the thermal stability of copolymers.

The surface properties of lignin copolymers, such as surface energy (wettability), surface charge, stability, are critical factors determining the applications of the developed materials. We have evaluated the surface energy and heterogeneity distributions of lignin-g-PCLs using iGC. Both the dispersive energy (γ_d) and specific (acid-base) energy (γ_{sp}) of the original KL and the copolymers are exponentially decreased under lower surface coverage and then tend to be constant under higher surface coverage (broad range of γ_d and γ_{sp}) in KL and copolymers (Figures 2-6A and 2-6B), indicating highly energetical heterogeneity on their surface.[120] Meanwhile, the median values of γ_d are apparently higher than those of γ_{sp} in all samples (Table 2-4), implying that PCL, KL and copolymers are dominated by London van der waals' force than dipole-dipole polar force.[121] Comparing

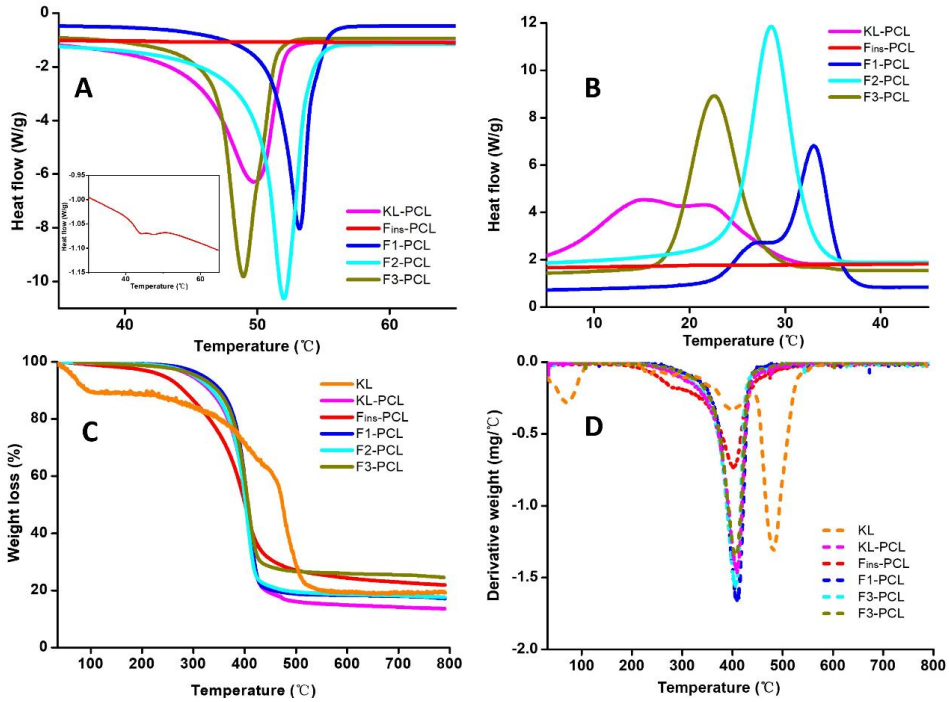


Figure 2 5 DSC heating (A), DSC cooling (B), TGA (C), and DTG (D) curves of KL and lignin-*g*-PCLs. The inserted figure is the heating curve of F_{ins}-PCL tested by DSC.

Table 2-3 Crystallization (T_c) and melting (T_m) temperatures, crystallinity degree (X_c), temperature at the onset of thermal degradation (T_{onset}) and temperature at maximum mass loss (T_{max}) of KL, PCL and lignin-*g*-PCLs

	T_c (℃)	T_m (℃)	X_c (%)	T_{onset} (℃)	T_{max} (℃)
PCL[45, 94]	26	56	73.3	--	373
KL	--	--	--	232	482
KL-PCL	15	50	34.5	232	409
F_{ins}-PCL	--	44	2.9	204	403
F1-PCL	33	53	45.9	244	409
F2-PCL	29	52	42.7	249	405
F3-PCL	23	49	45.8	258	408

with PCL and KL, KL-PCL exhibits broader γ_d distributions (Table 2-4), suggesting that after copolymerization the surface energetical heterogeneity of lignin-*g*-PCL is intensified. KL-PCL has a greater median value of γ_d than KL, but smaller than PCL (Table 2-4), illustrating that PCL segment may be the reason for its intensified dispersive interactions with alkane probes. Among lignin-*g*-PCLs, both F1-PCL and F2-PCL have relatively higher γ_d (median value: 66.28 and 66.54 mJ/m^2) and larger specific surface area (3.42 and 4.77 m^2/g) than F3-PCL (median value: 51.96 mJ/m^2 and 2.85 m^2/g, Table 2-4), suggesting that F1-PCL and F2-PCL presumably possess better dispersibility if blended with other non-polar polymers. The higher median values of γ_d of F1-PCL and F2-PCL than F3-PCL could be explained by their larger M_w or lower X_c with more amorphous regions that expose more active groups and intermolecular spaces on surface. Furthermore, the lowest median value of γ_{sp} of F1-PCL among all lignin-*g*-PCLs (Table 2-4) means the strongest polar-polar affinity with probes.[122] Additionally, higher hydrophilicity index, defined as the ratio of $\gamma_{sp}/(\gamma_{sp}+\gamma_d)$, of KL-PCL than that of KL, but lower than that of PCL (Table 2-4) indicates that lignin incorporation can intensify the hydrophobicity of PCL, which might be because lignin introduced aromatic groups to long-chain PCL esters.[122, 123] The lowest hydrophilicity index of F1-PCL (Table 2-4) may be ascribed to the highest content of hydrophobic group like ester and alkyl groups due to the longest PCL chains. However, although F2-PCL has a longer PCL chain length (more ester and alkyl groups) than F3-PCL, it still exhibits higher hydrophilicity index (0.24 *vs.* 0.19). The reason might be that F3-PCL with higher X_c is more difficult to be accessed by water molecules.[124] In general, the surface energy of copolymers is affected not only by their M_w, but also by the X_c.

The maximum mechanical properties of lignin-*g*-PCL films are 0.34 MPa for tensile strength and 40.92 MPa for impact strength (Table S1), which are lower than those reported in previous works where the maximum tensile strengths of 1.22 MPa[91] and 2.03 MPa[95]. This is likely due to the discrepancies in synthetic conditions, as well as structure features of synthesized copolymers. Compared with the neat PCL films, F1-PCL film exclusively exhibits higher tensile strength and impact strength (Figures 2-7A and 2-7B). It is primarily attributed to the high M_w where greater number of stable covalent bonds formed and high

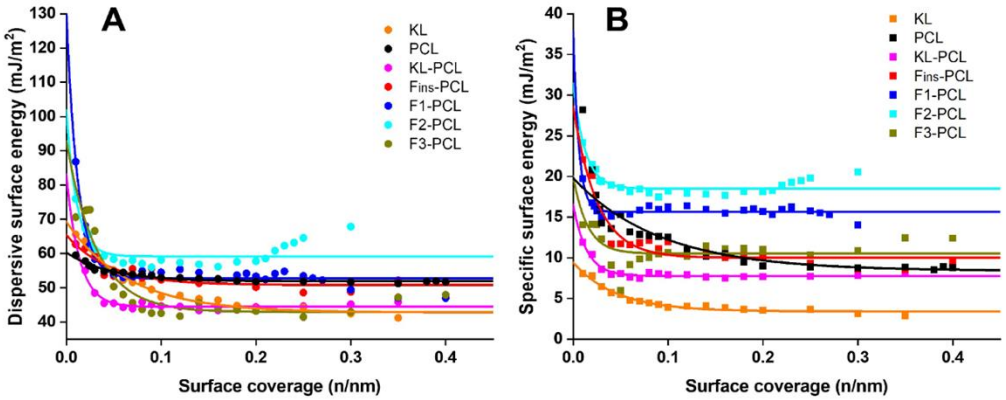


Figure 2-6 Dispersive (A) and specific (B) surface energy of KL, PCL, and lignin-*g*-PCLs

Table 2-4 The minimum, median and maximum values of g_d and g_{sp} as well as hydrophilicity index ($\gamma_{sp}/(\gamma_{sp}+\gamma_d)$) and specific surface area of KL and lignin-*g*-PCLs

Samples	γ_d (mJ/m^2)			γ_{sp} (mJ/m^2)			$\gamma_{sp}/(\gamma_{sp}+\gamma_d)$	Specific surface area (m^2/g)
	minimum	median	maximum	minimum	median	maximum		
PCL	53.65	57.64	59.28	8.38	18.31	22.39	0.27	1.10
KL	42.80	47.68	68.91	3.41	4.51	9.29	0.09	6.07
KL-PCL	44.56	51.36	80.85	7.78	9.32	16.00	0.16	1.15
F_{ins}-PCL	50.63	53.24	64.61	10.00	13.34	27.85	0.22	0.85
F1-PCL	52.75	66.28	125.02	2.69	7.01	17.51	0.08	3.42
F2-PCL	59.20	66.54	98.32	18.50	20.74	30.48	0.24	4.77
F3-PCL	42.93	51.96	91.26	10.52	12.18	19.40	0.19	2.85

X_c that exhibits mechanically tougher crystallinity.[125] But overall, the result of mechanical properties reveals that incorporation of lignin usually compromise the mechanical properties of lignin-based bio-composites, which is accordant with previous reports.[90, 95] KL is an excellent UV barrier due to the formation of unsaturated ethylene groups and condensed structures while the intermolecular β–O–4 linkages were cleaved during the pulping process.[126] This UV-blocking function can be imparted to KL-based composites.[127, 128] . In the current study, all the prepared lignin-*g*-PCL films, including both the non-fractionated and fractionated lignin precursors used, can effectively shield broad-spectrum UV radiation including UV-A (wavelength at 400-320 nm), UV-B (wavelength at 320-280 nm) and UV-C (wavelength at 280-200 nm) regions; on contrary, half-transparent neat PCL film shows inferior UV-shielding performance (Figure 2-7C). Hence, lignin incorporation plays an important role to enhance the UV-blocking effect of fabricated lignin-*g*-PCL films.

2.4.4. Biodegradability of lignin-g-PCLs

PCL is usually documented as a biodegradable polyester, but the full degradation could take over 200 days in landfill, and over 120 days in digester sludge.[129] We therefore, have evaluated the degradability of lignin-*g*-PCL using enzymatic hydrolysis approach that is widely employed for PCL and PCL-based polymers.[105, 130, 131]. In the present study, we have found that lipase can completely hydrolyze the neat PCL within 12 days, which is similar to a previous report of 15 days.[105] However, the degradation of lignin-*g*-PCLs using lipase exhibits much slower degradation rates (Figure 2-8). The reason might be that the presence of lignin caused a negative influence on the accessibility of lipase to copolymers,[132, 133] resulting in a reduced enzyme hydrolysis efficiency. In addition, lipase hydrolysis is affected by polymer structures e.g., M_w, X_c and chemical composition[105, 134].

This has been revealed by the different hydrolysis rates of the copolymers derived from the three representative F1, F2, and F3 fractions, showing that F3-PCL, F2-PCL, and F1-PCL are in the degradation order from high to low. It is likely associated with the differing X_c of PCL segments and M_w of the copolymer. As displayed, the degradation rate

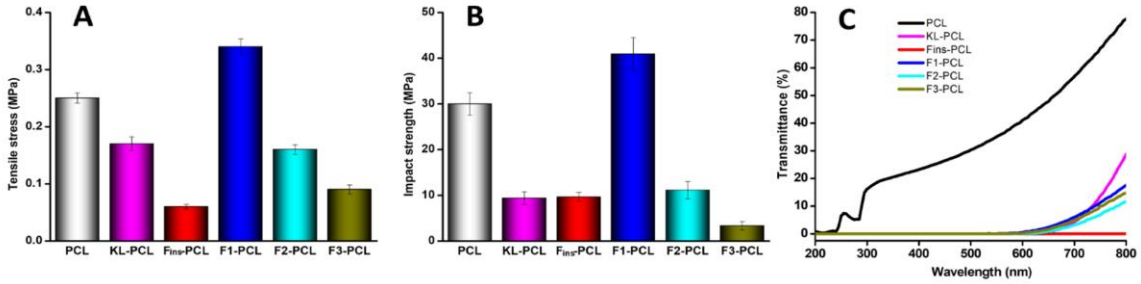


Figure 2-7 Tensile strength (A), impact strength (B), and UV-vis spectra (C) of PCL and lignin-*g*-PCL films

of all copolymers is fast in the early stage but slows down in the late stage. This means amorphous regions of copolymers are degraded firstly because of loose structures, while crystalline regions are degraded later because of compact alignment and difficult enzymatic accessibility.[134] Furthermore, F_{ins}-PCL presents the lowest degradation rate, which may be attributed to its relatively higher lignin content that is ineffective by lipase hydrolysis and restricts lipase accessibility.

2.4.5. Application of CFP with lignin-g-PCL for oil/water separation

With the rich hydroxyl groups serving as grafting sites, lignin can be chemically modified to substantially reduce hydrophilic groups, making it a good candidate to construct bio-based hydrophobic materials.[135] Lignin has been widely investigated to prepare filtration and adsorption materials for water/oil separation, such as lignin contained wood aerogel/polydimethylsiloxane membrane for chloroform separation from water[136] and silicane modified lignin particles used as a filler in filtration apparatus.[137] Lignin-*g*-PCL, as an environmentally friendly biomaterial, has shown potentials as surface coatings because of excellent UV-barrier capacity, good dispersibility, favorable film-forming ability, and stable surface characteristics including adhesion strength, abrasion, and gloss.[90, 94, 111] However, new applications of lignin-*g*-PCL as surface coatings remains to be explored. Combined with the excellent hydrophobicity obtained from iGC, lignin-*g*-PCL was coated on FP to evaluate the ability to purify oil-polluted water in the current work.

We have found that the WCA of neat PCL film is lower than that of lignin-*g*-PCL films (Figure 7-5A), confirming that lignin integration can enhance the hydrophobicity of PCL. This result agrees with the increased dispersive energy of copolymer measured using iGC previously. We also added SiO_2 and silicone oil to the FP coating process to further increase the hydrophobicity of CFP. FTIR spectra of the CFP verifies the presence of lignin-*g*-PCLs, SiO_2 and silicone oil on CFP-C surface (Figure 7-3). The coated filter paper (CFP) by copolymer, CFP-C, has shown apparently different surface morphology in comparison to the uncoated FP (Figures 2-9A and 2-9B) in that: on FP surface, cellulose fibers are entangled with each other to form a porous matrix (Figures 2-9A and 7-4), while CFP-C surface is much more compact and smoother due to the filled coating contents such as

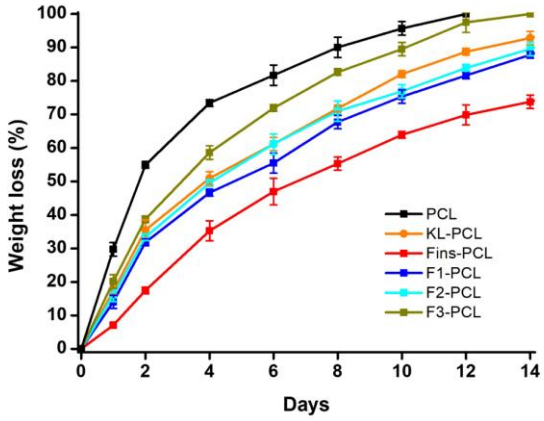


Figure 2-8 Lipase hydrolysis of neat PCL and lignin-*g*-PCL films

copolymers, SiO_2, and silicone oil in this case (Figures 2-9B and 7-4). The spherical particles on the CFP-C surface might be the SiO_2 particles (Figure 2-9B). CFP-C becomes more hydrophobic as revealed by the increased WCA with the increase of concentrations of lignin-*g*-PCL/acetone solutions, for example the WCA reaches up to 120° at a concentration of 1 mg/mL (Figure 7-5B). Moreover, water is adsorbed immediately once contacted with the hydrophilic FP substrate without forming a water drop; similar phenomenon is observed in CFP-B (Video S1). After FP being coated by PCL and F1-PCL, the surface becomes hydrophobic since the water drop with WCA over 90° is formed when the water drop contact with substrate at the very beginning. However, CFP-P displays much worse water-resistance ability than CFP-C owing to the fact that the water droplet gradually permeates the CFP-P substrate within 1 min, while holds still on the CFP-C substrate for more than 20 min (Video S1). Hence, we speculate that the lignin portion endows CFP-C a water barrier, and the hydrophobicity synergistically derives from multiple substances on the surface including lignin-*g*-PCL, SiO_2 and silicone oil.

For water-oil separation application, CFP with F1-PCL exhibits the highest separation efficiencies even though the superior performance to other copolymer CFPs is not substantial; besides, only CFP with F1-PCL exhibited relatively higher separation efficiencies than CFP with KL-PCL (Figure 7-6). The results suggest that F1-PCL featuring a higher M_w of lignin (*i.e.*, 4,461 Da), and longer grafted PCL length (*i.e.*, 40) shows better water-oil separation ability. However, the relationship observed is not applicable to CFPs with F2-PCL (lignin M_w of 3,086 Da and PCL size of 25) and F3-PCL (lignin M_w of 1,691 Da and PCL size of 20) because the structure differences of copolymers and lignin only caused slight influence on the separate efficiency. As a result, taking advantages of the best hydrophobicity (Figure 7-5) and oil-water separation efficiency (Figure 7-6) among all copolymers, CFP-C coated by F1-PCL/acetone solution with a concentration of 1.0 mg/mL was chosen to conduct the further water/oil separation experiment. FP (non-coated filter paper) and CFP-P (coated by 1.0 mg/mL PCL/acetone solution) were used as referral comparisons. In the first cycle, CFP-C is able to filter low-surface energy chloroform down to the vial and retain high-surface energy water in the conical funnel, displaying

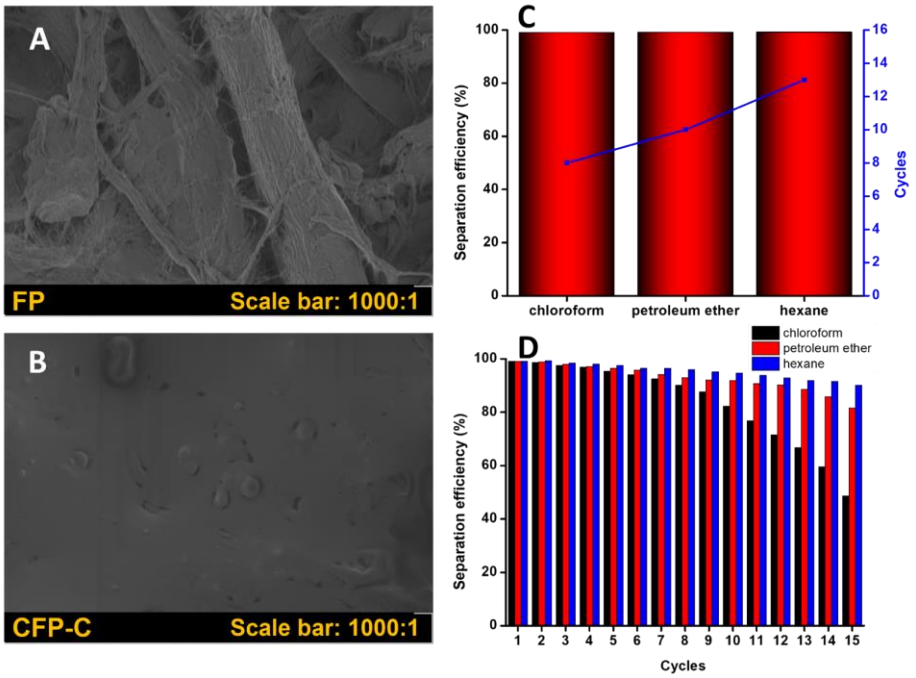


Figure 2-9 SEM images of FP (A) and CFP-C (B) under a scale bar of 1,000; Separation efficiencies at the first cycle, cycles with separation efficiencies over 92% (C) and separation efficiencies of CFP-C under 15 cycles (D) for separating chloroform-, petroleum ether- and hexane-water mixtures

outstanding separation efficiency of 99.0%; CFP-P otherwise displays poor separation efficiency of 12.8%; FP filtered the most of water because of its hydrophilicity (Figure 2-9C and Video S2). Thus, CFP-C in this work realized successful separation of water/oil mixture via a simple and fast conical-funnel filtration method. Apart from chloroform, CFP-C also exhibits maximum separation efficiencies of 99.1% and 99.2% for petroleum ether and hexane, respectively, in the first cycle (Figure 2-9C), showing a universality of CFP-C in oil/water separation. The separation efficiencies are outstanding and comparable with some reported lignin-based 2-demensional filtration biomaterials, such as CFP and membrane.[86, 100] For instance, an aerogel membrane fabricated by lignin, trimethoxymethylsilane, graphene oxide and sodium alginate displayed a maximum separating efficiency above 95% for chloroform and the separating efficiency was still above 90% after 10 reuses.[100] Moreover, the CFP constructed with acetonitrile extracted lignin and silica particles exhibited a maximum separating efficiency of 98.6% for chloroform (remained 96.6% at the fifth cycle), and above 95% for petroleum ether and hexane.[86] During separation, lignin component plays a role as a water-blocking barrier that stops water on the top, and the modified hydrophobic surface enables the infiltration of organic solvent through CFP-C. Reusability is a significant parameter for filtration materials applied for wastewater processing. Herein, CFP-C maintains separation efficiencies of above 90% for 8 cycles to chloroform, 12 times to petroleum ether, and 15 times to hexane (Figure 2-9C). The separation efficiency decreases as cycles progress because coated copolymers as well as silicon compounds are gradually leached by the organic solvents during each separation process. For petroleum ether- and hexane-water mixtures, the separation efficiency declines less conspicuously than chloroform, still reaching 90.1% at the fifteenth cycle when separating hexane (Figure 2-9D). The poorest reusability of CFP-C for chloroform/water separation is attributed by the dissolution of copolymers in chloroform that carries off chemicals from FP substrate little by little, leading to a reduction of water-resistance and hydrophobicity of CFP-C as cycles increased. Nevertheless, lignin-*g*-PCL is insoluble in petroleum ether and hexane, so the reusability

of CFP-C is superior. Overall, CFP-C exhibits excellent feasibility and reusability for oil/water separation.

In this study, the performance of applying CFP with lignin-*g*-PCL for oil/water separation are outstanding and comparable with most reported lignin-based filtration systems. We believe that the lignin-*g*-PCL is more attractive due to its biodegradability for both lignin and PCL components, low-cost, and sustainability. However, the reusability of the CFP with lignin-*g*-PCL for oil/water separation seems variable depending on the solvent used. For example, separation of chloroform from water is restricted due to the solubility of copolymers in chloroform. The results implies that oil/water separation coating with covalently modified, and highly biodegradable copolymers can be achieved with judicious design of the molecular structures. Future study on lignin-based hydrophobic or superhydrophobic materials are ongoing in our group.

2.5. Conclusions

KL was fractionated into four lignin fractions with decreasing M_w by acetone-methanol cosolvent (7:3, v/v) and hexane, which are F_{ins} (11,188 Da), F1 (4,461 Da), F2 (3,086 Da), and F3 (1,691 Da). Thereof, F_{ins} is a non-representative fraction that contains carbohydrate impurities, while F1, F2, and F3 are representative fractions whose M_w positively correlates with aliphatic OH content but negatively correlates with phenolic OH content. Lignin-*g*-PCL copolymers are successfully synthesized with lignin fractions and ε-CL monomers, during which ε-CL is inclined to interact with aliphatic OH in lignin. Higher M_w and richer aliphatic OH content of lignin is beneficial to the extension of PCL arms and M_w of lignin-*g*-PCLs. Fractionating KL into more homogeneous fractions is conductive to the crystallization of PCL segment. Generally, M_w and X_c play synergetic roles in thermal, surface, and mechanical properties of lignin-*g*-PCLs, where lignin incorporation improves the thermal stability, hydrophobicity, and UV-blocking ability, but slows down the lipase hydrolysis of PCL by reducing the enzymatic accessibility. Lignin-*g*-PCL, for the first time, successfully separate chloroform-, petroleum ether-, and hexane-

water mixtures by coated on filter paper with separation efficiency up to 99.2%. Cycles maintaining separation efficiencies above 90% reach up to 15. The structure differences of copolymers and lignin causes inconspicuous influence on the separate efficiency. This study shed light on the structural influence of lignin on the copolymerization and properties of lignin-*g*-PCL. It also provides important information for the development of lignin-derived composites and lignin valorization.

CHAPTER III

SYNTHESIS OF BIO-BASED REPAIRABLE POLYIMINES 1 WITH TAILORED PROPERTIES BY LIGNIN FRACTIONATION

A version of this chapter is originally written and published as:

Xie D., Pu Y., Bryant N. D., Harper D. P., Wang W., Ragauskas A. J., Li M. (2024). Synthesis of Bio-based Repairable Polyimines with Tailed Properties by Lignin Fractionation. *ACS Sustainable Chemistry and Engineering*.

Author contributions are listed as follows. D.X.: conceptualization, methodology, investigation, formal analysis, data curation, writing-original draft. Y.P.: resources, data curation, writing-review and editing. N.B.: investigation, writing-review and editing. D.H.: resources, writing-review and editing. W.W.: resources, writing-review and editing. A.R.: resources, writing-review and editing. M.L.: conceptualization, methodology, supervision, validation, writing-review and editing, project administration, and funding acquisition.

3.1. Abstract

Developing sustainable polymers with low-value lignin remains a challenge. Herein, lignin-containing repairable polyimines were synthesized with tailored properties using lignin fractionation. Firstly, softwood Kraft lignin is fractionated into a more homogeneous fraction with a lower molecular weight and a higher OH content. Next, Kraft lignin and its fraction are esterified by levulinic acid to introduce active ketone groups, and subsequently condensed with oleylamine (OAm) and bis(3-aminopropyl)-terminated-polydimethylsiloxane (PDMS) *via* catalyst-free Schiff-base reaction to form grafted lignin-OAm copolymers and crosslinked lignin-PDMS polymer networks (MKL-P & MFL-P), respectively. Results show that lignin-OAm polyimines can be self-repaired and hot reprocessed under pressure, while lignin-PDMS polyimines can be repaired with the assistance of a healing agent, heat, and pressure. Dynamic mechanical analyses demonstrate that the stress-relaxation behaviors of polyimines follow Arrhenius law under thermal-stress activation, indicating the occurrence of transimination. Moreover, compared with Kraft lignin, the lignin fraction ameliorates the grafting density of ketones, and enhances the crosslinking density of lignin-PDMS polyimine networks. The higher crosslinking density of MFL-P leads to superior stress-relaxation activation energy, thermal stability, hydrophobicity, and light-shielding ability, but inferior repairability and translucency. This work provides insights into the polymerization of lignin-based polymer networks and the potential application of lignin-PDMS polyimines for repairable, translucent, anti-UV, and hydrophobic coatings.

3.2. Introduction

To promote a green, sustainable, and circular economy, researchers are dedicated to developing chemically recyclable polymers using bio-derived polymers as a partial replacement to be applied in manufacturing industries.[19, 138, 139] One promising avenue is to prepare novel dynamic covalent polymer networks (DCPN), which typically can be chemically recycled (repaired, reshaped, reprocessed) *via* dynamic chemistries such as transimination, transesterification, transcarbamoylation, etc.[47] The reversible interaction between amines and ketone/aldehydes is one of the most common reactions to construct robust molecules by the formation of covalent imine bonds in organic chemistry.[53] The imine bonds can break and reform simultaneously under triggers like heat, pressure, excessive free amines, catalysts, or solvent *via* imine metathesis and exchange reactions.[16, 47, 53]

In terms of the DCPN developed by dynamic imine bonds, vanillin is a widely investigated bio-derived feedstock[54, 55] due to the aldehyde group that allows for the imine condensation, the capability of monomer recovery, and the retaining high-performance properties.[140] However, one vanillin molecule could only participate in one imine condensation due to the singular aldehyde group per molecule. Therefore, to obtain vanillin-based polyimines with highly crosslinked networks with favorable thermomechanical properties, vanillin is required to be modified to enrich the aldehydes and afterward crosslinked with multiamines.[54-56]

Apart from vanillin, bio-derived polymers such as lignin, cellulose, and vegetable oil also offer renewable alternatives to petroleum-based precursors commonly used in DCPN synthesis.[16, 141, 142] Lignin is one of the most challenging biomass feedstocks to be utilized because of its poor compatibility, dispersity, structural heterogeneity, and molecular rigidity.[13, 143] Nevertheless, lignin still attracts great attention due to its high abundance, low cost, rich reactive sites, good thermal stability, ultraviolet (UV)-shielding ability, and biodegradability.[57] Kraft lignin (KL), a byproduct of the pulp and paper industry, represents a readily available and inexpensive source of lignin.[32] The unique chemical structures of

KL comprise a variety of functional groups, including (phenolic, aliphatic, and carboxylic) hydroxyl (OH), methoxy, and carbonyl, etc., providing abundant reactive sites for polymerization reactions.[144] In addition, the structural heterogeneity of KL, resulting from its complex chemical structures, cooking processes, and plant sources, provides opportunities for tailoring the structures and properties of the synthesized polymers.[143, 145] More importantly, lignin features a natural three-dimensional polymer network with rich reactive sites ready for modification, endowing lignin a great candidate to act as a natural crosslinker for developing the DCPN.

Lignin, as a bio-derived component, has been widely investigated to develop novel DCPN (defined as bio-based DCPN) by integrating with multiple polymers such as polyurethane[46], poly(ethylene glycol)-epoxy (PEG-epoxy)[49], polyolefin[146], etc. For example, a mechanically strong polyurethane was catalytically synthesized with lignin and petroleum-derived polyols *via* dynamic (covalent) cross-linking networks and (non-covalent) interfacial hydrogen bonds, which could maintain the excellent mechanical strength after being hot reprocessed.[51] Besides, a thermoset was catalytically synthesized with lignin and PEG-epoxy *via* dynamic transesterification with adequate coating hardness and adhesion performances, which could be removed by mild alkaline and repaired with the assistance of glycol.[49] In addition, a new class of strong, tough, and ductile thermoplastic elastomers were constructed using lignin and modified polyolefin elastomer with the help of zinc chloride by dynamic coordination and interfacial bonds, which could remember shape with fixing and recovery ratios up to 94% and 82%, respectively.[146] The studies give us insight that lignin is feasible and promising for constructing high-performance chemically recyclable DCPN with minimal performance sacrifice. However, those DCNPs demand external stimuli of non-degradable metallic catalysts to activate the dynamic reactions. Therefore, catalyst-free activation of lignin-based DCNP is highly attractive because the absence of a catalyst eliminates the need for hazardous and refractory materials, simplifying the synthesis procedure, and reducing environmental impact.

Based on the prior study in Chapter II, lignin structures affect the copolymerization with poly(ε-caprolactone) due to the heterogeneous molecular weight and OH

concentrations. In the current study, a long-chain primary alkylamine (oleylamine, OAm) and a bis(3-aminopropyl) terminated poly(dimethyl siloxane) (PDMS) were selected to condense with lignin because of their versatility, flexible chains, low-surface energy, and other advantageous features for the consideration of further applications for hydrophobic coatings,[147, 148] which is expected to improve the film-forming ability, hydrophobicity, and other coating performances of lignin.[149] To enable the polymerization between lignin and amines, lignin is modified with sustainable levulinic acid (LA) to introduce active ketone groups.[15] OAm and PDMS, terminated with respective mono- and bi-primary amines, are expected to react with ketones in modified lignin *via* Schiff-base reactions. However, the type and complexity of the polymerizations with lignin are hypothesized to be different between OAm and PDMS: 1) The reaction with OAm is supposed to be more feasible than that with PDMS due to the smaller steric hindrance, and 2) the polymerization types are supposed to vary due to the different amounts of terminated amines/molecule. We hypothesize that lignin-OAm polyimines will afford grafting-polymerized thermoplastic-like properties, while lignin-PDMS polyimines are prone to be crosslinking-polymerized thermosets. Branched polyimines and crosslinked polyimine networks are therefore formed *via* Schiff-base reactions between modified lignin and OAm and PDMS, respectively.

3.3. Materials and Methods

3.3.1. Materials

Indulin AT softwood KL was provided by MeadWestvaco (Richmond, VA, USA). LA, DMSO, 4-dimethylaminopyridine (DAP), N, N'-dicyclohexylcarbodiimide (DCC), OAm, PDMS (number-average molecular weight (M_n): ~ 2500 Da), deuterated DMSO (DMSO-d_6), toluene, methanol, acetone, hexane, acetic anhydride, THF, TMDP (95%), N-hydroxy-5-norbene-2,3-dicarboxylic acid imide (NHND), nonane, octane, heptane, acetonitrile, ethyl acetate, dichloromethane were purchased from Sigma Aldrich (St. Louis, MO, USA). Anhydrous pyridine was purchased from Spectrum Chemical (New Brunswick,

NJ, USA). The filter paper (Porosity Coarse, Qualitative: P8) was purchased from Fisher Scientific (Pittsburgh, PA, USA). All chemicals and materials were used as received.

3.3.2. Lignin fractionation and modification

Fractionated lignin (FL, yield: 75.8%) was obtained by solvent fractionation of KL using acetone/methanol/ (7:3, v/v) as cosolvent and hexane as antisolvent (Figure S1).[150] KL and FL were modified by LA to graft ketone groups using a reported method.[15] Briefly, KL (20 g, 111.2 mmol OH) and LA (19.34 g, 166.8 mmol COOH), and DAP (1.36 g, 11.12 mmol) were dissolved in 500 mL DMSO solvent. The DCC (25.24 g, 122.32 mmol)/DMSO solution (30 mL) was then added dropwise and reacted at room temperature (RT) for 48 h. Next, the condensed liquid phase of the reaction product was obtained by successive filtration and rotary evaporation, and then precipitated in 50% methanol aqueous solution, followed by filtration, to obtain modified KL (MKL). Modified FL (MFL) was prepared with the same procedure with MKL, during which 20 g FL (123.4 mmol OH), 21.46 g LA (185.1 mmol COOH), 1.51 g DAP (12.34 mmol), 28.01 g DCC (135.74 mmol), and 30 mL DMSO were used as a batch. MKL and MFL were successively washed with deionized water three times to remove solvents and vacuum dried for later use. The yields of MKL and MFL were 66.8% and 68.7%, respectively, which are comparable with the yield (64.3%) in the previous report.[15] The OH decreasing percentage was calculated as the molar ratio of consumed phenolic and aliphatic OH in modified lignin (MKL and MFL) to the total available phenolic and aliphatic OH in lignin (KL and FL) in equation (1) based on the 31P NMR quantification results (Table S1) under an assumption that only aliphatic and phenolic OHs in KL and FL participated in the esterification with the COOH in LA. The content of ketones in modified lignin is calculated as the reduced aliphatic and phenolic OH after LA modification.

$$\text{OH decreasing percentage (\%)} = \left(1 - \frac{C_{OH,ML}}{C_{OH,L}}\right) \quad (1)$$

where $C_{OH,\,ML}$ is the sum of contents of aliphatic and phenolic OH in modified lignins, and $C_{OH,L}$ is the sum content of aliphatic and phenolic OH in lignins.

The ketone grafting density is calculated by the equation (2).

$$\text{Ketone grafting density} = (M_{ML}\text{-}M_L) / 98 \text{ g/mol} \quad (2)$$

where M_{ML} and M_L is the M_w of modified lignin and unmodified lignin, 98 g/mol is the increment molecular weight of a single grafted LA chain.

3.3.3. Synthesis of lignin-based polyimines

The preparation of lignin-based polyimines was conducted as follows. Firstly, MKL (1 g, ~ 3.99 mmol ketone groups) and MFL (1 g, ~ 4.77 mmol ketone groups) were fully dissolved in 50 mL THF, respectively. Then, OAm or PDMS with a ketone/amine groups molar ratio of 1:1 was added dropwise to the lignin/THF solutions, respectively. The mixture was pre-reacted at 80 ℃ for 24 h *via* Schiff base reaction. Subsequently, the products were poured into an aluminum dish (inner diameter: 114 mm) for solvent evaporation at RT overnight in a fume hood to yield gel-like films. The films were cured and post-cured under 130 ℃ and 150 ℃ in a vacuum oven for 12 h, respectively, to obtain film-shape polyimines. The lignin-OAm and lignin-PDMS polyimine films were named as MKL-O, MFL-O, MKL-P, and MFL-P respectively. The thickness of the lignin-OAm (MKL-O & MFL-O) and lignin-PDMS (MKL-P & MFL-P) polyimine films is ~ 1 mm and ~ 0.3 mm, respectively.

3.3.4. Characterization of lignin, modified lignin, and lignin-based polyimines

The weight-average molecular weight (M_w), M_n, and molar-mass dispersity ($Đ_M$) of lignin, modified lignin, and polyimines were measured by gel permeation chromatography (GPC) using an Agilent 1200 HPLC system (Agilent Technologies, Inc., Santa Clara, CA, USA) equipped with waters Styragel columns (HR1, HR2, and HR6; Waters Corporation, Milford, MA, USA) and an ultraviolet detector (wavelength: 270 nm). The mobile phase was THF that flowed at a rate of 0.5 mL/min. Polystyrene was used as the calibration standard. KL and FL samples were acetylated to be fully dissolved in THF for the GPC measurements referring to our previous study[143], while modified lignin and synthesized polyimines were dissolved in THF under shaking at 60 ℃ for 72 h. Lignin-PDMS

polyimines were partially dissolved in THF (gel fraction: MKL-P = 48.9% and MFL-P = 67.6%) with soluble portions used for GPC measurements.

The structural features of lignin, modified lignin, and polyimines were characterized by Fourier Transform Infrared Spectroscopy (FTIR), ^{1}H nuclear magnetic resonance (NMR), ^{31}P NMR, and ^{13}C NMR. FTIR spectra of samples were recorded by an FTIR spectrometer (Spectrum One FTIR system, PerkinElmer, Wellesley, USA) with a universal attenuated total reflection (ATR) accessory under wavenumbers using 4,000 cm^{-1} to 600 cm^{-1} with a resolution of 4 cm^{-1} for 32 scans. Samples were dissolved in DMSO-d_6 at a concentration of 100 mg/mL for the acquisition of NMR spectral data using a Bruker Avance III HD 500 MHz spectrometer (Bruker, Switzerland) equipped with a 5 mm N_2 cryogenically cooled BBO H&F probe. One-dimensional "zg30" and "zgpg" pulse sequences were employed for ^{1}H NMR and ^{13}C NMR spectra, respectively. The lignin-OAm and lignin-PDMS polyimines were dissolved in DMSO-d_6 under shaking at 60 ℃ for 24 h and 72 h, respectively. Lignin-OAm polyimines were fully dissolved, while lignin-PDMS polyimines were partially dissolved in DMSO-d_6 (gel fraction: MKL-P = 65.4% and MFL-P = 82.5%) with soluble portions used for NMR measurements. The number of scanning is 16 for the acquisition of ^{1}H NMR spectra, 1,024 * 2 for ^{13}C NMR spectra of lignin, modified lignin, and lignin-OAm polyimines, and 1,024 * 16 for ^{13}C NMR spectra of lignin-PDMS polyimines. An inverse-gated decoupling pulse sequence "Waltz-16" was used for ^{31}P NMR experiments to quantify the OH contents of samples using NHND as an internal standard and TMDP as a phosphitylation agent.[101] The acquired spectra were processed using Bruker Topspin 3.5 software.

The solvent stability of lignin-OAm polyimines and gel fraction (crosslinking degree) of lignin-PDMS polyimines were evaluated according to previous studies with minor modifications.[148, 151] In brief, polyimine films (~ 1 × 1 cm, vacuum-dried mass: m_0) were soaked in 10 mL of five different solvents, *i.e.*, toluene, acetone, THF, DMSO, and water, at RT and 60 ℃ for 24 h, respectively. Next, the films were taken out on a filter paper to remove extra solvent on the surface, and then vacuum dried at 100 °C overnight to completely remove the solvents. The oven-dried mass was recorded as m_1. The solvent

stability/gel fraction was calculated by equation (3) below. Solvent stability and gel fraction are used to denote lignin-OAm and lignin-PDMS polyimines, respectively. Each sample was measured twice with the means and standard deviations recorded. The solvent stability/gel fraction of films that were fully dissolved or unable to preserve the shape after the immersing were recorded as 0.

$$\text{Solvent stability/Gel fraction (\%)} = 100\% \times m_1/m_0 \qquad (3)$$

Thermal gravimetric analysis (TGA) was conducted using a Q-50 thermogravimetric analyzer (TA Instruments, USA) by the combustion of samples from 30 ℃ to 800 ℃ at a rate of 20 ℃/min under N_2. The heating temperatures against weight losses of samples during the combustion are recorded as TGA curves and differential TGA curves (DTG) were analyzed by Universal Analysis 2000 software. Differential scanning calorimetric (DSC) and thermal gravimetric analysis (TGA) were carried out using a Q-2000 differential scanning calorimeter (TA Instruments, USA). About 5 mg of each sample was hermetically sealed in an aluminum pan and afterwards subjected to a heating and cooling cycle twice, from -80 to 200 ℃, at a rate of 10 ℃/min under a nitrogen atmosphere. The second scanning DSC heating and cooling curves were used to determine glass-transition temperature (T_g).

The stress-relaxation behaviors of modified lignin and synthesized polyimines were measured by a rotational rheometer (ARES-G2, TA Instruments, USA) equipped with an 8-mm parallel-plate geometry. The polyimine films with a thickness of ~ 300 μm were cut into a circle shape with a diameter of 1 cm to fit the geometry. The stress-relaxation steps were tested under different temperatures (100 ℃ - 200 ℃) after equilibrations of temperature and geometry gaps for at least 5 min. An external axial force of 2 N and a strain of 1.5% were applied to the films. The stress-relaxation curves of modulus as a function of time were recorded. The Arrhenius law is fitted by the equation (4)[49] below:

$$ln\tau^* = \frac{E_a}{RT} - lnA \qquad (4)$$

where τ^* is the time (s) it takes for samples to relax to 1/e (~ 37%) of their initial modulus, E_a is the activation energy (the minimum energy required for chemical reactions

to occur, kJ/mol), R is the ideal gas constant (~ 8.315 J/(mol·K)), T is the absolute temperature (K), A is the pre-exponential factor.

The dispersive (γ_d) and specific (γ_{sp}) surface energies of lignin, modified lignin, and polyimines were measured by an inverse gas chromatography (iGC) surface energy analyzer (SEA) equipped with a flame ionization detector (Surface Measurements Systems, Ltd, Alperton, UK). Non-polar (nonane, octane, heptane, and hexane) and polar (acetone, ethanol, acetonitrile, ethyl acetate, and dichloromethane) probe molecules were injected successively under surface coverage from 0.01 n/n_m to 0.4 n/n_m. Data were analyzed by advanced SEA analysis software (Advance Version 1.4.2.0). Static water contact angle (WCA) of polyimine films were measured using a contact angle goniometer (Ramé-Hart Instrument Co., USA).

The UV-blocking ability of films was evaluated using UV-vis spectra as a function of light wavelength (ranges from 200 to 800 nm) against transmission recorded by an Evolution 60S UV-vis spectrometer (Thermo Fisher Scientific, USA).

3.3.5. Repairability of synthesized polyimines

The repairability of the polyimines was measured by referring to a previous study.[49] Briefly, the surface of polyimine films was scratched by a razor blade, and the damaged surface of MKL-O and MFL-O polyimine films was repaired by pressing under a flat plate with a pressure of 0.1 MPa. The damaged surface of MKL-P and MFL-P polyimine films was repaired at 150 °C in a vacuum oven for 12 h after filling a healing agent to the damaged gaps. The healing agent was prepared by pre-reacting modified lignin and PDMS in THF at 80 ℃ for 12 h. The optical microscopy images of the damaged surface were taken before and after the repair to make comparisons using a BX51 optical microscope (Olympus, Bartlett, TN, USA).

For statistical analysis, all data were processed using software including OriginPro 8.5 (OriginLab Corporation, Northampton, MA, USA) and Excel 2016 (Microsoft, Redmond, WA, USA)

3.4. Results and discussion

3.4.1. Lignin fractionation and modification

It has been a great challenge to utilize KL on a large scale because the structural heterogeneity of KL will affect the KL-based polymers or composites.[25] To investigate the effect of lignin structural non-uniformity on the synthesized polymers, a more homogeneous ($Đ_M$: 2.02 *vs.* 2.98) and lower-MW (M_w: 2,167 Da *vs.* 4,659 Da) FL is fractionated from KL successfully with a yield of 75.8% (Figure 8-1 and Table 3-1). From the OH quantification results by ^{31}P NMR analysis, the concentrations of phenolic, aliphatic, carboxylic, and total OH between FL and KL vary (Table 8-1), which will influence the further lignin modification and synthesis reactions.

To enable the functionality of KL reactive sites, chemical modifications such as esterification, hydroxylation, amination, etc. are typically required.[152-154] In the current study, lignin is grafted with active ketone groups through the esterification of the OHs by the carboxyl groups in LA to allow for the Schiff-base reaction with amines (Figure 3-1).[15] GPC, FTIR, ^{1}H NMR, ^{13}C NMR, and ^{31}P NMR analyses prove that KL and FL are successfully modified with the following observations: 1) the M_w of modified lignins are increased compared with the corresponding lignins (Table 3-1), which is attributed to the grafted LA and/or removal of low-MW lignin during methanol purification[15]; 2) the new signals of ketone groups show up at 1,710 cm^{-1} in the FTIR spectra of modified lignins (Figure 8-2)[15, 16]; 3) the new signals of methylene (signals a & b at ~ 2.73 ppm) and methyl (signal c at ~ 2.12 ppm) in LA appear at in ^{1}H NMR spectra of modified lignins[15] (Figure 8-3); 4) the new signal of ketone (signal C_d at 206.9 ppm) is observed in the ^{13}C NMR spectra of modified lignins (Figure 8-4)[15]; 5) the signals of aliphatic OH, guaiacyl phenolic OH, and *p*-hydroxyphenyl OH disappear and signal intensity of C_5-substituted OH apparently recedes in ^{31}P NMR spectra of modified lignins (Figure 8-5). The reduced content of aliphatic OHs and phenolic OHs in modified lignins (Table 8-1) is attributed to the esterification by the carboxyl of LA.[15] There are ~ 26% aliphatic and 22% phenolic OH were remained in MKL, and ~ 17% aliphatic and ~ 16% phenolic OH remained in MFL,

comparing with unmodified lignin (Table 8-1). The reasons could be 1) the OHs in lignin were not fully esterified by LA, and 2) a few OHs were newly formed during the purification by 50% methanol aqueous. It's worth noting that compared with MKL, the ketone grafting density of MFL is approximately twice as many as that of MFL (14.65 vs. 7.14), which is on account of the higher amount of OHs and lower MW of FL that favor the LA grafting.[143] Moreover, from Figure 8-4, the intensity of chemical shift of C_a (ester) in MFL is stronger than that in MKL, which is attributed by the fact that at a concentration of 100 mg/mL, the MFL/DMSO-d_6 solution contains more ester groups than the MKL/DMSO-d_6 solution because of the higher ketone grafting density (14.65 *vs.* 7.14) and lower M_w (3.603 kDa *vs.* 5.359 kDa) of MFL. However, there might be rare occurrence of the intramolecular and intermolecular esterification among lignin molecules[15] because the COOH content in both MKL (0.08 vs. 0.32 mmol/g) and MFL (0.09 vs. 0.46 mmol/g) is decreased compared with KL and FL, respectively (Table 8-1).

3.4.2. Synthesis and characterization of polyimines

Imine chemistry is one of the few synthetic strategies to construct robust molecules with chemical recyclability due to the formation of dynamic covalent bonds.[47, 53] Lignin is a widely used bio-derived precursor for the synthesis of high-performance polymers or DCPN due to the abundant functional groups.[27] Herein, lignin-OAm and lignin-PDMS polyimines are successfully synthesized *via* catalyst-free Schiff-base reaction between ketones in modified lignin and amines in OAm and PDMS, respectively (Figure 3-1). GPC, FTIR, and ^{13}C NMR analyses confirm the successful synthesis of polyimines. Firstly, the tested M_w of MKL-O, MFL-O, MKL-P, and MFL-P is significantly augmented compared with corresponding MKL and MFL (Table 3-1). It can also be assumed that the actual M_w of MKL-P and MFL-P is higher than the tested values (54.302 ± 1.680 kDa and 113.144 ± 21.531 kDa) due to the partial dissolution. Secondly, the newly formed C=N bonds are detected at around 1,660 cm^{-1} in the FTIR spectra of MKL-O, MFL-O, MKL-P, and MFL-P[15, 16] (Figure 3-2). Lastly, the ^{13}C NMR spectra verify the formation of the C=N bonds (signal C_d at ~ 164 ppm) in lignin-OAm polyimines and (signal C_d at 168.5 ppm) in MKL-

Table 3-1 Weight-average (M_w), number-average (M_n) molecular weight and molar mass dispersity ($Đ_M$) of lignin, modified lignin and lignin-based polyimines

	M_w (kDa)	M_n (kDa)	$Đ_M$
PDMS	5.463±0.034	2.983±0.023	1.83±0.00
Lignin and modified lignin			
KL	4.659±0.241	1.566±0.039	2.98±0.23
MKL	5.359±0.418	1.120±0.042	4.78±0.20
FL	2.167±0.099	1.071±0.019	2.02±0.06
MFL	3.603±0.0485	1.120±0.083	3.23±0.20
Polyimines			
MKL-O	6.388±0.721	2.150±0.055	2.98±0.41
MFL-O	6.486±0.793	1.724±0.038	3.77±0.54
MKL-P	54.302±1.680	26.664±1.113	2.04±0.02
MFL-P	113.144±21.531	100.915±10.514	1.11±0.10

Note: MKL-P and MFL-P were measured by partially dissolved in THF under shaking at 60 ℃ for 72 h. The data are in a form of mean ± standard deviation

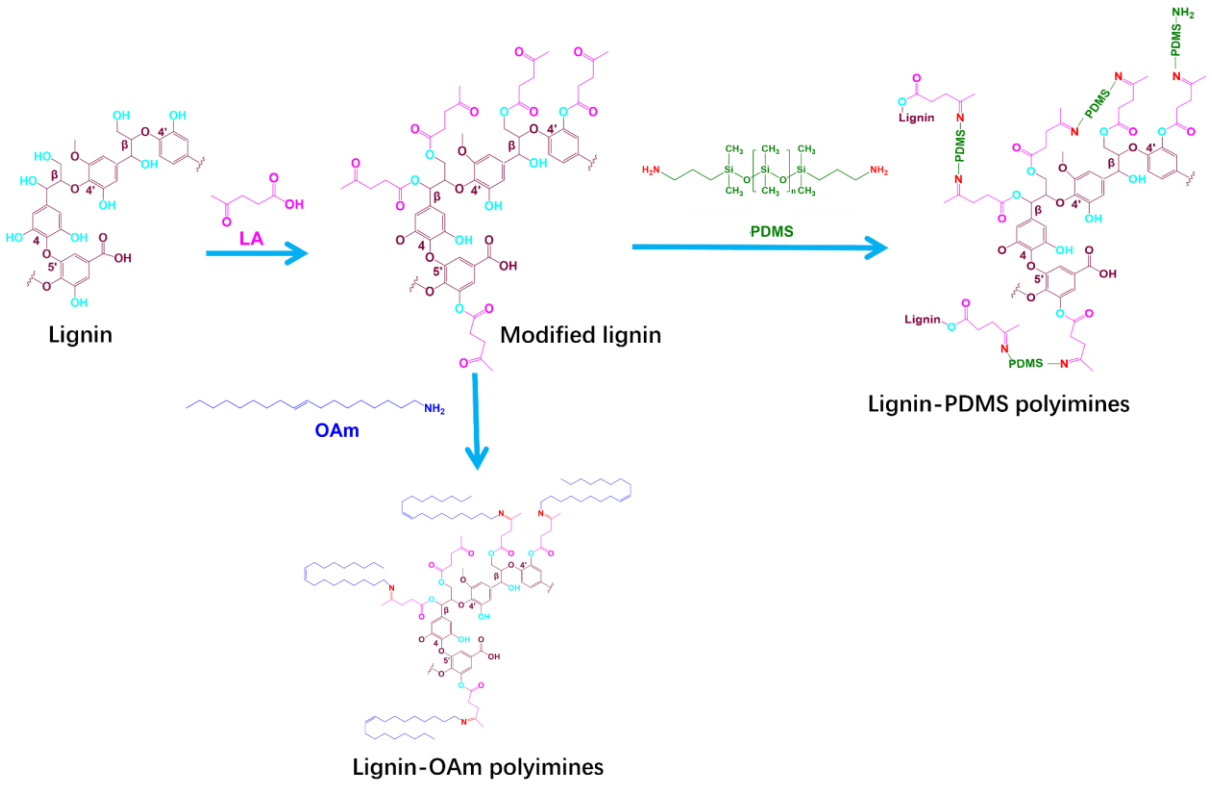


Figure 3-1 Proposed mechanisms of lignin modification and polyimine synthesis

P (Figure 3-3).[15, 155] With the similar method to calculate LA (ketone) grafting density based on the GPC results (Equation (2) and Table 3-1), the OAm grafting density can be calculated as 4.13 for MKL-O and 11.58 for MFL-O. Combined with the calculated ketone grafting density of MKL (7.14) and MFL (14.65), the OAm grafting efficiency of MKL-O and MFL-O is 57.8% and 79.0%, respectively. The results are verified by the peak integral ratio of C_a (ester) to C_d (imine) in the ^{13}C NMR spectra MKL-O (52.5%) and MFL-O (69.2%) (Figure 3-3). For lignin-PDMS polyimines, the peak integral ratio of C_a (ester) to C_d (imine) in the ^{13}C NMR spectra MKL-P is ~ 1.07; however, the imine bond was not detected in ^{13}C NMR spectra of MFL-P, which is attributed to its poor dissolution performance in DMSO-d_6 caused by the high MW. The solid-state ^{13}C NMR spectra exhibit weaker and broader signals of C=N bonds (C_d at 160-170 ppm, Figure 8-6) in MKL-P and MFL-P due to the immobility of molecules under scanning.

The better solubility of lignin-OAm than lignin-PDMS polyimines agrees with the noticeably larger tested M_w of the latter than the former, which suggests that OAm with singular amine group was grafted to modified lignins to form branched copolymers with modified lignins as skeletons and OAm as arms, while PDMS with double amine groups was crosslinked with modified lignins to form lignin-PDMS polymer networks. In addition, comparing MKL-based and MFL-based polyimines, the latter shows a higher testable M_w (Table 3-1), implying that lignin fractionation favors the grafting and crosslinking polymerization with amines. It could be attributed to the enhanced reactive (phenolic and aliphatic) OH sites in FL (Table 8-1), reduced steric hindrance effect of lower-M_w MFL,[156] and the increased ketone grafting density of MFL compared with MKL in the current study. As for the lignin-OAm polyimines, the $Đ_M$ is slightly decreased compared with modified lignin (Table 3-1), which could be related to the negative relationship between the content of active OHs and lignin MW[150] that favor higher-MW lignin grafted less LA and OAm arms and vice versa, thus to homogenize the MW distribution of synthesized lignin-OAm polyimines.

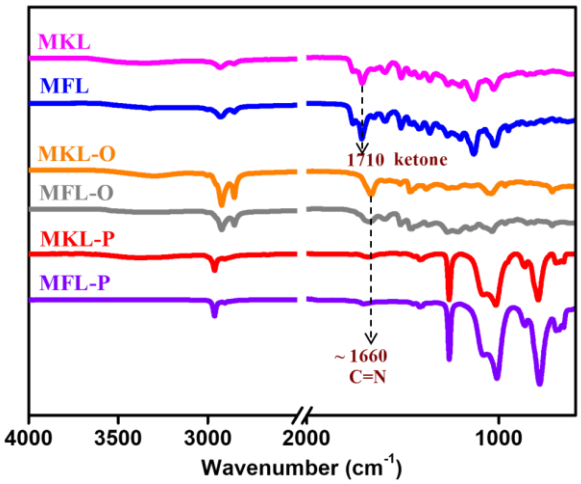


Figure 3-2 FTIR spectra of lignin-based polyimines

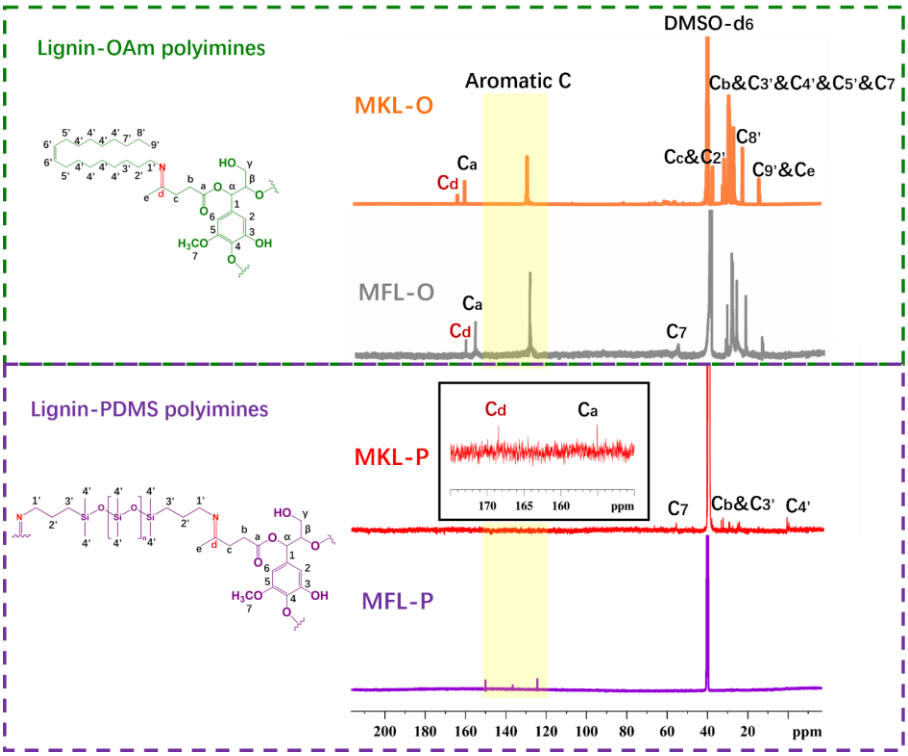


Figure 3-3 ^{13}C NMR spectra of lignin-based polyimines with DMSO-d_6 as a solvent

3.4.3. Physicochemical properties of polyimines

For the sake of future applications, it is of great significance to have a thorough understanding of the physicochemical properties of the synthesized lignin-based polyimines. During the solvent stability test, MKL-P and MFL-P were swollen into transparent gels after immersing under toluene, acetone, THF, and DMSO while no swelling occurred to MKL-O and MFL-O, which aligns with our hypothesis that lignin-PDMS polyimines are in form of a crosslinked polymer network while lignin-OAm polyimines are in form of grafted copolymers. Furthermore, the gel fractions of the synthetic lignin-PDMS polyimines reach over 85% after being immersed under polar solvents including acetone, DMSO, and water; however, their gel fractions are below 80% in less-polar solvents including THF and toluene (Table 3-2). It suggests an overall non-polarity of lignin-PDMS polyimines. Theoretically, the Schiff-base condensation reaction proceeds with water as a byproduct and the reversible hydrolysis reaction will also proceed if water exists[53, 157], which could lead to the humidity instability. However, in the current study, the gel fractions of lignin-PDMS polyimines are 100% after being immersed under water for 24 h at RT (Table 3-2). We reason that it may be related to the facts that i) the incorporation of low-surface energy PDMS restrains the water uptake to the polyimines, ii) the hydrophobic functional groups in lignin (like aromatics and esters and the long-chain alkyls in OAm) prevent water from penetrating into the polymers, and iii) the compact structures of covalent crosslinking polymer network of lignin-PDMS polyimines enhance the water-resistance to imine hydrolysis, allowing more water stability. In addition, the gel fraction of MKL-P is lower than that of MFL-P under five tested solvents, together with the testable M_w (Table 3-1), indicating a higher crosslinking density of MFL-P. The higher crosslinking density of MFL-P results from the more active sites (reacted with PDMS) in MFL caused by the increased ketone grafting density of FL (Table 8-1) and the reduced steric hindrance effect of MFL with a lower M_w (Table 3-1)[31], and would further lead to various physicochemical properties of the synthesized polyimines.[158]

To understand the thermal properties of lignins and the synthesized polyimines, T_g and thermal stability are characterized by DSC and TGA (Table 3-3 and Figure 3-4). First

Table 3-2 Solvent stability and gel fraction of synthesized lignin-based polyimines

Solvent	Solvent stability (%)				Gel fraction (%)			
	MKL-O		MFL-O		MKL-P		MFL-P	
	25 ℃	60 ℃	25 ℃	60 ℃	25 ℃	60 ℃	25 ℃	60 ℃
Toluene	35.2±0.4	32.5±2.5	46.9±0.9	42.9±0.8	78.5±0.5	75.3±0.3	84.5±2.2	82.5±0.4
Acetone	74.3±2.9	0	80.7±2.9	0	85.2±0.3	83.8±0.5	91.9±0.6	90.5±0.5
THF	0	0	0	0	67.5±1.1	58.6±3.1	82.1±1.6	80.1±2.5
DMSO	74.5±2.8	0	83.8±2.2	0	87.2±5.3	81.6±4.0	92.1±3.8	90.8±3.7
H_2O	99.5±0	98.4±0.6	99.5±0	99.1±0.1	100.0±0	99.9±0.2	100.0±0	100.0±0

Note: The data are in a form of mean ± standard deviation

of all, T_g of modified lignin and polyimines is just slightly discrepant from lignin. Furthermore, the thermal stability of FL increases compared with KL due to a higher T_{max} (385 ℃ *vs.* 363 ℃, Table 3-3), which is triggered by the cleavage of less stable ether bonds of KL and the augmentation of more stable C-C bonds in FL.[11] Besides, modified lignin exhibits a broader thermal degradation range than unmodified lignin, which is due to the more complex compositions including lignin core and grafted LA arms that lead to multiple degradation pathways.[159] Also, the thermal stability of synthesized polyimines is much higher than the corresponding modified lignin (T_{max}: ~ 400 ℃ *vs.* ~ 500 ℃, Table 3-3), which may be explained by the introduction of thermally stable structures such as C-C and silicones and elevated MW caused by the polymerization. For lignin-PDMS polyimines, the dual (lignin-lignin and lignin-PDMS) crosslinking network further contributes to a higher thermal stability. Compared with MKL-P, MFL-P displays higher thermal stability (T_{max}: 576 ℃ *vs.* 518 ℃, Table 3-3), which further advocates our previous finding of gel fraction (Table 3-2) that the crosslinking density of MFL-P is higher than MKL-P.

Dynamic imine chemistry has been investigated to be stimulated by heat, pressure, excess primary amine, and polar solvents.[16, 157] In the present study, no product purification protocol was addressed. Theoretically, all the amines are supposed to be consumed since the ketone/amine groups molar ratio is 1:1. However, the ketone molar amount in modified lignin is calculated based on equation (1) ignoring the intermolecular and intramolecular esterification. Besides, as mentioned above, the OAm grafting efficiency of MKL-O and MFL-O is 57.8% and 79.0%, respectively. Therefore, excess amines are present in the final products. To further testify the associate imine bond exchanging process of synthesized polyimines, dynamic mechanical compression analysis was conducted. As a result, all four synthesized polyimines recovered to the original shape and hardness after the removal of heat and stress without using a mold. They also show observable temperature-dependent stress-relaxation behaviors and follow the Arrhenius law (Figure 3-5), suggesting that chemical reactions took place under thermal and stress activation.[47] On the one hand, lignin-OAm polyimines are more thermoplastics-like whose relaxation modulus decreases

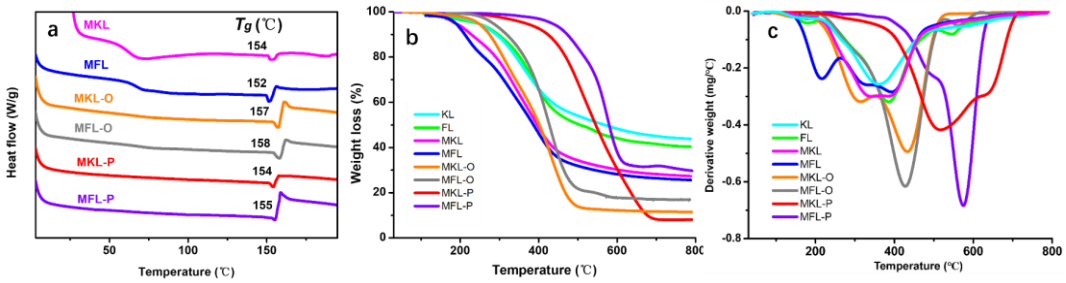


Figure 3-4 DSC (a), TGA (b), and DTG (c) curves of lignin, modified lignin, and lignin-based polyimines

Table 3-3 Glass transition temperature (T_g), temperatures at the onset of thermal degradation (T_{onset}) and maximum mass loss (T_{max}), residual carbon content (C_r), and calculated average activation energy (E_a) of lignin, modified lignin, and lignin-based polyimines

	T_g (℃)	T_{onset} (℃)	T_{max} (℃)	C_r (%)	E_a (kJ/mol)
KL	154	252	363	43.6	N/A
FL	158	261	385	40.0	N/A
MKL	154	157	342-387	27.2	N/A
MFL	152	164	326-394	25.6	N/A
MKL-O	157	222	434	11.3	43.5
MFL-O	158	251	429	16.7	44.8
MKL-P	154	325	518	7.9	100.0
MFL-P	155	385	576	29.7	130.2

exponentially in the early stage and tends to be constant in the late stage (Figures 3-5a and 3-5b), indicating that lignin-OAm polyimines are copolymers mainly consist of noncovalent hydrogen networks that are easily to overcome, and the imine bonds act as chain extenders of the lignin core.[160] On the other hand, traditional thermosets are hard to stress-relax under heating because of the irreversible covalent bonds.[49] However, in this work, the relaxation modulus of lignin-PDMS polyimines is released slowly first and significantly later (Figures 3-5c and 3-5d), indicating that they are adaptable thermoset-like networks mainly consisting of dynamic imine covalent networks that are responsible for their stress-relaxation effect.[161] In other words, the occurrence of imine exchange and metathesis leads to their network rearrangement and stress-relaxation behavior.[148, 162] Comparing lignin-PDMS and lignin-OAm polyimines, the latter exhibit much faster relaxation rates under the same temperatures and applied strain (Figure 3-5), as well as a lower E_a (Table 3-3), which could be explained by the fact that the covalent crosslinking network of lignin-PDMS polyimines is more complex and rigid than the core-branch-shape lignin-OAm polyimines, leading to a higher difficulty in chain mobility and rearrangement and a reduced ability to dissipate stress over time.[163]

Herein, both MKL-P and MFL-P relax faster as the temperature increases (Figures 3-5c and 3-5d), which is due to the fact that elevated temperature and pressure promote the mobility and diffusion of the silicone chains, allowing for the rearrangement of imine bonds in response to the applied pressure.[148] Besides, MKL-P shows comparable E_a with reported transamination of Schiff-base bonds[148, 164, 165], while MFL-P shows a higher E_a than MKL-P (Table 3-4), indicating that their stress-relaxation behaviors highly depend on the crosslinker, *i.e.*, lignin. We speculate the reason is that MFL-P synthesized by more homogeneous and lower-MW FL possesses an increased covalent crosslinking density and a less flexible network than MKL-P, restricting the intermolecular and intramolecular mobility of the amine and imine groups, thus, to hamper the dynamic imine metastasis and exchange reactions and the reformation of the polymers.[162] It may also be attributed to the reduction of noncovalent interactions (H-bonding) among lignin, PDMS, and polyimines

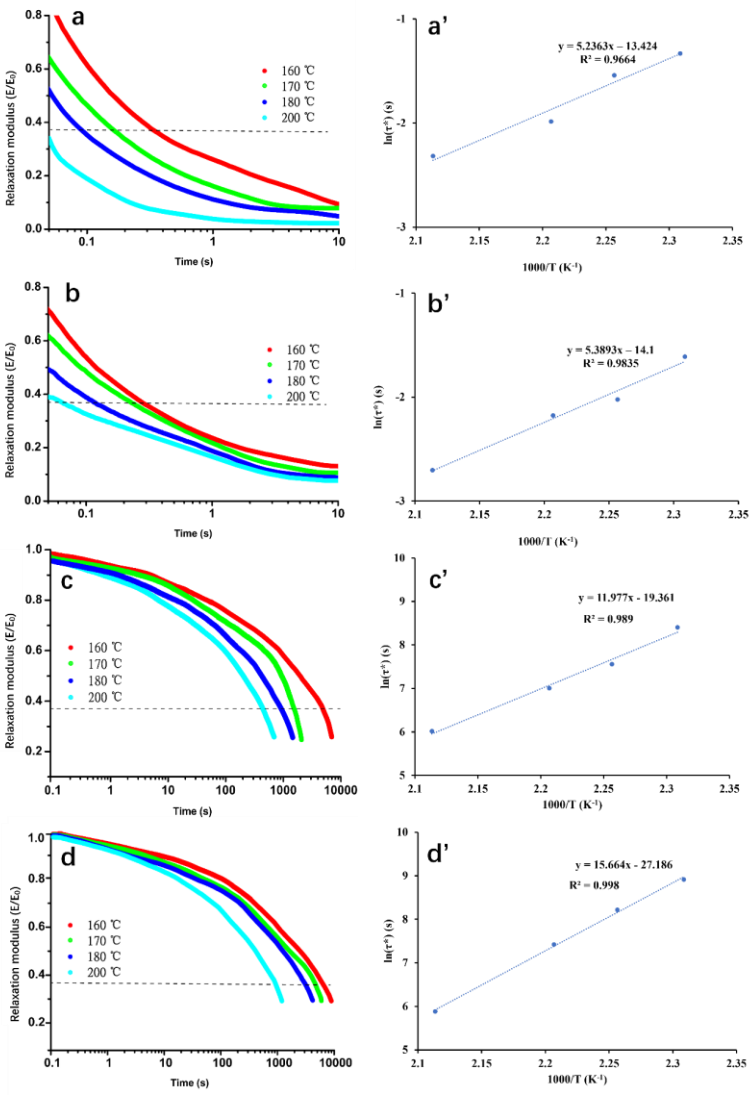


Figure 3-5 Stress-relaxation curves (a-d) and the Arrhenius equation plots (a'-d') of MKL-O (a, a'), MFL-O (b, b'), MKL-P (c, c'), and MFL-P (d, d'). The dashed line refers to the 1/e (~ 0.37) of the initial modulus.

that favor the melting and reshaping of MFL-P under heat.[148] Therefore, MFL-P requires longer time and/or higher temperature to relax.

The surface properties including dispersive and specific surface energy, hydrophilicity index, and WCA are also characterized. As expected, both the dispersive and specific surface energy of modified lignin are more heterogeneous (*i.e.*, the difference between maximum and minimum surface energy is more significant) than original lignin because the grafted active arms introduce more diverse functional groups and more complicated structures, whereas they become more homogeneous after the synthesis with amines because the incorporations of long-chain OAm and low-surface-energy PDMS[149] lower down the maximum surface energy of modified lignin (Figures 3-6a and 3-6b). However, it is pointed out that the specific surface area of the polyimine products in this study is very low (< 1 m^2/g), which easily leads to a disparity of the surface coverage and surface energy quantification. Further verification with large samples running needs to be conducted. The decreased hydrophilic index of polyimines implies that the introduction of OAm and PDMS weakens the water affinity of modified lignin (Table 3-4). It is worth noting that the WCA of MFL-P reaches 111°, higher than many of the reported lignin-based hydrophobic thermosets.[19, 49, 166, 167] What's more, the WCA of MFL-P is higher than that of MKL-P (111° *vs.* 106°), which is align with the hydrophilic index (0.10 *vs.* 0.06) tested by iGC (Table 3-4). The difference might be attributed to the lower surface energy and higher water resistance of MFL-P caused by the higher crosslinking density. However, the WCA shows a minimal difference between the two lignin-OAm polyimines. The increased hydrophilicity index of MFL-O than MKL-O (0.09 *vs.* 0.05, Table 3-4) may be attributed to the higher LA grafting efficiency of MFL that brought more polar-polar interactions between MFL-O and probes.

Overall, compared with KL, FL has a relatively higher OH content ready for LA esterification (5.71 mmol/g *vs.* 5.24 mmol/g) and more homogeneous MW distribution ($Đ_M$: 2.98 vs. 2.02). Compared with MKL, MFL has higher OH decreasing percentage (83.54% & vs. 76.15%), ketone grafting density (14.65 *vs.* 7.14), and lower M_w (3.603 kDa *vs.* 5.359 kDa, Table 3-1), which causes little differences in the structures and properties between

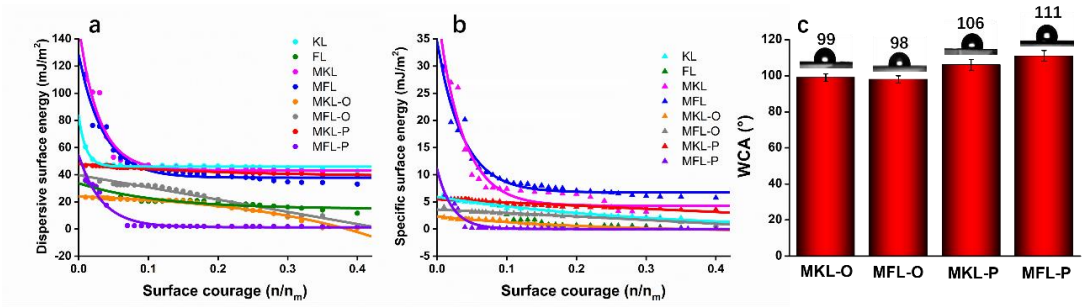


Figure 3-6 Dispersive (a) and specific (b) surface energy and WCA (c) of lignin, modified lignin, and synthesized lignin-based polyimines

Table 3-4 The minimum, median and maximum values of γ_d and γ_{sp} as well as hydrophilicity index ($\gamma_{sp}/(\gamma_{sp}+\gamma_d)$) and specific surface area of lignin, modified lignin and lignin-based polyimines

Samples	γ_d (mJ/m^2)			γ_{sp} (mJ/m^2)			$\gamma_{sp}/(\gamma_{sp}+\gamma_d)$	WCA (°)
	minimum	median	maximum	minimum	median	maximum		
KL	42.60	46.74	60.51	0.71	3.56	6.45	0.08	N/A
FL	11.63	20.10	35.57	0.17	0.71	4.38	0.04	N/A
MKL	42.19	45.57	110.20	11.27	6.81	26.99	0.15	N/A
MFL	33.08	41.88	114.05	5.74	7.92	20.15	0.19	N/A
MKL-O	0.68	21.12	23.41	0.03	1.02	2.14	0.05	99
MFL-O	0.93	28.85	39.52	0.70	2.73	3.19	0.09	98
MKL-P	39.74	43.57	46.80	3.59	4.54	5.49	0.10	106
MFL-P	2.25	12.93	59.41	0.11	0.83	10.88	0.06	111

MKL-O and MFL-O but causes obvious differences between MKL-P and MFL-P. In particular, MFL-P possesses higher crosslinking density than MKL-P, which further leads to different thermal stability (T_{max}: 576 ℃ *vs.* 518 ℃, Table 3-3) and hydrophobicity (WCA: 111° vs. 106°; hydrophobicity index: 0.06 vs. 0.10, Figure 3-6 and Table 3-4). The differences are not only originated from the discrepant OH content in lignin and grafting density of LA, but also from the discrepant steric hinderance of modified lignin that influences the lignin-amine polymerization.

The synthesized polyimine films exhibit an excellent ability to shield broad-spectrum UV radiation including UV-A (wavelength: 400 - 320 nm), UV-B (wavelength: 320 - 280 nm) and UV-C (wavelength: 280 - 200 nm) with 0% transmittance of UV light. Among them, lignin-OAm films exhibit better ability to shield visible light (wavelength: 400 - 800 nm) than lignin-PDMS films (Figure 3-7a). Their UV-blocking ability mainly is attributed to the conjugated C=C double bonds, unsaturated ethylene groups, and condensed structures in lignin.[126] Moreover, synthesized lignin-PDMS polyimine films are translucent. As we can see from Figures 3-7b and 3-7c, the letters "Center for Renewable" could be seen through the MKL-P and MFL-P films. The transparency mainly derives from the PDMS component, and the brownish color is mainly derived from the chromophore groups such as C=C, C=O, and COOH in the lignin component.[168, 169] However, MKL-P displays better visuality than MFL-P, which is accordant to the higher visible-light transmittance of MKL-P in Figure 3-7a. Overall, the synthesized lignin-PDMS polyimines could act as a potential candidate for translucent, anti-UV, and hydrophobic coatings.

3.4.4. Reprocessing ability and repairability of polyimines

Imine exchange and metathesis are the two primary reactions responsible for the reprocess ability and recyclability of polyimines without requiring catalysts.[16, 47, 53, 54] In a previous report, a lignin-based polyimine thermoset was successfully reprocessed under hot press *via* dynamic imine chemistries with a minimally detrimental effect on mechanical strength.[16] The dynamic imine exchange and metathesis are closely influenced by the polymer structures, molecular chain flexibility and rigidity, etc.[15, 16] In the current study,

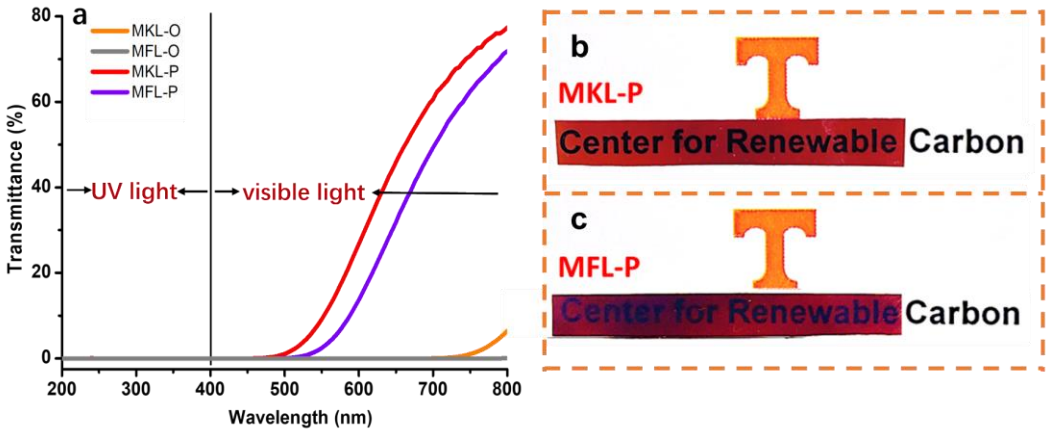


Figure 3-7 UV light blocking ability (a) and images of MKL-P (b) and MFL-P (c) translucent films

lignin-OAm polyimine films can be repurposed into new films under 160 ℃ and 1 MPa for 3 h after being cut into small pieces (Figure 8-9); however, it was arduous for lignin-PDMS films to be reprocessed in the present study. It echoes the stress-relaxation analyses that lignin-OAm polyimines are more thermoplastic-like while lignin-PDMS polyimines are more thermoset-like.

To reduce the difficulty in reprocessing polyimines, repairability measurements were conducted by re-healing razor scratches on the films under (hot) press. As a result, the scratches on lignin-OAm polyimine films could be self-healed under RT and 0.1 MPa for 20 min (Figure 8-10). Nevertheless, a healing agent of a pre-reacted lignin and PDMS solution under 80 ℃ for 12 h was required to repair the damaged lignin-PDMS polyimine films under 150 ℃ and reduced pressure for 12 h (Figure 8-11). Under a micro-scale, the scratches on lignin-OAm polyimine films are nearly invisible after repair (Figures 3-8a' and 3-8b'), while the scratches on lignin-PDMS polyimine films are repaired significantly but still observable (Figures 3-8c' and 3-8d'). Meanwhile, based on the differences in the width of repaired scratches, MKL-P displays better repairability than MFL-P, which could be explained by the higher crosslinking density of MFL-P that rises the difficulty in chain mobility and polymer re-healing.[170] Overall, lignin-OAm polyimine films can be self-healed by simply applying pressure, while lignin-PDMS polyimine films can be repaired with the help of a healing agent, heat and pressure.

Combined with the structural characterization results, possible dynamic bonds are imine and ester bonds in synthesized polyimines. To investigate whether transesterification occurred, dynamic mechanical analyses of esterified lignin (MKL & MFL) were also conducted. As shown in Figure 8-8, although MKL and MFL exhibit classic stress-relaxation behavior (viscosity-temperature dependence), however, the weak Arrhenius correlations (R^2 = 0.84 and 0.65, respectively) provide limited evidence for transesterification. As a result, the stress-relaxation behavior of modified lignin is highly-possibly attributed by the polymer melt. Therefore, dynamic imine chemistries including imine exchange and metathesis are mainly responsible for the repairability of the synthesized polyimines.

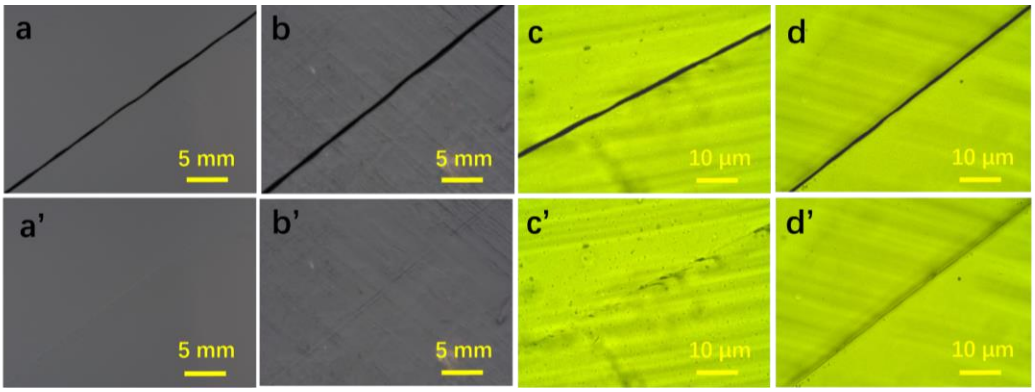


Figure 3-8 Optical microscopy images of MKL-O (a, a'), MFL-O (b, b'), MKL-P (c, c'), and MFL-P (d, d') before (a-d) and after (a'-d') repair

Several factors are considered to affect the dynamic imine chemistries: 1) higher temperatures can increase the reaction rate by i) providing more thermal energy to the reactant molecules[171] and ii) increasing the chain mobility of the silicone[148], thereby promoting the breaking and formation of C=N bonds and bond rearrangement in response to heat and pressure; 2) pressure can affect imine exchange and metathesis reactions indirectly by influencing the solubility and diffusion of reactants to impact the reaction kinetics.[172] 3) Excessive amines play an important role in initiating the dynamic imine exchange and metathesis. A prior report investigated that the amine concentrations affect the dynamic imine bond exchange kinetics by taking part in non-covenant interactions, and higher amine concentration is beneficial to the decreasing the activated energy of relaxation of the vanillin-PDMS polyimines.[148] As discussed above, excess amines are present in the final products in this study. Under the stimulation of unreacted amines, the polyimines were repairable *via* the imine exchange and metathesis.

The proposed reactions during repairing are displayed in Figure 3-9. As for lignin-OAm polyimines, unreacted ketones in modified lignin further condense with excessive amines in OAm to form imine bonds. Meanwhile, lignin-OAm polyimine molecules exchange imine bonds and metathesize imine bonds with amines in unreacted OAm under pressure reversibly (Figure 3-9a). As for lignin-PDMS polyimines, unreacted ketones in modified lignin are stimulated to condense with free PDMS by heat and pressure. Simultaneously, imine exchange reactions occurred among the existing and newly formed imine bonds, and imine metathesis reactions occurred between imines and uncondensed amines in PDMS or lignin-PDMS polyimines (Figure 3-9b).

It cannot be denied that there are a few limitations in the current study. Firstly, a more efficient lignin pretreatment method will be beneficial to further decrease the MW and ketone grafting density of KL, so that the tailoring effect of lignin would be more obvious. Secondly, the repair time is long, which is energy consuming. Further studies on lignin pretreatment and application of lignin-PDMS polyimines for coatings are ongoing in our group.

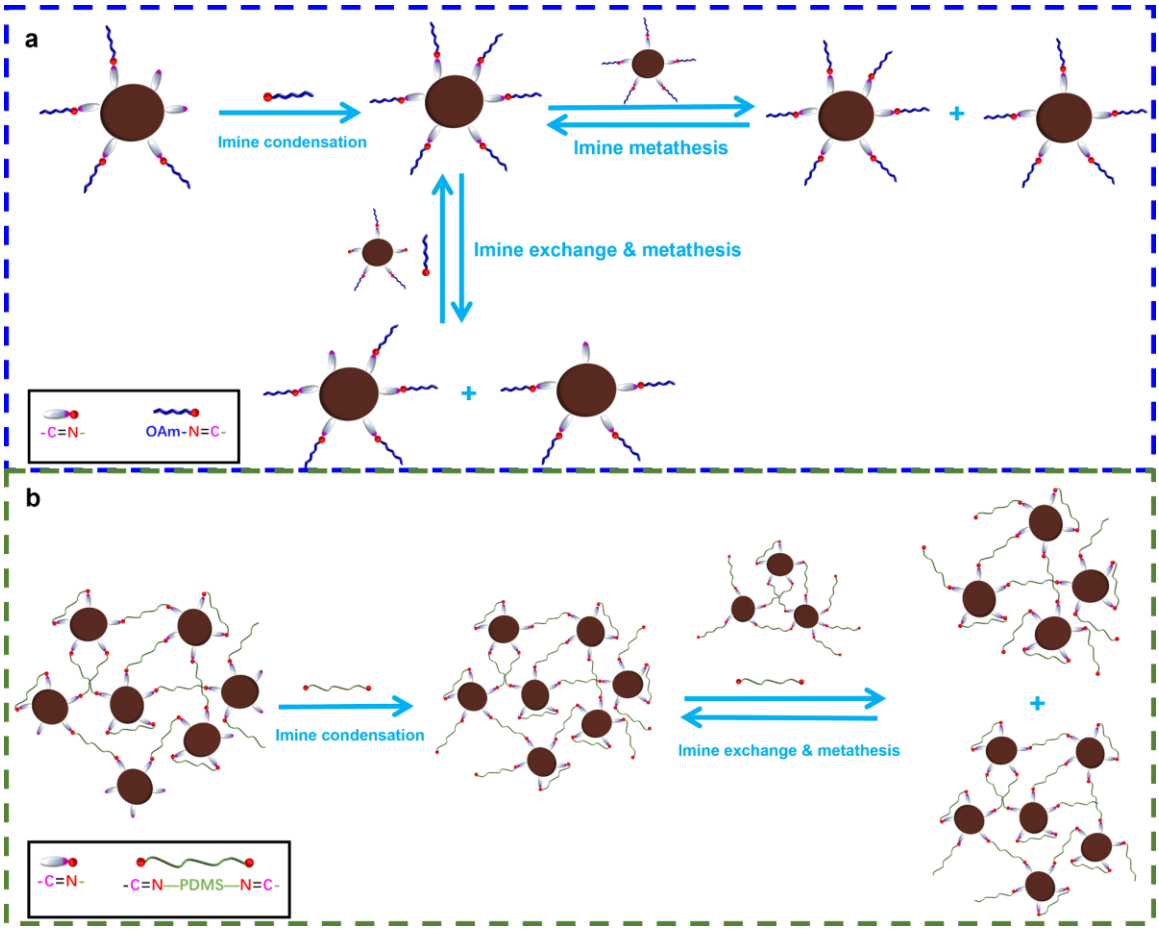


Figure 3-9 Proposed mechanisms of imine condensation, exchange, and metathesis reactions during repairing of lignin-OAm (a) and lignin-PDMS (b) polyimines

3.5. Conclusions

Lignin-based polyimines are successfully prepared *via* catalyst-free Schiff-base reaction between the ketone groups in modified lignins and amine groups in OAm and PDMS. The ketone grafting density of MFL is higher than that of MKL, resulting in a higher M_w of MFL-O and a denser crosslinking network of MFL-P. Additionally, lignin-OAm polyimines are linear grafted copolymers with modified lignin as skeletons and OAm as arms, while lignin-PDMS polyimines are 3-dimensional crosslinked polymer networks. The stress-relaxation behaviors of synthesized polyimines indicate the occurrence of transimination under thermal-stress activation. As a result, lignin-OAm polyimines are self-repairable and hot reprocessable, while lignin-PDMS polyimines are repairable with the assistance of a healing agent, heat, and stress. Moreover, lignin-PDMS polyimines exhibit excellent hydrophobicity, thermal stability, translucency, and UV-blocking ability. Thereof, MFL-P features better hydrophobicity and light-shielding ability but inferior repairability and translucency because of the intensified crosslinking density and a more rigid network structure. The synthesized lignin-PDMS polyimines hold a great potential to be applied for repairable, translucent, anti-UV, and hydrophobic coatings.

CHAPTER IV

APPLICATION OF LIGNIN-PDMS POLYIMINES FOR REMOVABLE HYDROPHOBIC COATINGS

4.1. Abstract

Having synthesized lignin-PDMS polyimines with excellent hydrophobicity, water resistance, film-forming ability, anti-UV ability, and translucency in the last chapter, we believe that the synthesized polyimines are promising to be applied for hydrophobic coatings. As a result, both MKL-P and MFL-P were used to fabricate uniform coatings on paper and glass by dip coating followed by curation, and post-curation in this chapter. The fabricated coated paper (CP) and glass (CG) are transformed to hydrophobic surface with WCA over 90°. The hydrophobicity increased along with the concentration of the lignin-PDMS polyimines. Compared with glass, polyimines show improved coating adhesion on paper mainly due to the good biocompatibility between lignin and cellulose, and improved hydrophobicity due to the higher roughness of paper surface. Moreover, MKL-P coatings exhibit inferior hydrophobicity than MFL-P coatings, which can be explained by the stronger water resistance caused by the higher crosslinking density and M_w of MFL-P. Both CP and CG showed efficient UV blockage and they can be removed in acidic THF efficiently. After removal, the residual substances are mainly lignin on paper while PDMS on glass. The study provides an innovative routine to utilize lignin-based polyimines for hydrophobic coatings.

4.2. Introduction

Hydrophobic coatings, usually coupled with water-resistant, anti-UV light, anti-corrosion, self-cleaning properties and so forth, have displayed various applications and application potentials in packaging, construction, biomedical, automotive, marine and energy industries, etc.[77]

Our prior study exhibited that the synthesized lignin-PDMS polyimines to be applied for translucent, anti-UV, repairable, and removable hydrophobic coatings. Besides, lignin structures cause variations in the structures and properties of synthesized lignin-PDMS polyimines which could further influence the coating performances. Considering the great demand in paper-based packaging industry (such as food and beverage packaging) and good biocompatibility between lignin and cellulose, paper was used as the main substrate to evaluate the coating performances of synthesized MKL-P and MFL-P polyimines in this chapter. It is expected that the lignin-PDMS polyimines would be coated on paper a with good coating adhesion; meanwhile, the various coating performances of MKL-P and MFL-P will provide insights for a better design of coating formulas. Moreover, due to the DCPN structures of lignin-PDMS polyimines, it is hypothesized that the polyimine coatings could be less difficult to be chemically removed and repaired.

Herein, dipping coating (easy to operate in lab scale) and followed by hot press processes were used to prepare the coatings with MKL-P and MFL-P on two substrates including cellulose-based paper sheet and glass slides (as a comparison) in the present study. The basic coating performances including hydrophobicity, adhesion, thickness, surface density, and UV-blocking ability were evaluated. The removability and repairability of the coatings were also assessed.

4.3. Materials and Methods

4.3.1. Preparation of coating agents

The coating agent was prepared by pre-reacting 1 g MKL (~ 6.99 mmol ketones) and 9.74 g PDMS (~ 6.99 mmol amines) in 50 mL THF at 80 ℃ for 24 h to obtain MKL-P/THF solutions for the first-step dip coating. MFL-P/THF solutions were prepared with the same method.

4.3.2. Preparation of hydrophobic coatings

The coatings are fabricated as displayed in Figure 4-1 by modifying a previous report[49]. The substrates paper and glass slides were dip coated in polyimines/THF solutions for 6 h, followed by solvent evaporation in fume hood overnight. Subsequently, coated substrates are cured under 130 ℃ for 6 h, and then post-cured under 150 ℃ for 2 h under 1 MPa using a hot press machine. The obtained products are coated paper (CP) and glass (CG) with MKL-P and MFL-P, respectively, *i.e.,* CP-MKL-P, CP-MFL-P, CG-MKL-P, and CG-MFL-P.

4.3.3. Characterizations of fabricated coatings

The hydrophobicity was measured with WCA using a goniometer (Ramé-Hart Instrument Co., USA) under RT for three times to record the average and standard deviation. The coating adhesion level was measured using ASTM D3359-17 (Test method B).[173] The surface density is the added weight of substrates after coating per area unit. The thickness is obtained by subtracting the thickness of neat substrates from the thickness of coated substrates. Five points were taken to calculate the mean and standard deviation values of the thickness. The UV-shielding ability will be determined by the UV transmittance under different light wavelength (200 - 800 nm) using an Evolution 60S UV-vis spectrometer (Thermo Fisher Scientific, USA) to obtain plots of UV-light transmittance against wavelengths.

The chemical degradability of lignin-PDMS polyimine film (MFL-P was selected as an example due to its higher MW) was tested by referring a prior study.[15] MFL-P films (~

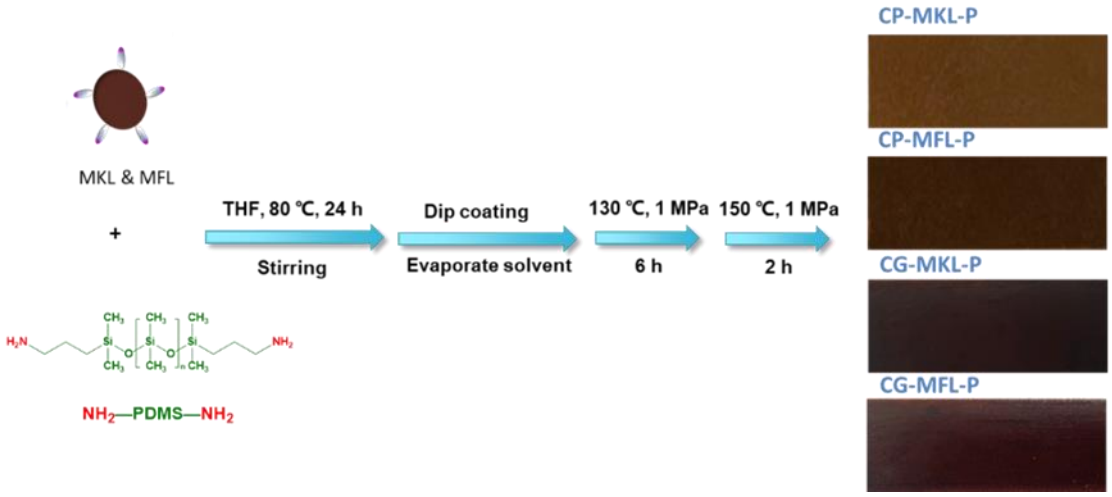


Figure 4-1 The procedures to prepare polyimine coatings on paper and glass slides

1 * 1 cm, ~ 40 mg) was placed into 10 mL of HCl/THF solutions with different concentrations of 0.1, 0.5, 1.0, 1.5, and 2.0 M at 80 °C under 400 rpm stirring, respectively, until they were fully degraded. Every 24 h, the residual films were removed and dried at 60 °C overnight under reduced pressure to record the dried weight and placed into the new solvents. The weight loss (%) was defined as the equation below:

$$\text{Weight loss (\%)} = 100\% \times (w_0 - w_1)/w_0$$

where w_0 and w_1 are the weight of polyimine films before and after degradation, respectively. The degradability was evaluated by the weight loss as a function of time.

The removability[49] of fabricated coatings was evaluated by the reduced thickness, surface density, and hydrophobicity of coatings after removal by immersing the lower half of the CP and CG under 0.1 M HCl solution/THF solutions for 130 ℃, compared with coatings before removal.

4.4. Results and discussion

4.4.1. Coating performances of polyimines

The MKL-P and MFL-P polyimines can be coated on paper and glass slides to form uniform coating surfaces by dip coating and hot press (Figure 4-1). During the dip coating, pre-reacted lignin-PDMS solutions were gelatinized after THF evaporation. The gelation was formed by the Schiff-base reactions between the ketones in modified lignin and the amines in PDMS, which was thoroughly investigated in the previous chapter. Followingly, the gel-like products were further crosslinking polymerized during curation and post-curation at 130 ℃ and 150 ℃ under heat and pressure, forming uniformed and brown-color coating surfaces on paper and glass. It is expected that the final products do not contain any solvent residuals.

Firstly, the coating hydrophobicity differs from the four fabricated coatings and is influenced by the concentrations of coating reagents. Figures 4-2 shows that 1) as the concentration of coating agents increases, the hydrophobicity improves; 2) the MFL-P coatings (WCA up to 129°) have higher hydrophobicity than that of MKL-P (WCA up to

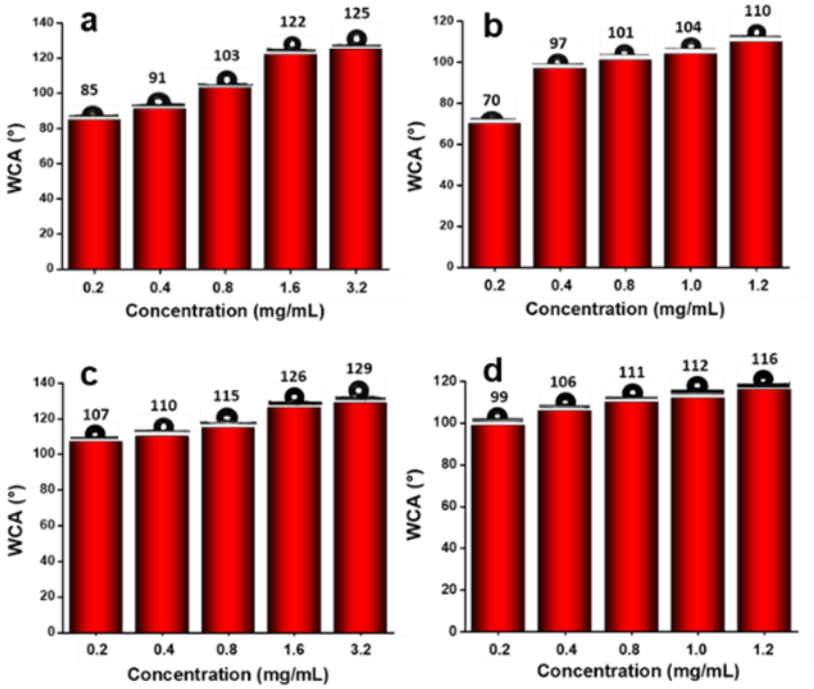


Figure 4-2 WCA of CP coated with MKL-P (a) and MFL-P (c), and CG coated with MKL-P (b) and MFL-P (d)

125°) on both paper and glass; 3) the coated paper (WCA up to 129°) exhibits higher hydrophobicity than coated glass (WCA up to 116°). The higher hydrophobicity of MFL-P coatings than MKL-P coating may be due to the higher water-resistance caused by compact structures of higher crosslinking degree. The higher hydrophobicity of coated paper than coated glass can be explained by the rougher surface texture of paper. Moreover, the coating adhesion of both MKL-P and MFL-P reaches 5B level (with 0% area damaged after tape peeling) on paper (Figure 4-3). The better adhesion of polyimines to paper than glass may be because of the better biocompatibility between lignin and cellulose fibers due to the similar surface groups. Lastly, the coatings also show excellent UV-blocking ability, which can shield UV light with wavelength between 200 nm and 400 nm completely, which is benefited from the lignin incorporation. (Figure 4-4).

4.4.2. Chemical degradation of polyimines

To evaluate the removable potential of the coatings, chemical degradation of MFL-P, with a higher crosslinking density and M_w, was tested by immersing in acidic THF. Results show that MFL-P can be chemically degraded completely in 1.5 M and 2 M HCl/THF solution within 2 h under 130 ℃ with 100% mass losses (Figure 4-5b). As we can observe in Figure 4-5a, the MFL-P film in acidic THF starts to degrade after the application of heat, and the degradation degree is intensified as time moves forward. After 2 h, the films are fully degraded in 1.5 M and 2 M HCl/THF solutions, while still leave pieces in 0.1 M, 0.5 M, and 1 M HCl/THF solutions.

4.4.3. Coating removability of polyimines

To measure the removability of the lignin-PDMS coatings, CP and CG are washed using the conditions tested from chemical degradation experiment to remove the coated polyimines. Figure 4-6 demonstrates the half unremoved and half removed coatings on paper and glass. The removal of the coatings was testified to occur after immersing in 1.5 M HCL/THF solution under 130 ℃ for 2 h, the thickness, surface density, and WCA of polyimine coatings on CP and CG dropped significantly compared with unremoved

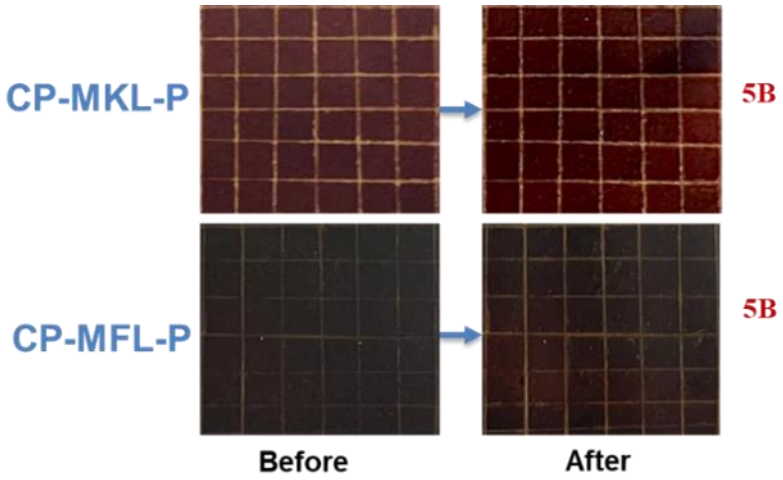


Figure 4-3 Coating adhesion of lignin-PDMS polyimines on paper

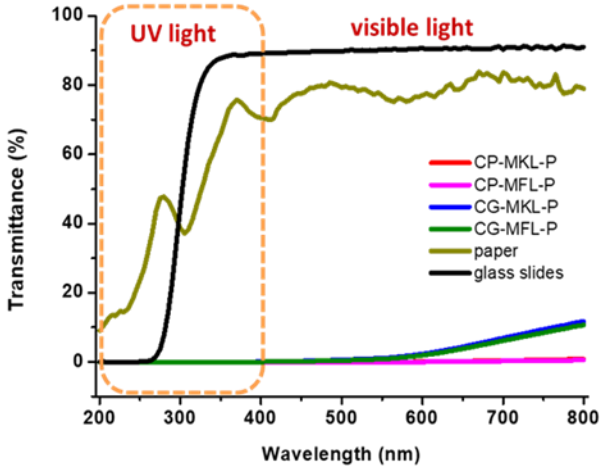


Figure 4-4 UV-blocking ability of paper and glass coated with and without lignin-PDMS polyimines

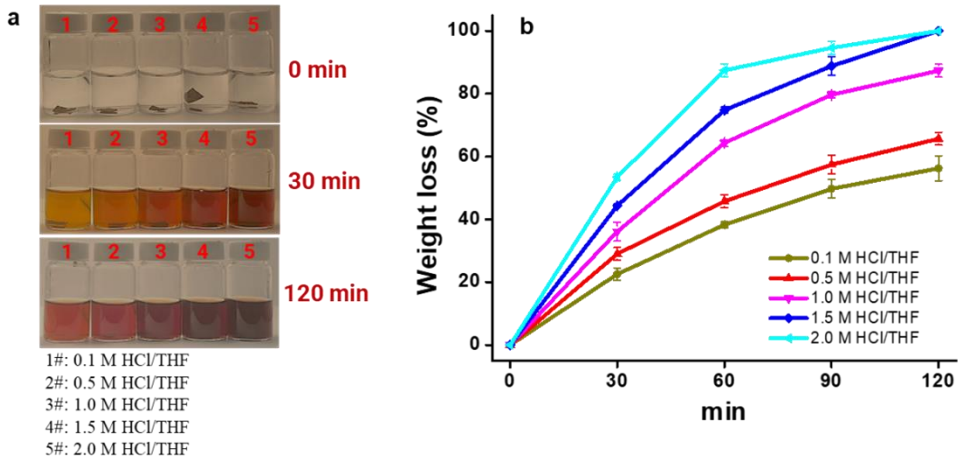


Figure 4-5 Chemical degradation of lignin-PDMS polyimines

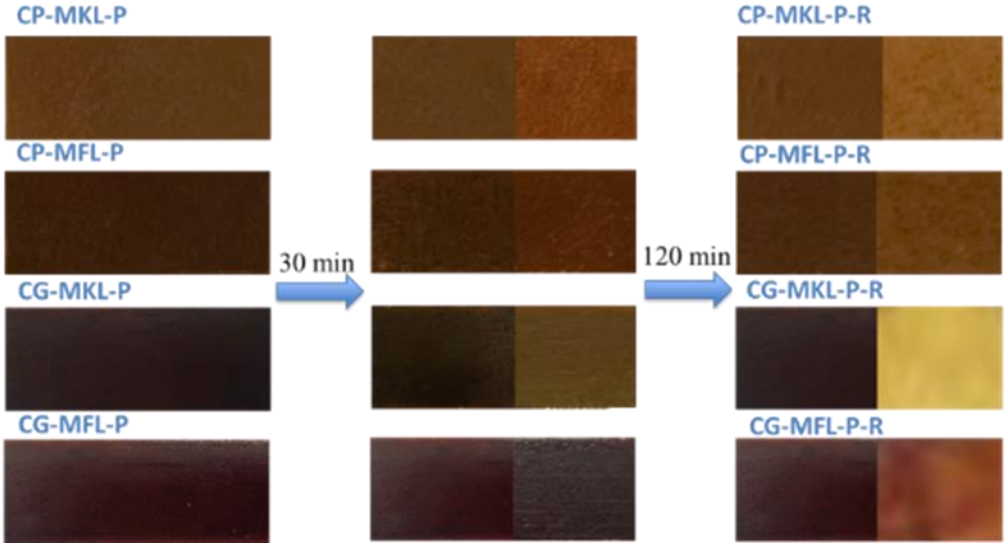


Figure 4-6 Removability of lignin-PDMS polyimine coatings

coatings (Table 4-1). The residues on coated paper are mainly lignin, while mainly PDMS on the coated glass after removal. Therefore, we propose that lignin-PDMS polyimines are expected to prepare a hydrophobic coating with removability.

4.5. Conclusions

The synthesized lignin-PDMS polyimines including MKL-P and MFL-P can be applied for uniform hydrophobic coatings on paper and glass by dip coating followed by curation, and post-curation in this chapter. The fabricated CP and CG are transformed to hydrophobic surface with WCA over 90°. The hydrophobicity increases as the concentration of the lignin-PDMS polyimines increases. Compared with glass, polyimines show improved coating adhesion on paper due to the good biocompatibility between lignin and cellulose, and improved hydrophobicity due to the higher roughness of paper surface. Moreover, MKL-P coatings exhibit inferior hydrophobicity than MFL-P coatings, which can be explained by the stronger water resistance caused by the higher crosslinking density and M_w of MFL-P. Both CP and CG can be removed in acidic THF under 130 ℃ and block UV light efficiently. After removal, the residual substances are mainly lignin on paper while PDMS on glass. This study indicates the feasibility of lignin-PDMS polyimines to be applied for hydrophobic coatings on cellulose-based substrates.

Table 4-1 Coating properties of lignin-PDMS polyimines on paper and glass before and after removal

Samples	Thickness (μm)	Surface density (mg/cm^2)	Adhesion level	WCA (°)
paper	101±3	0.00	N/A	N/A
Glass slide	1005±0	0.00	N/A	13
CP-MKL-P	285±10	6.38±0.04	5B	125
CP-MFL-P	334±9	7.20±0.05	5B	129
CG-MKL-P	1187±6	3.27±0.07	2B	110
CG-MFL-P	1202±5	3.57±0.02	3B	116
CP-MKL-P-R	167±2	1.63±0.01	N/A	70
CP-MFL-P-R	183±3	2.01±0.04	N/A	75
CG-MKL-P-R	1026±1	0.21±0.01	N/A	72
CG-MFL-P-R	1034±1	0.25±0.00	N/A	82

Note: The data are in a form of mean ± standard deviation

CHAPTER V

ROBUST SUPERHYDROPHOBIC COATINGS WITH LIGNIN-PDMS POLYIMINE CROSSLINKING NETWORK AND LIGNIN MICRO-NANOSPHERES

A version of this chapter is originally written and considered for submission as:

Xie D., Alipanahrostami M., Wang W., Harper D., Pu Y., Ragauskas A. J., Li M. (2024). Robust Superhydrophobic Coatings with Polyimine Crosslinking Network and Lignin Micro-nanospheres.

Author contributions are listed as follows. D.X.: conceptualization, methodology, investigation, formal analysis, data curation, writing-original draft. M.A.: investigation, writing-review and editing. W.W.: resources, writing-review and editing. D.H.: resources, writing-review and editing. Y.P.: resources, writing-review and editing. A.R.: resources, writing-review and editing. M.L.: conceptualization, methodology, supervision, validation, writing-original draft, project administration, and funding acquisition.

5.1. Abstract

Superhydrophobic coatings, usually coupled with water-resistant, self-cleaning, non-fouling properties and so forth, are promising to be applied for construction, packaging, and automotive industries, etc. However, the use of toxic fluorocarbons or non-degradable inorganic materials causes heavy environmental burdens. Herein, a two-step coating process using dip coating of lignin-polydimethylsiloxane crosslinked polymer networks and drop casting of LMNS was used to fabricate hydrophobic coatings on cellulose-based substrates including wood, paper, and fabric. Results show that the water contact angle reaches up to 173° and the roll-off angle low to 5° on coated cross-section of wood block (WB-C) with excellent self-cleaning ability. Multiple daily liquids including 5wt% NaCl aqueous, tea, coffee, and milk can also be repelled efficiently. The liquid repellency of the coatings is not only related with the coating process, but the natural textures of substrates. Durable superhydrophobic coating surface was successfully fabricated on WB-C, exhibiting outstanding resistance to tape peeling, knife scratch, waterdrop impact, water and medium-alkaline impregnations. Furthermore, the coatings can bring extra UV-blocking ability, improved thermal stability and stiffness of paper and fabric. The current study proposed a novel, simple, efficient, and environmentally friendly method of superhydrophobic coatings on cellulose-based substrates to be applied in construction and food packaging materials.

5.2. Introduction

In wood science, bionics has been integrated to overcome the limitations of raw wood including poor resistance to moisture, harsh chemical and high-temperature environment, deformation, decay, etc.[83, 84, 174] Superhydrophobic coating technologies on wood have been investigated to improve wood quality and extend wood serve life.[84, 174, 175] However, to lower down the surface energy and construct hierarchical micro-nano surface structure, fluorocarbon, petroleum-based additives, and inorganic nanomaterials are commonly used. For example, Yang et al. manufactured robust superhydrophobic wood surfaces using a polyethylene glycol-functionalized SiO_2/poly(vinylalcoho1)/poly(acrylic acid)/fluoropolymer hybrid coating to establish a micro-nano binary rough surface on the cross-section of *fraxinus chinensis* Rob wood.[174] Tu et al. fabricated mechanically stable, self-cleaning superhydrophobic wood surface using spray coating of perfluoroalkyl methacrylic copolymer/TiO_2 nanocomposites after polydimethylsiloxane pre-coating.[84] The above coating agents containing toxic and undegradable materials are hazardous to our eco-system. The negative environmental impact urges researchers to seek biodegradable, organic, natural materials such as lignin[6, 59], cellulose[176], chitosan[177] and so on, etc. as alternatives. Thereof, lignin features natural hydrophobicity, wet stability, good thermal stability, and excellent anti-UV/antioxidant activities, making it a good candidate to construct bio-based hydrophobic coatings.

To apply KL for hydrophobic coatings, hydrophobic modification is typically needed. Reported lignin hydrophobization methods include esterification with long-chain alkyls[58], silanization[14], lignin nanosizing[59], lignin (catalytic) pyrolysis[61], etc. Lignin esterification takes advantage of the newly formed ester groups, and other grafted non-polar groups such as alkyls, ethers, etc. from the esterification agents to increase the hydrophobicity of modified lignin. For example, Singam *et al.* esterified lignin with propionic acid, and then coated esterified lignin-cellulose acetate blends on paper sheets to achieve a hydrophobic coating with a WCA over 130°.[62] In another study, Antoine *et al.* esterified lignin with phoretic acid, and then synthesized with amines to obtain lignin-based benzoxazines thermosets for hydrophobic coatings on glass, showing a WCA up to 91°.[19] However, the

hydrophobicity of modified lignin closely relates to the surface properties of esterifying agent, so the hydrophobicity is hard to be enhanced significantly. Therefore, further reducing surface energy and surface roughening are still required.

A widely used method to reduce surface energy is to introduce low-surface-energy chemicals like silica and/or siloxane to decrease the surface energy. For instance, a lignin-based polyurethane coating was prepared through covalent immobilization of polydimethylsiloxane as a de-wetting agent, which can repel water (WCA up to 105 °), self-clean, and block UV light. In another study, KL was modified by a silylating agent containing silane groups through the reaction of the OHs and isocyanate groups, which greatly improved the hydrophobicity, rubber compatibility, rubber dispersibility of lignin.[14] Even though the hydrophobicity is greatly improved, it is still far away from super-hydrophobicity due to the lack of rough surface microstructures.

LMNS, formed by self-assembly of lignin molecules, possess a spherical morphology with a hydrophobic core and hydrophilic surface. We herein hypothesize that LMNS could be used to replace, or even perform better than, inorganic micro-nano fillers for superhydrophobic coatings on wood for the following reasons: 1) LMNS deposition and/or anchor could have a surface roughening effect on wood surface by the formation of hierarchical micro-nano morphology to enhance the hydrophobicity to coatings[6]; and 2) LMNS have better interfacial compatibility and bonding with hydrophilic cellulose-based substrates than inorganic particles to enhance the mechanical durability of coatings.[178] So far, a few studies used LMNS to fabricate superhydrophobic coatings. For example, LMNS was prepared by self-assembly and hydrothermal treatment to coat on a silicon board to form a superhydrophobic surface with WCA up to 151.9°.[59] For another example, Ma *et al.*'s fabricated a LMNS-based superhydrophobic wood with WCA up to ~ 164° and multiple advanced properties like self-cleaning, excellent mechanical and organic solvent stability, great photothermal effect, antibacterial activity, etc.[6] Although the above reports present that LMNS allows for functional superhydrophobic coatings, the relevant investigations is still scarce.

Our prior study shows that LA modified KL with grafted ketone groups could successfully synthesize with bis(3-aminopropyl)-terminated Polydimethylsiloxanes to form crosslinked polyimine networks *via* imine condensations, exhibiting a great potential in anti-UV, translucent, hydrophobic coatings. However, the hydrophobicity and coating stability remain to be enhanced. In this study, robust superhydrophobic coating surface is expected to be constructed with by the combination of lignin-PDMS crosslinking polyimine networks and LMNS. Lignin-PDMS polyimine coating agent was prepared by reacting MKL and PDMS in THF for dip coating. LMNS were prepared from KL by solvent-antisolvent exchange, and then dispersed in ethanol for drop casting. The robust superhydrophobic coating surfaces are expected to be fabricated by successive dip coating, drop casting, curation, and post-curation steps on wood, paper, fabric, and glass slides.

5.3. Materials and Methods

5.3.1 Materials

Indulin AT softwood KL was provided by MeadWestvaco (Richmond, VA, USA). γ-valerolactone (GVL), glycerol, LA, PDMS (number-average molecular weight: ~ 2500 Da), THF, ethanol, nonane, octane, heptane, hexane, acetone, acetonitrile, ethyl acetate, and dichloromethane were purchased from Sigma Aldrich (St. Louis, MO, USA). Wood block and chip is Balsa wood purchased from Fisher Scientific. Paper is standard A4 paper purchased from Georgia Pacific LLC. Fabric made of poly-cellulose is cleanroom wipes purchased from Fisher Scientific. All chemicals and materials were used as received.

5.3.2. Preparation of LMNS

The LMNS was prepared using the method reported by Wang et al.[179] Briefly, KL was fully dissolved in GVL in a concentration of 20 mg/mL, and then added to glycerol with a GVL/glycerol volume ratio of 1:4, followed by constant stirring (200 rpm) under 80 ℃ for 12 h to form a homogeneous solution. Afterwards, the solution was cooled down to room temperature (RT) and added to deionized (DI) water with a GVL/water volume

ratio of 1:4 quickly under 200-rpm stirring. The LMNS were obtained by successive centrifugation (8,000 rpm, RT) for 10 min, water washing for 3 times, and vacuum-drying overnight.

5.3.3. Preparation of coating agents

There were two coating reagents used in this work. Firstly, KL was modified with LA to graft active ketone groups using a reported method to get MKL.[150] Followingly, 1 g MKL (~ 6.99 mmol ketones) and 9.74 g PDMS (~ 6.99 mmol amines) were reacted in 50 mL THF at 80 ℃ for 24 h to obtain MKL-P/THF solutions. MKL-P/THF solutions at a concentration of 214.8 mg/mL were prepared by THF dilution as the first coating agents. The second coating agents were prepared by suspending LMNS in ethanol at concentrations of 0.5 mg/mL using sonication for 5 min.

5.3.4. Preparation of superhydrophobic coatings

The coatings were fabricated as displayed in Figure 5-1. The two-step coating includes dipping coating in MKL-P/THF solutions for 6 h first, and physical deposition of LMNS/ethanol suspensions followed by solvent evaporation in fume hood overnight. Subsequently, coated substrates are cured under 130 ℃ for 6 h, and then post-cured under 150 ℃ for 2 h in an oven with reduced pressure. The coating substrates used in this work are wood block (WB), wood chip (radical section, WC), fabric, and paper. Glass slides were also used for substrates as comparisons. During dip coating, WB was bottom-up soaking from the cross sections. Control 1 is prepared with the same-concentration PDMS/THF solutions replacing MKL-P/THF solutions in the dip coating, with other steps the same as above prepared products. Control 2 is prepared with the same procedures shown in Figure 5-1 excluding the LMNS/ethanol deposition step. The cross-, tangential-, and radical-sections of coated WB are named as WB-C, WB-T, and WB-R, respectively. The coated (and neat) wood chip, paper, fabric, and glass slides are named as CW (NW), CP (NP), CF (NF), and CG (NG), respectively.

5.3.5. Characterizations of LMNS and superhydrophobic coatings

The particle size distribution of prepared LMNS was measured using a Zetasizer Nano-ZS series instrument (Malvern Instruments Ltd., Worcestershire, UK) by suspending o.d. LMNS in DI water at a concentration of ~ 1 mg/mL under RT for triple scans to obtain the average and standard deviation.

Fourier Transform infrared spectroscopy was used to characterize the structural features of LMNS and functional groups on coating surface. The FTIR spectra of samples were recorded by a FTIR spectrometer (Spectrum One FTIR system, PerkinElmer, Wellesley, USA) under wavenumbers from 4,000 cm^{-1} to 500 cm^{-1} with a resolution of 4 cm^{-1} for 32 scans.

For statistical analysis, all data were processed using software including OriginPro 8.5 (OriginLab Corporation, Northampton, MA, USA) and Excel 2016 (Microsoft, Redmond, WA, USA).

The CA and ROA of coating surface were determined using a goniometer (Ramé-Hart Instrument Co., USA) under RT for three times to record the average and standard deviation. The volume of liquid, including water, 5wt% NaCl aqueous, milk, tea, and coffee drops is 8 μL for CA and 10 μL for ROA.

The self-cleaning behavior[180] of the coating surfaces is recorded by the goniometer. The dust silica powder was placed on the surface of the coatings by a tweezer. Water drops injected by a syringe needle were fallen by gravity on the silica-contaminated surface of coated wood that was tilted 10° to the horizontal.

The dispersive (γ_d) and specific (γ_{sp}) surface energies of samples were measured by an inverse gas chromatography (iGC) surface energy analyzer (SEA) equipped with a flame ionization detector (Surface Measurements Systems, Ltd, Alperton, UK).[150] Non-polar (nonane, octane, heptane, and hexane) and polar (acetone, ethanol, acetonitrile, ethyl acetate, and dichloromethane) probe molecules were injected successively under surface coverage from 0.01 n/nm to 0.4 n/nm. Data were analyzed by advanced SEA analysis software (Advance Version 1.4.2.0).

The surface morphology of gold sputtered LMNS and coated substrates was detected

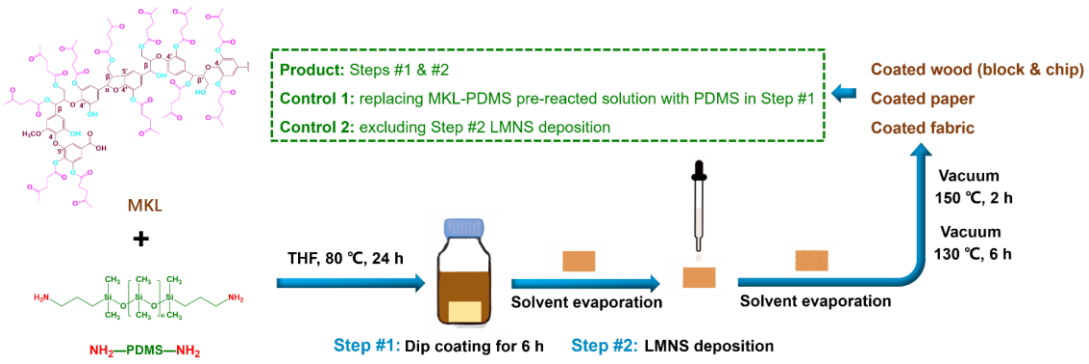


Figure 5-1 Schematic diagram of the preparation of coatings on wood, paper, fabric, and glass slides. MKL: modified kraft lignin; PDMS: polydimethylsiloxane; THF: tetrahydrofuran; LMNS: lignin micro-nanospheres

by a Zeiss EVO scanning electron microscopy (SEM, Zeiss group, USA). The surface element compositions were measured by an energy dispersive X-ray spectroscopy (EDS, Zeiss group, USA) connected to SEM.

The ultraviolet (UV)-blocking ability of the coatings was evaluated by an Evolution 60S UV-vis spectrometer (Thermo Fisher Scientific, USA) using a plot of UV-light transmittance against wavelengths from 200 to 800 nm.

Thermal gravimetric analysis (TGA) was conducted using a Q-50 thermogravimetric analyzer (TA Instruments, USA) by the combustion of samples from 30 to 800 ℃ at a rate of 20 ℃/min under N_2. The heating temperatures against weight losses of samples during burning are recorded as TGA curves and derivative TGA curves (DTG) were analyzed by Universal Analysis 2000 software.

The mechanical stability of coatings was evaluated by knife scratch[70], tape peeling[181], and waterdrop impact[70] tests. The coating surface was scratched 10 times horizontally and 10 times diagonally by a blade. The polyester tape (3M 850, Minnesota, USA) was adhered on the coating surface by rolling a metal rod on the coating surface twice, and then peeled by hand in a constant gesture and speed as a cycle. New tape was used every cycle. The waterdrop height is 5 cm and speed is ~ 2 drops per second.

The water stability[70] was assessed by comparing the WCA of the coatings before and after immersing the wood blocks in DI water for 5 min, 10 min, 1 h, 1.5 h, 3 h, 6 h, 12 h, 24 h, 48 h, and 72 h. The chemical stability[180] was evaluated by comparing the WCA of the coatings by immersing the coatings in the liquids with different pH values (1, 6, 9, and 13) for 12 h.

The Young's modulus, maximum tensile strength, and extension (tensile strain at the maximum tensile strength) of CP, CF, NP, and NF was measured using an Instron 5943 universal tensile tester (Instron Co., USA) according to the standard ASTM 882-10.[182] The samples were cut into a rectangle shape (5 × 1 cm), and tested by being stretched with an initial grip separation distance of 3 cm and a crosshead speed of 50 mm/min at RT. The average values of five replicates are reported.

5.4. Results and discussion

5.4.1. LMNS formation

To enhance the coating hydrophobicity, surface roughening with micro- and nano-particles would play a key role.[183] Herein, LMNS, prepared from industrial waste KL by self-assembly, is hypothesized to be able to increase the water repellency of the coatings in virtue of its micro- and nano- morphology.[81] Additionally, the coating adhesion on cellulosic substrates could also be strengthened due to the stronger interactions between the hydrophilic surface of LMNS and cellulose compared with inorganic nanoparticles like nano-SiO_2[184] or nano-Fe_3O_4[185], or nano-$Cu_2(OH)_3Cl$[180].

In the current study, LMNS was successfully fabricated with solvent exchange using a GVL/glycerol biphasic system and water.[179] Firstly, KL was fully dissolved in GVL, and then homogeneously dispersed in glycerol with the addition of heat. After cooling down to RT, the KL/GVL/glycerol solution was emulsified, leading to the lignin molecules stacked in GVL droplet and the KL/GVL droplets dispersed in glycerol due to the solubility of KL in GVL and insolubility in glycerol. Followingly, water was added to remove the solvents because of its miscibility with both GVL and glycerol. Thus, LMNS was formed after centrifugation by the self-assembly of stacked lignin molecules and the cluster-cluster aggregation of lignin molecules *via* hydrophobic interactions, hydrogen bonding, $\pi - \pi$ interactions, and *van der Waals* force.[179, 186]

The solvent exchange does not change the functional groups of LMNS according to the FTIR spectra (Figure 5-2a). The particle size of prepared LMNS ranges from 295 nm to 2,480 nm with an average particle size of 627.3 ± 255.6 nm, which is much smaller than that of KL (3,001.8 ± 1,575.0 nm, Figure 5-2b). The micro- and nano-scale spherical morphology of LMNS was detected in the SEM image (Figure 5-2c).

5.4.2. Enhancement of coating hydrophobicity

The superhydrophobic coatings using LMNS and lignin-based polyimines were successfully prepared on cellulose-based substrates including wood, paper, and fabric

(Figure 5-1). Firstly, MKL was pre-reacted with PDMS in THF for the first step of dip coating. Next, LMNS/ethanol suspension was used for the second step of physical deposition. The two-step coated products were obtained after curing and post curing, during which MKL and PDMS are further crosslinked and LMNS was anchored on the coating surface by the MKL-P polyimine networks. Two controls were prepared as well to investigate the effects of LMNS deposition and polyimine crosslinking network on the coating performances.

To construct superhydrophobic coatings, low-surface-energy chemistry is crucial.[81] The most commonly used low-surface-energy materials such as fluorocarbon or petroleum-based additives are toxic and hazardous to ecosystem.[187] Thus, greener alternatives are highly required. In our prior study, MKL was successfully polymerized with low-surface-energy PDMS to form crosslinked polyimine networks with excellent hydrophobicity, film-forming and anti-UV ability, good translucency, and water stability. Given the great potential in coatings, bio-based polyimines were employed to fabricate (super)hydrophobic coatings in the present study (Figure 5-1). As a result, superhydrophobic surface was achieved on WB-C (WCA=173°, ROA=5°), WB-C-c1 (WCA=158°, ROA=7°), WB-T (WCA=166°, ROA=6°), and CW (WCA=157°, ROA=9°) with their WCA over 150° and ROA below 10° (Figure 5-3a). Moreover, they exhibited self-cleaning behaviors that the silica dust can be carried by free waterdrops when the substrates were 10° tilted from a horizontal plane (Figure 5-3i and Video S3), which provides evidence of a Cassie-Baxter state of the waterdrop.

To study the effect of polyimine crosslinking reaction on the hydrophobicity, controls 1 which were fabricated by replacing polyimines with PDMS in step #1 are compared with their corresponding products. The analyses of variance (ANOVA) results evidence that lignin-PDMS crosslinking significantly affect the hydrophobicity of the coatings (*P*-value ≈ 0.0026 Table 9-1). As displayed in Figure 5-3a, a higher WCA is detected on products compared with their corresponding control 1, which indicates that lignin-PDMS crosslinking polymerization is beneficial to the non-wettability of the coatings. Possible

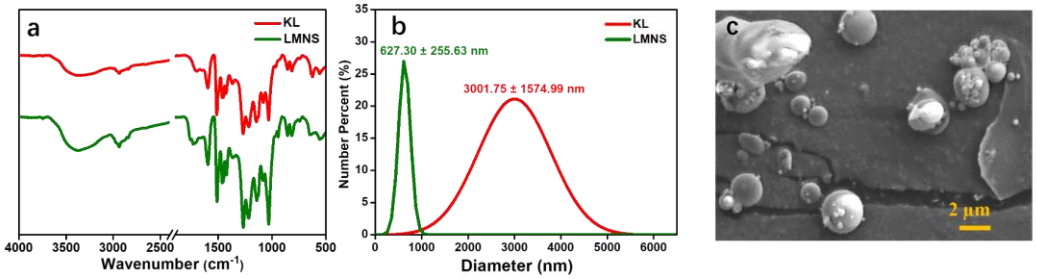


Figure 5-2 FTIR spectra (a) and particle size distribution (b) of KL and LMNS; SEM image of LMNS (c)

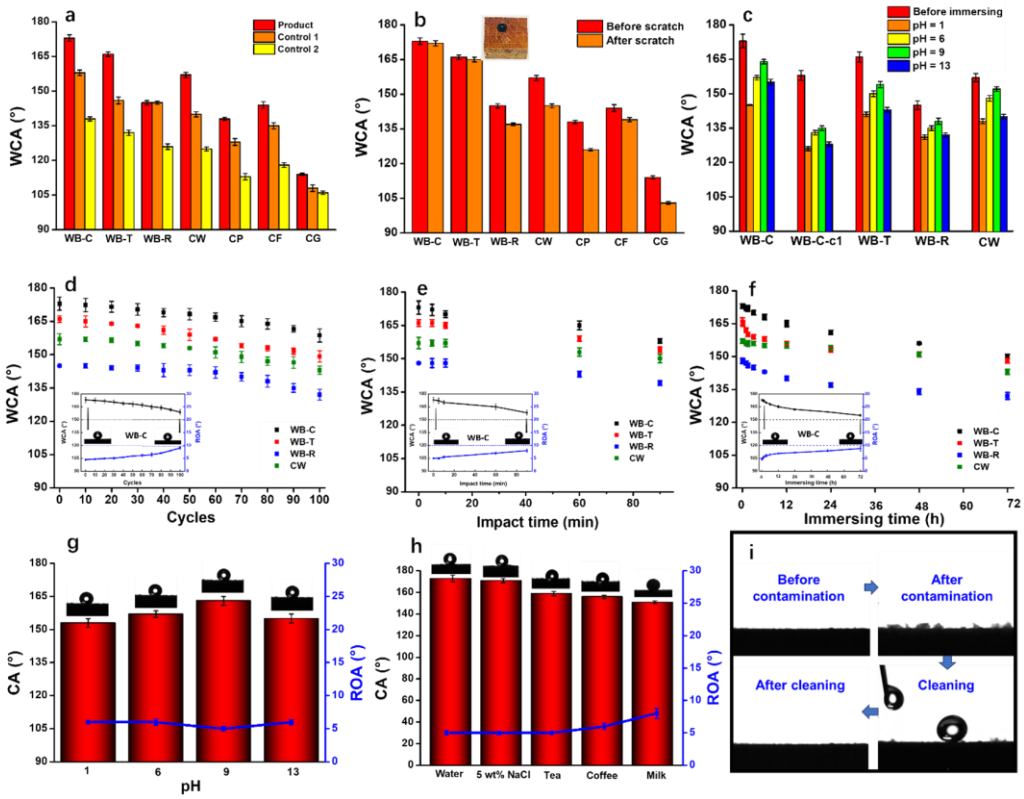


Figure 5-3 WCA of the products and controls of WB-C, WB-T, WB-R, CW, CP, CF, and CG (a); WCA of WB-C, WB-T, WB-R, CW, CP, CF, and CG products before and after knife scratch (b); WCA of WB-C, WB-T, WB-T, and CW products, and WB-C-control 1 (WB-C-c1) after immersing under liquids with different pH values (1, 6, 9, 13) for 12 h at RT (c); WCA of WB-C, WB-T, WB-T, and CW products after different tape-peeling cycles (d); WCA of WB-C, WB-T, WB-T, and CW products under different waterdrop impact time (e); WCA of WB-C, WB-T, WB-T, and CW products after immersing under water at RT for different time (f); CA of WB-C using liquids with

different pH values (g), and different daily liquids (h); self-cleaning silica dust on WB-C. The inserted graph in Figure 5-3b refers to WB-R. The inserted graphs in Figures 5-3d – 5-3f refer to WB-C product.

reasons are 1) the lignin-PDMS polyimines formed a film that could cover the substrate surface. Even if PDMS could lower down the surface energy of controls 1, it is hard for PDMS to self-crosslink (form a film), leading to ununiformed coating surface and weak interactions with surface groups on controls 1. Therefore, the water repellency of the products is superior; 2) the hydrophilic terminal groups -NH_2 in PDMS are freely exposed on the surface of controls 1, while -NH_2 was consumed by the Schiff-base reaction with ketones in MKL, leading to a more hydrophobic surface of products; 3) the compact structures of crosslinking network and high M_w of polyimines provide extra resistance to water affinity on the surface of products.

Together with low-surface-energy chemistry, surface roughness is another key factor to develop superhydrophobic surface.[81, 188] Typically, micro- and/or nano-particles, such as nano SiO_2[189, 190], ZnO[191], TiO_2[192], etc., are used to build up microrough and nanorough surface. Considering the non-degradability of these materials, LMNS, featured with greater biodegradability and biocompatibility with cellulose-based substrates, is expected to be a good alternative due to its micro- and nano-morphology. In this study, the hydrophobicity of prepared coatings was successfully enhanced by the deposition of LMNS. As shown in Figure 5-3a, the WCA of WB-C, WB-T, WB-R, CW, CP, CF, and CG products is higher than those of corresponding control 2 (no LMNS deposition). Besides, the ANOVA further demonstrate that the LMNS deposition in step#2 significantly influences the WCA (hydrophobicity) of the coatings (P-value ≈ 0.0003, Table 9-2). Moreover, the SEM images of products and controls 2 of six coating surface are compared in Figure 5-4. As we can observe, the LMNS was armored on the coating surface in a form of micro- and nano-papillae wrapped by the polyimine film. The surface morphology of products (upper row) exhibits rougher texture than the controls 2 (middle row) which were coated by polyimines exclusively, which also indicates that the deposition of LMNS is mainly responsible for the higher hydrophobicity of products.

Apart from the coating procedures, the surface roughness is also influenced by the surface morphology of neat substrates (lower row in Figure 5-4). Thereof, the cross-section of neat WB is obtained by cutting perpendicular to the growth rings of trees, leading to the

ring-shape edges of cell walls on the surface. Comparing radical- and tangential-sections, although they display similar surface texture, however, tangential section possesses more unregular alignment of fiber cells, vessels, and growth rings, as well as more complexed pattern because it includes both earlywood and latewood with different densities and hardness[193]. Combined with the topography detected in the SEM images (Figure 5-4), we can order the roughness degree of three sections of the balsa wood as cross section > tangential section > radical section, which explains why the WCA of WB-C is the highest, followed by WB-T, and then WB-R (Figure 5-3a). The ANOVA result further suggests that the different wood sections cause significant effect on the hydrophobicity of coated surface (*P*-value ≈ 0.004, Table 9-3). Regarding the two-dimensional (2D) substrates (wood chip, paper, fabric, and glass slide), the coating method proposed in this study shows the highest hydrophobicity on CW product (WCA up to 157°), followed by fabric, paper, and glass slide successively (Figure 5-3a). The ANOVA result also implies that the hydrophobicity of these coatings is significantly different from each other (*P*-value ≈ 0.003, Table 9-4). The variation could be attributed by the fact that 1) the surface textures of neat substrates cause various surface roughness of coated substrates, and 2) the different bonding and adhesion interactions between coating agents and substrates cause variance to the surface energy of the coating surface. Overall, the non-wetting water repellency and self-cleaning behavior of the superhydrophobic coatings could be explained by 1) the irregular arrangement of micro and nanostructures of LMNS, 2) the introduction of low-surface-energy and water-resistant lignin-PDMS polyimine network, and 3) the natural rough texture of the wood sections.

5.4.3. Enhancement of coating durability

The results of tape-peeling tests show that as the peeling cycles increase, the WCA of the coating products, controls 1 and 2 decrease slightly (Figures 5-3d and 9-1), which is attributed to the removal of coatings on the surface and/or the damage of surface texture due to the adhesion and pressure applied by the tapes for multiple times. It's worth noting that the WB-C still maintains a WCA of 158.7° and a ROA of 9° after 100 cycles (inserted

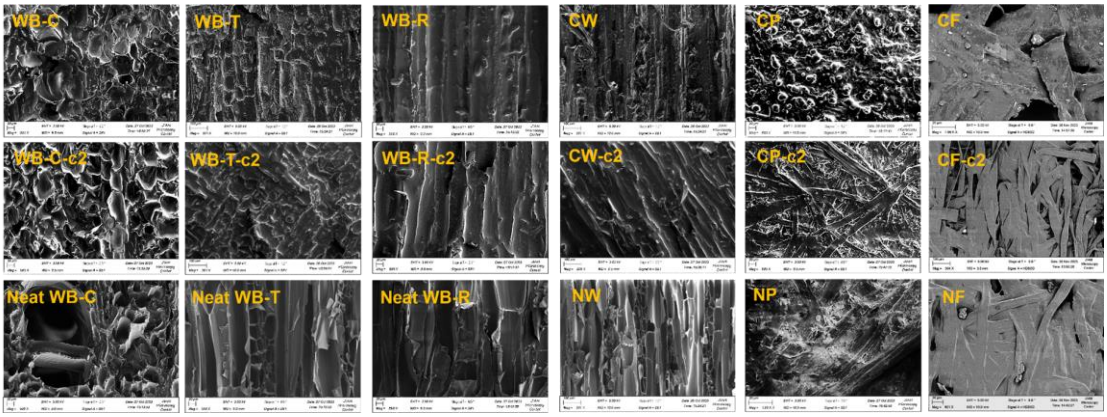


Figure 5-4 SEM images of the products (upper row), control 2 (middle row), and neat substrates (lower row) of WB-C, WB-T, WB-R, CW, CP, and CF

graph in Figure 5-3d), exhibiting a robust superhydrophobicity. As for the knife scratching test, the WCA does not change a lot on the hydrophobicity of coated wood block products, especially WB-C and WB-T, but changes that of coated 2D products (Figure 5-3b). The ANOVA analyses verify that knife scratching did not cause significant impacts on the hydrophobicity (WCA) of coated wood blocks (*P*-value ≈ 0.1367, Table 9-5), whereas caused significant impacts the hydrophobicity of coated 2D substrates (*P*-value ≈ 0.0095, Table 9-6). The results further support that a robust superhydrophobic surface was obtained on coated wood block in this study.

To further investigate the effect of coating processes on the mechanical stability of the coatings, the WCA decreasing percentages after 100-cycle tape peeling and 1.5-h waterdrop impact of products, controls 1 and 2 were calculated in Table 5-1. As we can see, the decreasing percentage of the WCA after 100 cycles (compared with 0 cycles) of WB-C products is obviously lower than that of WB-C-c1 (8.27% vs. 25.32%). The same phenomenon is observed between WB-T (10.12% vs. 19.86%), WB-R (8.96% vs. 24.83%), and CW (8.92% vs. 17.86%), compared with their corresponding control 1 where lignin-PDMS/THF solution was replaced by PDMS/THF solution in step #1 (Table 5-1). It implies that the crosslinking network of polyimines could enhance the mechanical stability of the coatings. Possible reason is that the crosslinked network structures of lignin-PDMS polyimines with higher molecular weight and covalent bond density than pure PDMS provide stronger resistance to tape peeling. However, the WCA decreasing percentages of products after 100 cycles is not obviously lower than those of their corresponding controls 2 (no LMNS deposition), suggesting that LMNS plays limited role in enhancing the coating mechanical robustness. These findings could also be supported by the decreasing percentages of the WCA after 1.5-hour waterdrop impact between WB-C, WB-T, WB-R, and CW, and their corresponding controls 1 (Table 5-1). Thereof, WB-C and WB-T still maintain superhydrophobic surface with WCA above 150° and ROA below 10° even after 80-cycle tape peeling and 1.5-hour waterdrop impact herein (Figures 5-3d, 5-3e, 9-1c and 9-2c).

Table 5-1 Decreasing percentage (%) of WCA of coated woody substrates after 100-cycle tape peeling and 1.5-h waterdrop impact

Samples	WB-C			WB-T			WB-R			CW		
	prod.	c1	c2	prod.	c1	c2	prod.	c1	c2	prod.	c1	c2
Decreasing percentage of WCA after 100-cycle tape peeling	8.27	25.32	8.70	10.12	19.86	4.55	8.97	24.83	8.73	8.92	17.86	4.00
Decreasing percentage of WCA after 1.5-h waterdrop impact	4.62	22.78	2.90	4.22	19.18	3.79	5.41	21.38	1.59	2.55	25.00	1.60

Secondly, the chemical resistance of prepared polyimines-LMNS coatings to acidic (pH = 1 and 6) and strong alkaline (pH = 13) liquids is relatively weaker than that to medium alkaline (pH = 9, Figure 5-3c). It could be explained by the fact that the imine bonds can be disassociated by the H^+ in acidic medium[47], while LMNS is unstable in strong alkaline, leading to the destructions of polyimine networks and micro-/nano- surface morphology. Finally, the hydrophobicity of the coating samples declined. Overall, the prepared coatings are more chemically resistant to alkaline medium with a pH value around 9. The results can also be advocated by the CA of liquids with different pH values on WB-C surface (Figure 5-3g).

Thirdly, the water stability of the coatings is also outstanding in this study, especially WB-C whose WCA is 155.2° and ROA is 9° after 72-hour immersing under water (Figure 5-3f). The WCA and ROA of WB-T is 150.1° and 11°, respectively, after 72-hour immersing under water (Figure 9-3). The water-proofing ability of the coatings is prominently due to the formed water-resistant polyimine films fill the pores and cover the hydrophilic groups (such as hydroxyls) on the cellulose-based substrate surface. The water resistance of polyimine films mainly derives from the introduction of low-surface-energy PDMS that repels water affinity, and the high crosslinking density of lignin-PDMS networks that prevents water penetration. In general, the mechanical-, water-, and chemical-stability of prepared coating products were enhanced prominently due to the crosslinked polyimine networks. Lastly, the WB-C also shows superhydrophobicity when repelling multiple daily liquids including 5wt% NaCl aqueous, tea, coffee, and milk efficiently (Figure 5-3h), exhibiting great application potentials in food packaging and household furniture.

5.4.4. Characterization of coatings

To further investigate the possible physiochemical changes during coating process, multiple characterization methods were applied on the coating products and their neat substrates. Firstly, signals of Si-O bond in PDMS appear at ~ 1256 cm^{-1}, and the signals of hydroxyl groups become less obvious in the FTIR spectra of CW, CP, and CF, compared with those of NW, NC, and NF (Figure 5-5a). Regarding the signal of aromatic rings in

lignin, it is located at 1592 cm^{-1} in the FTIR spectra of both CW and NW (Figure 9-5a), while newly shows up at ~ 1598 cm^{-1} in FTIR spectra of CP and CF, compared with NP and NF, respectively (Figure 9-5b). As for the signals of imine bond, weak shoulders at ~ 1660 cm^{-1} show up in the FTIR spectra of CW, CP, and CF (Figure 9-5). All above observations suggest that the lignin-PDMS polyimines were successfully coated on the wood, paper, and fabric substrates. It's worth noting that ketone groups in MKL can still be detected at ~ 1705 cm^{-1} in the FTIR spectra of coatings, which alerts us that the feedstock ratio of the coating agents still needs to be improved to make sure all ketones are consumed. Another detail needs to be pointed out is that minor peaks appear at ~ 1685 cm^{-1} in the FTIR spectra of both CP and CF (Figure 9-5b), which could be the amides formed by the coupling reaction between carboxylic groups on paper and fabric surface and amines in PDMS.[194, 195]

The EDS spectra exhibit that C, O, Si are main elements on coatings, while C and O are main elements on neat substrates (Figure 5-5b). Moreover, the normalized atomic concentration of Si is obviously higher than that of uncoated wood, paper, and fabric (Figure 5-5b and Table 5-2), suggesting that the fabricated coatings carry PDMS. Due to the relatively low concentration of imine bonds, the atomic concentration of detectable N is negligible on coatings (Table 5-2).

The fabricated CW, CP, CF, and CG display excellent anti-UV ability. The transmittance of UV-A (wavelength: 400 - 320 nm), UV-B (wavelength: 320 - 280 nm) and UV-C (wavelength: 280 - 200 nm) light is 0% for all four tested coatings (Figure 5-5c). Their enhanced UV-blocking ability is brought by the conjugated C=C double bonds, unsaturated ethylene groups, and condensed structures in lignin.[143]

The mechanical performances of paper and fabric vary before and after coating. The stiffness of CP and CF is much higher than that of NP and NF, respectively (Table 5-3). The stress-strain curves exhibit that the maximum tensile strength of CP is approximately doubled compared with that of NP (12.9 ± 1.8 MPa vs. 6.6 ± 0.5 MPa), while the maximum tensile strength of CF is close to that of NP (7.2 ± 1.1 MPa vs. 7.3 ± 0.8 MPa, Figure 5-5d and Table 5-3). However, the tensile strain at maximum tensile stress of CP and CF is

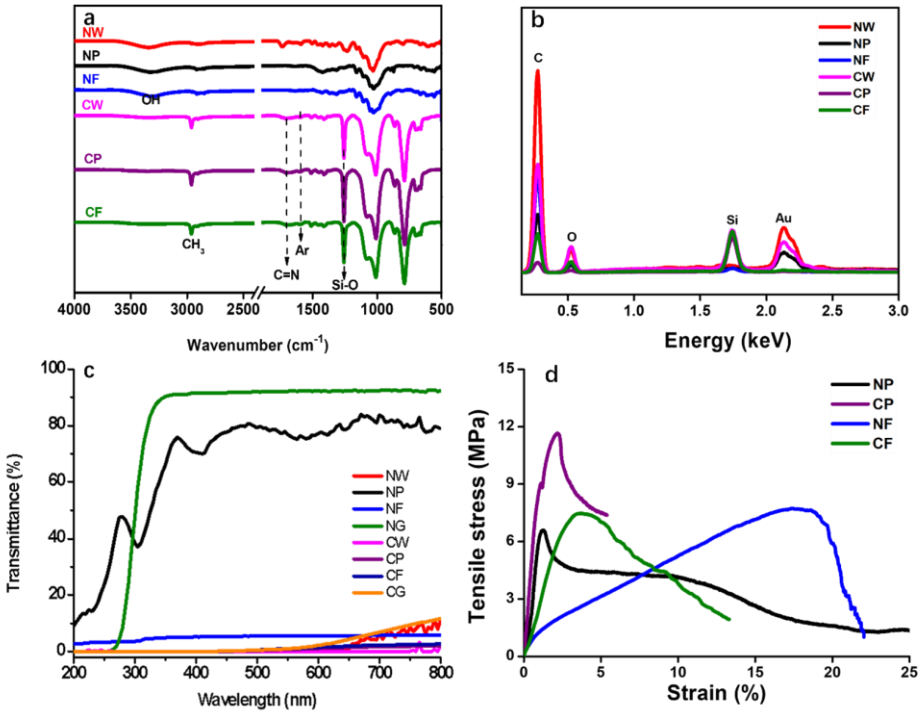


Figure 5-5 FTIR (a), EDS (b), UV transmittance (c), and stress-strain curve (d) of neat and coated cellulosic substrates. NW: neat wood, NP: neat paper, NF: neat fabric, CW: coated wood, CP: coated paper, CF: coated fabric

Table 5-2 Normalized atomic concentration (%) of surface elements on coated and neat cellulosic substrates

samples	C	N	O	Si	S	Cl	K	Ca	Au
NW	81.1±1.8	0	14.1±0.5	0.1±0.1	0	0.1±0.1	0.8±0.1	0.4±0.2	3.4±0.5
CW	71.9±2.5	0	19.0±2.1	6.5±1.9	0	0	0.1±0.0	0.1±0.0	2.4±0.1
NP	74.1±5.2	0.2±0.1	23.2±2.8	0	0	0	0	0	2.5±0.3
CP	65.0±6.8	0.5±0.1	20.5±0.7	10.6±3.4	0	0	0	0	3.4±0.5
NF	78.9±6.0	0.1±0.1	17.7±3.5	0	0.4±0.1	0	0	0	2.9±0.8
CF	65.8±2.4	0.1±0.1	20.2±4.1	10.3±3.5	0.3±0.1	0	0	0	3.3±0.7

Note: The data are in a form of mean ± standard deviation

decreased after coating, among which the decreasing intensity of CF is much remarkable (Table 5-3). We can conclude that the effect of coating process on the mechanical strength of coating products is different with respect to different substrates. As for paper, coatings can enhance the stiffness and tensile strength. As for fabric, coatings can enhance the stiffness, but sacrifice the ductility. The reason could be explained by the discrepant mechanical performances and adhesion or bonding interactions between coating agent and substrate.

The thermal stability of the cellulosic substrates is also improved after coating. As TGA and DTG results show, the $Tonset$ and $Tmax$ of CW, CP, and CF are larger than those of NW, NP, and NF, respectively (Figures 5-6a and 5-6b, and Table 5-4). There are a few peaks measured in DTG curves of the samples (Figure 5-6b). The thermal degradation of NW can be classified into three stages. The first stage mainly is drying and initial decomposition (RT - 189 ℃). The second stage is the main decomposition stage (194 ℃ - 313 ℃), which is attributed to the primary carbohydrate components of wood (cellulose and hemicellulose). The third stage is occurred mainly due to the lignin decomposition, and char formation (313 ℃ - 700 ℃).[196] For paper and fabric, the decomposition can also be divided into three stages including the first moisture evaporation and small-molecule carbohydrates stage (RT - ~ 255 ℃), the second cellulose decomposition stage (~ 255 ℃ - ~ 400 ℃), and the third char formation stage (above 400 ℃). The char was formed as carbon-rich materials after the volatile components were released. After the coating treatment, the thermal stability of CW, CP, and CF are increased based on the increased T_{onset} and T_{max} results in Table 5-3. The number of thermal degradation stages is also increased due to the enhanced covalent bond density caused by the introduction of lignin-PDMS polyimines, and the introduction of LMNS with high C/H ratio.

The hydrophilicity index and WCA show that 1) the hydrophilic surface of NW is modified to hydrophobic surface after coating, and 2) the hydrophobicity of CW is enhanced after 2-step coating. As we can see, both dispersive and specific surface energy

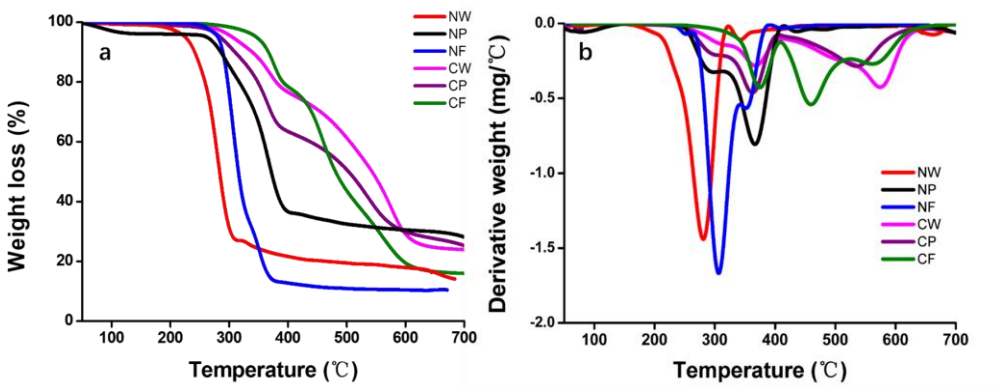


Figure 5-6 TGA (a), DTG (b) curves of neat and coated cellulosic substrates. NW: neat wood, NP: neat paper, NF: neat fabric, CW: coated wood, CP: coated paper, CF: coated fabric.

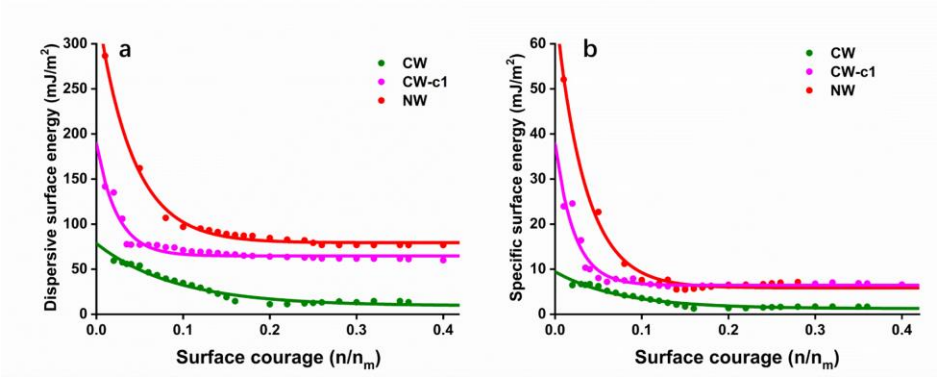


Figure 5-7 Dispersive (a) and specific (b) surface energy of CW, CW-c1, and NW. CW: coated wood product, CW-c1: coated wood control 1, NW: neat wood

Table 5-3 Young's modulus, maximum tensile strength, and tensile strain at maximum tensile stress (Extension) of neat and coated substrates

Samples	Young's modulus (MPa)	Maximum tensile stress (MPa)	Extension (%)
NP	584.6±45.3	6.6±0.5	2.7±0.5
NF	114.8±5.4	7.2±1.1	17.5±1.3
CP	1167.4±114.2	12.9±1.8	2.1±0.0
CF	325.4±31.5	7.3±0.8	3.5±0.3

Note: The data are in a form of mean ± standard deviation

Table 5-4 Temperatures at the onset of thermal degradation (T_{onset}) and maximum mass loss (T_{max}), residual carbon content (C_r) of neat and coated substrates

Samples	T_{onset} (°C)	T_{max} (°C)	C_r (%)
NW	188.9	281.0	14.3
NP	259.4	367.7	28.4
NF	255.5	307.4	10.0
CW	253.4	575.1	23.7
CP	264.0	363.7	26.1
CF	376.9	460.8	15.7

of coated wood go down compared with uncoated wood, which is mainly because of the introduction of low-surface-energy PDMS and LMNS (Figure 5-7). Comparing CW-c1, the surface energy and hydrophilic index of CW is further declined, which could be mainly attributed by the better film-forming ability of polyimine crosslinking network compared with neat PDMS. Although amide formation reaction could happen between amines in PDMS and carboxyl in cellulose as described in FTIR analysis, the lack of catalyst limits the occurrence of the amide formation. Therefore, PDMS could barely form a film on the CW-c1 surface, leading to exposed hydroxyls on the surface. While in our previous study, lignin-PDMS polyimines can form a uniform film, which could cover the surface of CW and reduce the exposed hydrophilic groups, thus to decrease the surface energy. It can also be supported by the surface energy heterogeneity (*i.e.*, the difference between maximum and minimum surface energy) of CW-c1 and CW (Table 5-5). The low surface energy heterogeneity of CW also prove that a uniform coating surface is fabricated.

5.5. Conclusions

A two-step coating method using lignin-based coating agents was proposed for the effective hydrophobic modification of cellulose-based substrates in this study. The hydrophobicity of coatings could be enhanced by LMNS surface roughening, lignin-PDMS polymerization, and selection of substrates with rougher surface texture. The mechanical-, water-, and chemical-stabilities of coatings are prominently enhanced by lignin-PDMS polymerization. Durable superhydrophobic coating surface was successfully fabricated on WB-C. The WCA reaches up to 173° and the ROA low to 5° with excellent self-cleaning ability. Multiple daily liquids including 5wt% NaCl aqueous, tea, coffee, and milk can also be repelled efficiently. Moreover, WB-C exhibits outstanding mechanical robustness and water resistance. The coated wood is more medium alkaline-stable (pH = 9). Furthermore, the coatings can bring extra UV-blocking ability, improved thermal stability and stiffness of paper and fabric.

Table 5-5 The minimum, median and maximum values of γ_d and γ_{sp} as well as hydrophilicity index ($\gamma_{sp}/(\gamma_{sp}+\gamma_d)$) and WCA of CW, CW-c1, and NW

Samples	γ_d (mJ/m^2)			γ_{sp} (mJ/m^2)			$\gamma_{sp}/(\gamma_{sp}+\gamma_d)$	WCA (°)
	minimum	median	maximum	minimum	median	maximum		
NW	76.7	87.9	286.6	5.5	16.8	52.1	0.19	75.2
CW-c1	60.0	67.3	141.7	6.0	7.7	24.6	0.12	140.0
CW	11.1	26.2	59.4	1.3	2.5	6.7	0.09	156.8

CHAPTER VI
SUMMARY AND OUTLOOK

6.1. Summary

KL, as an underused industrial waste, deserves great attentions to its valorization. The current dissertation focuses on the application of KL for hydrophobic coatings. However, KL itself is difficult to be used directly for hydrophobic coatings due to the structural heterogeneity, low compatibility with other materials, and insufficient hydrophobicity, film-forming, etc. Therefore, KL is treated like solvent fractionation, nanosizing, chemical modification and polymerization herein to benefit the coating performances.

To build up structure-properties relationships of lignin-based copolymers, the effects of lignin structural heterogeneity on the structures and properties of lignin-based copolymers and biomaterials are investigated. Solvent fractionation is conducted to obtain lignin fractions with different M_w and OH contents. Together with more homogeneous lignin fractions, KL is synthesized with ε-CL and OAm to form lignin-based thermoplastics and synthesized with PDMS to form lignin-based thermosets. The synthesized lignin-based copolymers are coated on cellulose-based substrates including filter paper, A4 paper, wood, and fabric to explore further applications like water/oil separation, packaging and construction materials. Given the important role of surface roughness and microstructures, LMNS with a micro- and nano-morphology is employed to enhance the hydrophobicity and durability the coatings. Based on the results and discussion in the current dissertation, some conclusions can be drawn as follows:

1) KL and its fractions are successfully copolymerized with ε-CL *via* ROP to form star-shape lignin-*g*-PCL copolymers with a lignin skeleton and PCL arms, among which high-MW lignin favors the ROP polymerization because the higher aliphatic OH content provides more grafting sites for ε-CL.
2) KL and FLs are successfully copolymerized with OAm and PDMS to form lignin-OAm grafted and lignin-PDMS crosslinked polyimines, respectively, after LA modification *via* the Schiff-base reactions between ketones and amines. In this case, low-MW lignin favors grafting and crosslinking polymerization with amines due to the higher ketone grafting efficiency and lower steric hinderance.
3) The prepared lignin-OAm polyimines can be self-repaired, while lignin-PDMS

polyimines can be repaired with the assistance of a healing agent, heat and pressure.

4) Lignin-*g*-PCL coated filter paper shows great performances in separating water-hexane, water-petroleum ether, and water-chloroform mixtures with an outstanding separation efficiency up to 99% and an excellent reusability.
5) Lignin-PDMS polyimines also exhibit good coating hydrophobicity, adhesion, and removability on paper.
6) The hydrophobicity of polyimine coatings is further enhanced by LMNS surface roughening. As a result, robust superhydrophobic coating surfaces are achieved on wood by dip coating MKL-PDMS polyimines and drop casting LMNS. The WCA reaches up to 173° and the ROA reaches low to 5° on WB-C. The superhydrophobicity of WB-C mountains when repelling daily liquids including 5wt% NaCl aqueous, tea, coffee, and milk.
7) The WB-C product displays excellent mechanical resistance to knife scratch, 100-cycle tape peeling, and 1.5-hour waterdrop impact, chemical resistance to medium alkaline (pH = 9), and water resistance.
8) The polyimine-LMNS coatings bring improved stiffness and tensile strength of paper and improved the stiffness and ductility of fabric.
9) Lignin incorporation could affect the hydrophobicity, thermal stability, and UV-blocking abilities of synthesized lignin-g-PCL, lignin-OAm, and lignin-PDMS copolymers, which can be further impart to the lignin-based coating products.

This project is expected to provide new insight into lignin-based polymerization and versatility of lignin valorization for hydrophobic coatings.

6.2. Outlook

The dissertation studies the effects of lignin structures on the structures and performances of the synthesized copolymers and fabricated coatings, conducts multiple

lignin treatments to enable the synthesis and fabrication. Even so, some proposed further investigations would be interesting to conduct, and some limitations remain to be addressed.

Firstly, while lignin fractionation and nanosizing were used, more efficient lignin pretreatments that further decrease the MW and increase the OH content of KL will benefit the tailoring effect of lignin. Secondly, the repair time of lignin-based polyimines is long, which is energy-consuming.

In addition, lignin-PDMS polyimine films can be re-healed under 150 ℃ in vacuum oven for 12 h after a healing agent of lignin and PDMS pre-reaction solution was added (Figure 3-8). The healing ability of polyimines indicates the repairability potential of lignin-PDMS polyimine coatings. Therefore, further studies on the repairability of lignin-PDMS polyimine coatings remain to be investigate.

Although robust superhydrophobic surfaces were obtained on wood with an innovative method in this study, the effects of LMNS deposition density and polyimine concentration in dip coating step on the hydrophobicity and coating durability will be interesting to investigate..

To evaluate the universality of lignin-based coatings, multiple lignin species such as alkaline lignin, modification and treatment pathways, coating methods such as spraying coating, coating substrates such as metal, remain to be surveyed.

To reduce the fabricating cost and energy input, simpler coating procedure without solvent evaporation or oven curation, cheaper feedstocks, and more scalable and applicable technologies would be required for the industry manufacturing in real world.

LIST OF REFERENCES

1. Wise, L. E.; Brown, H. P., *Wood chemistry*. Reinhold publishing corporation: New York, 1944.

2. Constant, S.; info:eu, r. d. n.; Wienk, H. L. J.; info:eu, r. d. n.; Frissen, A. E.; Peinder, P. D.; info:eu, r. d. n.; Boelens, R.; info:eu, r. d. n.; Van Es, D. S.; Grisel, R. J. H.; Weckhuysen, B. M.; info:eu, r. d. n.; Huijgen, W. J. J.; Gosselink, R. J. A.; Bruijnincx, P. C. A.; info:eu repo/dai/nl, X.; Spectroscopy, N. M. R.; Sub Inorganic, C.; Catalysis; Sub, N. M. R. S.; Inorganic, C.; Catalysis, New insights into the structure and composition of technical lignins: A comparative characterisation study. *Green chemistry : an international journal and green chemistry resource : GC* **2016,** *18* (9), 2651-2665.

3. Rencoret, J.; Prinsen, P.; Gutiérrez, A.; Martínez, A. n. T.; del Río, J. C., Isolation and Structural Characterization of the Milled Wood Lignin, Dioxane Lignin, and Cellulolytic Lignin Preparations from Brewer's Spent Grain. *Journal of agricultural and food chemistry* **2015,** *63* (2), 603-613.

4. Brebu, M.; Tamminen, T.; Spiridon, I., Thermal degradation of various lignins by TG-MS/FTIR and Py-GC-MS. *Journal of Analytical and Applied Pyrolysis* **2013,** *104*, 531-539.

5. Bajwa, D. S.; Pourhashem, G.; Ullah, A. H.; Bajwa, S. G., A concise review of current lignin production, applications, products and their environmental impact. *Industrial Crops and Products* **2019,** *139*, 111526.

6. Ma, B.; Xiong, F.; Wang, H.; Qing, Y.; Chu, F.; Wu, Y., Tailorable and scalable production of eco-friendly lignin micro-nanospheres and their application in functional superhydrophobic coating. *Chemical engineering journal (Lausanne, Switzerland : 1996)* **2023,** *457*, 141309.

7. Pang, T.; Wang, G.; Sun, H.; Sui, W.; Si, C., Lignin fractionation: Effective strategy to reduce molecule weight dependent heterogeneity for upgraded lignin valorization. *Industrial crops and products* **2021,** *165*, 113442.

8. Gigli, M.; Crestini, C., Fractionation of industrial lignins: opportunities and challenges. *Green chemistry : an international journal and green chemistry resource : GC* **2020,** *22* (15), 4722-4746.

9. Jiang, X.; Abbati de Assis, C.; Kollman, M.; Sun, R.; Jameel, H.; Chang, H.-m.; Gonzalez, R., Lignin fractionation from laboratory to commercialization: chemistry, scalability and techno-economic analysis. *Green chemistry : an international journal and green chemistry resource : GC* **2020,** *22* (21), 7448-7459.

10. Tindall, G. W.; Chong, J.; Miyasato, E.; Thies, M. C., Fractionating and Purifying Softwood Kraft Lignin with Aqueous Renewable Solvents: Liquid–Liquid Equilibrium for the Lignin–Ethanol–Water System. *ChemSusChem* **2020,** *13* (17), 4587-4594.

11. Wang, Y.-Y.; Li, M.; Wyman, C. E.; Cai, C. M.; Ragauskas, A. J., Fast Fractionation of Technical Lignins by Organic Cosolvents. *ACS sustainable chemistry & engineering* **2018,** *6* (5), 6064-6072.

12. Tagami, A.; Gioia, C.; Lauberts, M.; Budnyak, T.; Moriana, R.; Lindström, M. E.; Sevastyanova, O., Solvent fractionation of softwood and hardwood kraft lignins for more efficient uses: Compositional, structural, thermal, antioxidant and adsorption properties. *Industrial crops and products* **2019,** *129*, 123-134.

13. Li, M.; Pu, Y.; Chen, F.; Ragauskas, A. J., Synthesis and Characterization of Lignin-grafted-poly(ε-caprolactone) from Different Biomass Sources. *New biotechnology* **2021,** *60*, 189-199.

14. Shorey, R.; Gupta, A.; Mekonnen, T. H., Hydrophobic modification of lignin for rubber composites. *Industrial crops and products* **2021,** *174*, 114189.

15. Huang, K.; Ma, S.; Wang, S.; Li, Q.; Wu, Z.; Liu, J.; Liu, R.; Zhu, J., Sustainable valorization of lignin with levulinic acid and its application in polyimine thermosets. *Green chemistry : an international journal and green chemistry resource : GC* **2019,** *21* (18), 4964-497.

16. Buzoglu Kurnaz, L.; Bension, Y.; Tang, C., Facile Catalyst-Free Approach toward Fully Biobased Reprocessable Lignin Thermosets. *Macromolecular chemistry and physics* **2023,** *224* (3), 2200303-n/a.

17. Lisý, A.; Ház, A.; Nadányi, R.; Jablonský, M.; Šurina, I., About Hydrophobicity of Lignin: A Review of Selected Chemical Methods for Lignin Valorisation in Biopolymer Production. *Energies (Basel)* **2022,** *15* (17), 6213.
18. Dong, H.; Tang, S.; Zhang, L.; Tong, Z.; Wu, Z.; Zhan, P.; Shao, L.; Qing, Y.; Liu, J., Wood-derived bio-coating materials incorporating hydrophobic lignin and hierarchically porous biochar for high-efficiency coating slow-release fertilizers. *International journal of biological macromolecules* **2023,** *242* (Pt 1), 124769-124769.
19. Adjaoud, A.; Puchot, L.; Federico, C. E.; Das, R.; Verge, P., Lignin-based benzoxazines: A tunable key-precursor for the design of hydrophobic coatings, fire resistant materials and catalyst-free vitrimers. *Chemical engineering journal (Lausanne, Switzerland : 1996)* **2023,** *453*, 139895.
20. de Haro, J. C.; Allegretti, C.; Smit, A. T.; Turri, S.; D'Arrigo, P.; Griffini, G., Biobased Polyurethane Coatings with High Biomass Content: Tailored Properties by Lignin Selection. *ACS sustainable chemistry & engineering* **2019,** *7* (13), 11700-11711.
21. Li, R.; Zhu, X.; Peng, F.; Lu, F., Biodegradable, Colorless, and Odorless PLA/PBAT Bioplastics Incorporated with Corn Stover. *ACS sustainable chemistry & engineering* **2023,** *11* (24), 8870-8883.
22. Zhu, X.; Wang, D.; Li, N.; Sun, X. S., Bio-Based Wood Adhesive from Camelina Protein (a Biodiesel Residue) and Depolymerized Lignin with Improved Water Resistance. *ACS omega* **2017,** *2* (11), 7996-8004.
23. Alipoormazandarani, N.; Fatehi, P., Lignin-methyl methacrylate polymer as a hydrophobic multifunctional material. *Industrial crops and products* **2020,** *154*, 112728.
24. Zhang, C.; Zhang, P.; Li, Y.; Sandeep, S. N.; Li, J.; Ji, M.; Peng, S.; Yan, N.; Li, F., Fully biodegradable, hydrophobic, enhanced barrier starch bio-composites with sandwich structure by simulating wood. *Industrial crops and products* **2023,** *197*, 116603.
25. Gellerstedt, G., Softwood kraft lignin: Raw material for the future. *Industrial crops and products* **2015,** *77*, 845-854.

26. Sen, S.; Patil, S.; Argyropoulos, D. S., Thermal properties of lignin in copolymers, blends, and composites: a review. *Green chemistry : an international journal and green chemistry resource : GC* **2015,** *17* (11), 4862-4887.

27. Naseem, A.; Tabasum, S.; Zia, K. M.; Zuber, M.; Ali, M.; Noreen, A., Lignin-derivatives based polymers, blends and composites: A review. *International journal of biological macromolecules* **2016,** *93* (Pt A), 296-313.

28. Kong, F.; Wang, S.; T. Price, J.; Konduri, M. K. R.; Fatehi, P., Water soluble kraft lignin–acrylic acid copolymer: synthesis and characterization. *Green chemistry : an international journal and green chemistry resource : GC* **2015,** *17* (8), 4355-4366.

29. Martín-Sampedro, R.; Santos, J. I.; Fillat, Ú.; Wicklein, B.; Eugenio, M. E.; Ibarra, D., Characterization of lignins from Populus alba L. generated as by-products in different transformation processes: Kraft pulping, organosolv and acid hydrolysis. *International journal of biological macromolecules* **2019,** *126*, 18-29.

30. Zhang, R.; Du, Q.; Wang, L.; Zheng, Z.; Guo, L.; Zhang, X.; Yang, X.; Yu, H., Unlocking the response of lignin structure for improved carbon fiber production and mechanical strength. *Green chemistry : an international journal and green chemistry resource : GC* **2019,** *21* (18), 4981-4987.

31. Duval, A.; Layrac, G.; Zomeren, A.; Smit, A. T.; Pollet, E.; Avérous, L., Isolation of Low Dispersity Fractions of Acetone Organosolv Lignins to Understand their Reactivity: Towards Aromatic Building Blocks for Polymers Synthesis. *ChemSusChem* **2021,** *14* (1), 387-397.

32. Araújo, L. C. P.; Yamaji, F. M.; Lima, V. H.; Botaro, V. R., Kraft lignin fractionation by organic solvents: Correlation between molar mass and higher heating value. *Bioresource technology* **2020,** *314*, 123757-123757.

33. Izaguirre, N.; Gordobil, O.; Robles, E.; Labidi, J., Enhancement of UV absorbance and mechanical properties of chitosan films by the incorporation of solvolytically fractionated lignins. *International journal of biological macromolecules* **2020,** *155*, 447-455.

34. Crestini, C.; Lange, H.; Sette, M.; Argyropoulos, D. S., On the structure of softwood kraft lignin. *Green chemistry : an international journal and green chemistry resource : GC* **2017,** *19* (17), 4104-4121.

35. Wang, G.; Pang, T.; Xia, Y.; Liu, X.; Li, S.; Parvez, A. M.; Kong, F.; Si, C., Subdivision of bamboo kraft lignin by one-step ethanol fractionation to enhance its water-solubility and antibacterial performance. *International journal of biological macromolecules* **2019,** *133*, 156-164.

36. Delgado, N.; Ysambertt, F.; Ochoa, R.; Chavez, G.; Bravo, B.; Santos, J.; Garcia, D. E., Esterified lignins from Pinus caribaea as bentonite-dispersing agents. *Clay minerals* **2018,** *53* (1), 41-51.

37. Dohendou, M.; Pakzad, K.; Nezafat, Z.; Nasrollahzadeh, M.; Dekamin, M. G., Progresses in chitin, chitosan, starch, cellulose, pectin, alginate, gelatin and gum based (nano)catalysts for the Heck coupling reactions: A review. *International journal of biological macromolecules* **2021,** *192*, 771-819.

38. Jiang, B.; Chen, C.; Liang, Z.; He, S.; Kuang, Y.; Song, J.; Mi, R.; Chen, G.; Jiao, M.; Hu, L., Lignin as a Wood-Inspired Binder Enabled Strong, Water Stable, and Biodegradable Paper for Plastic Replacement. *Advanced functional materials* **2020,** *30* (4), 1906307-n/a.

39. Pradyawong, S.; Shrestha, R.; Li, P.; Sun, X. S.; Wang, D., Effect of pH and pH-Shifting on Lignin–Protein Interaction and Properties of Lignin-Protein Polymers. *Journal of polymers and the environment* **2021,** *30* (5), 1908-1919.

40. An, L.; Chen, J.; Heo, J. W.; Bae, J. H.; Jeong, H.; Kim, Y. S., Synthesis of lignin-modified cellulose nanocrystals with antioxidant activity via Diels–Alder reaction and its application in carboxymethyl cellulose film. *Carbohydrate polymers* **2021,** *274*, 118651-118651.

41. Gabov, K.; Oja, T.; Deguchi, T.; Fallarero, A.; Fardim, P., Preparation, characterization and antimicrobial application of hybrid cellulose-lignin beads. *Cellulose* **2016,** *24* (2), 641-658.

42. Dong, J.; Su, Y.; Jiang, T.; Li, D.; Ma, X., Insight into the complex coupling agents on thermal, mechanical, and barrier properties of lignin-poly(3-hydroxybutyrate-co-3-hydroxyhexanoate) biocomposites. *Polymer composites* **2022,** *43* (4), 2431-2439.
43. Yan, Y.; Zhang, L.; Zhao, X.; Zhai, S.; Wang, Q.; Li, C.; Zhang, X., Utilization of lignin upon successive fractionation and esterification in polylactic acid (PLA)/lignin biocomposite. *International journal of biological macromolecules* **2022,** *203*, 49-57.
44. Zhang, X.; Liu, W.; Liu, W.; Qiu, X., High performance PVA/lignin nanocomposite films with excellent water vapor barrier and UV-shielding properties. *International journal of biological macromolecules* **2020,** *142*, 551-558.
45. Abdollahi, M.; Bairami Habashi, R.; Mohsenpour, M., Poly(ε-caprolactone) chains grafted from lignin, hydroxymethylated lignin and silica/lignin hybrid macroinitiators: Synthesis and characterization of lignin- based thermoplastic copolymers. *Industrial crops and products* **2019,** *130*, 547-557.
46. Huang, J.; Wang, H.; Liu, W.; Huang, J.; Yang, D.; Qiu, X.; Zhao, L.; Hu, F.; Feng, Y., Solvent-free synthesis of high-performance polyurethane elastomer based on low-molecular-weight alkali lignin. *International journal of biological macromolecules* **2023,** *225*, 1505-1516.
47. Zheng, N.; Xu, Y.; Zhao, Q.; Xie, T., Dynamic Covalent Polymer Networks: A Molecular Platform for Designing Functions beyond Chemical Recycling and Self-Healing. *Chemical reviews* **2021,** *121* (3), 1716-1745.
48. Krishnakumar, B.; Sanka, R. V. S. P.; Binder, W. H.; Parthasarthy, V.; Rana, S.; Karak, N., Vitrimers: Associative dynamic covalent adaptive networks in thermoset polymers. *Chemical engineering journal (Lausanne, Switzerland : 1996)* **2020,** *385*, 123820.
49. Hao, C.; Liu, T.; Zhang, S.; Brown, L.; Li, R.; Xin, J.; Zhong, T.; Jiang, L.; Zhang, J., A High-Lignin-Content, Removable, and Glycol-Assisted Repairable Coating Based on Dynamic Covalent Bonds. *ChemSusChem* **2019,** *12* (5), 1049-1058.

50. Tu, Z.; Liu, W.; Wang, J.; Qiu, X.; Huang, J.; Li, J.; Lou, H., Biomimetic high performance artificial muscle built on sacrificial coordination network and mechanical training process. *Nature communications* **2021,** *12* (1), 2916-2916.

51. Liu, W.; Fang, C.; Wang, S.; Huang, J.; Qiu, X., High-Performance Lignin-Containing Polyurethane Elastomers with Dynamic Covalent Polymer Networks. *Macromolecules* **2019,** *52* (17), 6474-6484.

52. Wang, H.; Huang, J.; Liu, W.; Huang, J.; Yang, D.; Qiu, X.; Zhang, J., Tough and Fast Light-Controlled Healable Lignin-Containing Polyurethane Elastomers. *Macromolecules* **2022,** *55* (19), 8629-8641.

53. Belowich, M. E.; Stoddart, J. F., Dynamic imine chemistry. *Chemical Society reviews* **2012,** *41* (6), 23-224.

54. Yang, X.; Ke, Y.; Chen, Q.; Shen, L.; Xue, J.; Quirino, R. L.; Yan, Z.; Luo, Y.; Zhang, C., Efficient transformation of renewable vanillin into reprocessable, acid-degradable and flame retardant polyimide vitrimers. *Journal of cleaner production* **2022,** *333*, 130043.

55. Hong, K.; Sun, Q.; Zhang, X.; Fan, L.; Wu, T.; Du, J.; Zhu, Y., Fully Bio-Based High-Performance Thermosets with Closed-Loop Recyclability. *ACS sustainable chemistry & engineering* **2022,** *10* (2), 1036-1046.

56. Geng, H.; Wang, Y.; Yu, Q.; Gu, S.; Zhou, Y.; Xu, W.; Zhang, X.; Ye, D., Vanillin-Based Polyschiff Vitrimers: Reprocessability and Chemical Recyclability. *ACS sustainable chemistry & engineering* **2018,** *6* (11), 15463-15470.

57. Shu, F.; Jiang, B.; Yuan, Y.; Li, M.; Wu, W.; Jin, Y.; Xiao, H., Biological Activities and Emerging Roles of Lignin and Lignin-Based Products A Review. *Biomacromolecules* **2021,** *22* (12), 4905-4918.

58. Meng, H.; Zhao, Y.; Wang, S.; Wang, Y.; Xiao, Z.; Wang, H.; Liang, D.; Xie, Y., Turning the morphology and wetting ability of self-assembled hierarchical structures from lignin stearoyl esters. *Industrial crops and products* **2022,** *183*.

59. Wang, H.; Xiong, F.; Tan, Y.; Yang, J.; Qing, Y.; Chu, F.; Wu, Y., Preparation and Formation Mechanism of Covalent–Noncovalent Forces Stabilizing Lignin Nanospheres

and Their Application in Superhydrophobic and Carbon Materials. *ACS sustainable chemistry & engineering* **2021,** *9* (10), 3811-3820.

60. Li, D. C.; Xu, W. F.; Cheng, H. Y.; Xi, K. F.; Xu, B. D.; Jiang, H., One-Step Thermochemical Conversion of Biomass Waste into Superhydrophobic Carbon Material by Catalytic Pyrolysis. *Global challenges* **2020,** *4* (4), 1900085-n/a.

61. Gao, R.; Huang, Y.; Gan, W.; Xiao, S.; Gao, Y.; Fang, B.; Zhang, X.; Lyu, B.; Huang, R.; Li, J.; Wei, X.; Deng, Y.; Lu, Y., Superhydrophobic elastomer with leaf-spring microstructure made from natural wood without any modification chemicals. *Chemical engineering journal (Lausanne, Switzerland : 1996)* **2022,** *442*.

62. Singh, S. S.; Zaitoon, A.; Sharma, S.; Manickavasagan, A.; Lim, L.-T., Enhanced hydrophobic paper-sheet derived from Miscanthus × giganteus cellulose fibers coated with esterified lignin and cellulose acetate blend. *International journal of biological macromolecules* **2022,** *223* (Pt A), 1243-1256.

63. Gordobil, O.; Herrera, R.; Llano-Ponte, R.; Labidi, J., Esterified organosolv lignin as hydrophobic agent for use on wood products. *Progress in organic coatings* **2017,** *103*, 143-151.

64. Hua, Q.; Liu, L.-Y.; Karaaslan, M. A.; Renneckar, S., Aqueous Dispersions of Esterified Lignin Particles for Hydrophobic Coatings. **2019,** *7*.

65. Buono, P.; Duval, A.; Verge, P.; Averous, L.; Habibi, Y., New Insights on the Chemical Modification of Lignin: Acetylation versus Silylation. *ACS Sustainable Chemistry & Engineering* **2016,** *4* (10), 5212-5222.

66. Li, S.; Xie, W.; Wilt, M.; Willoughby, J. A.; Rojas, O. J., Thermally Stable and Tough Coatings and Films Using Vinyl Silylated Lignin. *ACS Sustainable Chemistry & Engineering* **2018,** *6* (2), 1988-1998.

67. Chen, J.; Yang, H.; Qian, Y.; Ouyang, X.; Yang, D.; Pang, Y.; Lei, L.; Qiu, X., Translucent Lignin-Based Omniphobic Polyurethane Coating with Antismudge and UV-Blocking Dual Functionalities. *ACS sustainable chemistry & engineering* **2023,** *11* (6), 2613-2622.

68. Pang, T.; Wang, G.; Sun, H.; Wang, L.; Liu, Q.; Sui, W.; Parvez, A. M.; Si, C., Lignin Fractionation for Reduced Heterogeneity in Self-Assembly Nanosizing: Toward Targeted Preparation of Uniform Lignin Nanoparticles with Small Size. *ACS sustainable chemistry & engineering* **2020,** *8* (24), 9174-9183.

69. Wang, G.; Pang, T.; Chen, S.; Sui, W.; Si, C.; Ni, Y., Fabrication of lignin nanospheres by emulsification in a binary γ-valerolactone/glycerol system and their application as a bifunctional reducer and carrier for Pd nanoparticles with enhanced catalytic activity. *Green chemistry : an international journal and green chemistry resource : GC* **2020,** *22* (24), 8594-863.

70. Ma, B.; Xiong, F.; Wang, H.; Qing, Y.; Chu, F.; Wu, Y., Tailorable and scalable production of eco-friendly lignin micro-nanospheres and their application in functional superhydrophobic coating. *Chemical Engineering Journal* **2023,** *457*.

71. Yearla, S. R.; Padmasree, K., Preparation and characterisation of lignin nanoparticles: evaluation of their potential as antioxidants and UV protectants. *Journal of Experimental Nanoscience* **2016,** *11* (4), 289-302.

72. Chen, L.; Zhou, X.; Shi, Y.; Gao, B.; Wu, J.; Kirk, T. B.; Xu, J.; Xue, W., Green synthesis of lignin nanoparticle in aqueous hydrotropic solution toward broadening the window for its processing and application. *Chemical Engineering Journal* **2018,** *346*, 217-225.

73. Luo, X.; Liu, C.; Yuan, J.; Zhu, X.; Liu, S., Interfacial Solid-Phase Chemical Modification with Mannich Reaction and Fe(III) Chelation for Designing Lignin-Based Spherical Nanoparticle Adsorbents for Highly Efficient Removal of Low Concentration Phosphate from Water. *ACS Sustainable Chemistry & Engineering* **2017,** *5* (8), 6539-6547.

74. Beisl, S.; Miltner, A.; Friedl, A. Lignin from Micro- to Nanosize: Production Methods *International Journal of Molecular Sciences* [Online], 2017.

75. Tang, Q.; Zhou, M.; Li, Y.; Qiu, X.; Yang, D., Formation of Uniform Colloidal Spheres Based on Lignosulfonate, a Renewable Biomass Resource Recovered from Pulping Spent Liquor. *ACS Sustainable Chemistry & Engineering* **2018,** *6* (1), 1379-1386.

76. Qian, Y.; Deng, Y.; Qiu, X.; Li, H.; Yang, D., Formation of uniform colloidal spheres from lignin, a renewable resource recovered from pulping spent liquor. *Green chemistry : an international journal and green chemistry resource : GC* **2014,** *16* (4), 2156-2163.
77. Hooda, A.; Goyat, M. S.; Pandey, J. K.; Kumar, A.; Gupta, R., A review on fundamentals, constraints and fabrication techniques of superhydrophobic coatings. *Progress in organic coatings* **2020,** *142*, 105557.
78. Liu, X.; Liu, Q.; Wang, S.; Liu, Z.; Yang, G.; Wang, H.; Xiong, W.; Li, P.; Xu, F.; Xi, Y.; Kong, F., Effect of functional group and structure on hydrophobic properties of environment-friendly lignin-based composite coatings. *International journal of biological macromolecules* **2022,** *215*, 132-140.
79. Camargos, C. H. M.; Poggi, G.; Chelazzi, D.; Baglioni, P.; Rezende, C. A., Protective Coatings Based on Cellulose Nanofibrils, Cellulose Nanocrystals, and Lignin Nanoparticles for the Conservation of Cellulosic Artifacts. *ACS Applied Nano Materials* **2022,** *5* (9), 13245-13259.
80. Henn, K. A.; Forsman, N.; Zou, T.; Österberg, M., Colloidal Lignin Particles and Epoxies for Bio-Based, Durable, and Multiresistant Nanostructured Coatings. *ACS applied materials & interfaces* **2021,** *13* (29), 34793-34806.
81. Wang, D.; Sun, Q.; Hokkanen, M. J.; Zhang, C.; Lin, F.-Y.; Liu, Q.; Zhu, S.-P.; Zhou, T.; Chang, Q.; He, B.; Zhou, Q.; Chen, L.; Wang, Z.; Ras, R. H. A.; Deng, X., Design of robust superhydrophobic surfaces. *Nature (London)* **2020,** *582* (7810), 55-59.
82. Miljkovic, N.; Wang, E. N., Condensation heat transfer on superhydrophobic surfaces. *MRS bulletin* **2013,** *38* (5), 397-406.
83. Liu, M.; Qing, Y.; Wu, Y.; Liang, J.; Luo, S., Facile fabrication of superhydrophobic surfaces on wood substrates via a one-step hydrothermal process. *Applied Surface Science* **2015,** *330*, 332-338.
84. Tu, K.; Wang, X.; Kong, L.; Guan, H., Facile preparation of mechanically durable, self-healing and multifunctional superhydrophobic surfaces on solid wood. *Materials & Design* **2018,** *140*, 30-36.

85. Cassie, A. B. D.; Baxter, S., Wettability of porous surfaces. *Transactions of the Faraday Society* **1944,** *40*, 546-551.

86. Gong, X.; Meng, Y.; Zhu, J.; Wang, X.; Lu, J.; Cheng, Y.; Tao, Y.; Wang, H., Construct a stable super-hydrophobic surface through acetonitrile extracted lignin and nano-silica and its application in oil-water separation. *Industrial Crops and Products* **2021,** *166*, 113471.

87. Ikeo, Y.; Aoki, K.; Kishi, H.; Matsuda, S.; Murakami, A., Nano clay reinforced biodegradable plastics of PCL starch blends. *Polymers for advanced technologies* **2006,** *17* (11-12), 940-944.

88. Labet, M.; Thielemans, W., Synthesis of polycaprolactone: a review. *Chemical Society reviews* **2009,** *38* (12), 3484-3504.

89. Li, P.; Fu, L.; Liao, Z.; Peng, Y.; Ning, C.; Gao, C.; Zhang, D.; Sui, X.; Lin, Y.; Liu, S.; Hao, C.; Guo, Q., Chitosan hydrogel/3D-printed poly(ε-caprolactone) hybrid scaffold containing synovial mesenchymal stem cells for cartilage regeneration based on tetrahedral framework nucleic acid recruitment. *Biomaterials* **2021,** *278*, 121131-121131.

90. Jang, S.-H.; Kim, D.-H.; Park, D. H.; Kim, O. Y.; Hwang, S.-H., Construction of sustainable polyurethane-based gel-coats containing poly(ε-caprolactone)-grafted lignin and their coating performance. *Progress in organic coatings* **2018,** *120*, 234-239.

91. Tian, J.; Yang, Y.; Song, J., Grafting polycaprolactone onto alkaline lignin for improved compatibility and processability. *International journal of biological macromolecules* **2019,** *141*, 919-926.

92. Liang, R.; Zhao, J.; Li, B.; Cai, P.; Loh, X. J.; Xu, C.; Chen, P.; Kai, D.; Zheng, L., Implantable and degradable antioxidant poly(ε-caprolactone)-lignin nanofiber membrane for effective osteoarthritis treatment. *Biomaterials* **2020,** *230*, 119601.

93. Wang, D.; Jang, J.; Kim, K.; Kim, J.; Park, C. B., "Tree to Bone": Lignin/Polycaprolactone Nanofibers for Hydroxyapatite Biomineralization. *Biomacromolecules* **2019,** *20* (7), 2684-2693.

94. Liu, X.; Zong, E.; Jiang, J.; Fu, S.; Wang, J.; Xu, B.; Li, W.; Lin, X.; Xu, Y.; Wang, C.; Chu, F., Preparation and characterization of Lignin-graft-poly (ε-caprolactone)

copolymers based on lignocellulosic butanol residue. *International journal of biological macromolecules* **2015,** *81*, 521-529.

95. Laurichesse, S.; Avérous, L., Synthesis, thermal properties, rheological and mechanical behaviors of lignins-grafted-poly(ε-caprolactone). *Polymer (Guilford)* **2013,** *54* (15), 3882-3890.

96. Pérez–Camargo, R. A.; Saenz, G.; Laurichesse, S.; Casas, M. T.; Puiggalí, J.; Avérous, L.; Müller, A. J., Nucleation, Crystallization, and Thermal Fractionation of Poly (ε-Caprolactone)-Grafted-Lignin: Effects of Grafted Chains Length and Lignin Content. *Journal of polymer science. Part B, Polymer physics* **2015,** *53* (24), 1736-1750.

97. Liu, Z.-H.; Hao, N.; Shinde, S.; Pu, Y.; Kang, X.; Ragauskas, A. J.; Yuan, J. S., Defining lignin nanoparticle properties through tailored lignin reactivity by sequential organosolv fragmentation approach (SOFA). *Green chemistry : an international journal and green chemistry resource : GC* **2019,** *21* (2), 245-260.

98. Yue, Y.; Wang, Y.; Li, J.; Cheng, W.; Han, G.; Lu, T.; Huang, C.; Wu, Q.; Jiang, J., High strength and ultralight lignin-mediated fire-resistant aerogel for repeated oil/water separation. *Carbon (New York)* **2022,** *193*, 285-297.

99. Cao, M.; Hu, Y.; Cheng, W.; Huan, S.; Bai, T.; Niu, Z.; Zhao, Y.; Yue, G.; Zhao, Y.; Han, G., Lignin-based multi-scale cellular aerogels assembled from co-electrospun nanofibers for oil/water separation and energy storage. *Chemical engineering journal (Lausanne, Switzerland : 1996)* **2022,** *436*, 135233.

100. Jiang, Y.-H.; Zhang, Y.-Q.; Gao, C.; An, Q.-D.; Xiao, Z.-Y.; Zhai, S.-R., Superhydrophobic aerogel membrane with integrated functions of biopolymers for efficient oil/water separation. *Separation and purification technology* **2022,** *282*, 120138.

101. Meng, X.; Crestini, C.; Ben, H.; Hao, N.; Pu, Y.; Ragauskas, A. J.; Argyropoulos, D. S., Determination of hydroxyl groups in biorefinery resources via quantitative 31P NMR spectroscopy. *Nature protocols* **2019,** *14* (9), 2627-2647.

102. Standard Test Method for Tensile Properties of Thin Plastic Sheeting. *West Conshohocken* **2010,** (West Conshohocken), PA 19428-2959, United States.

103. Korbag, I.; Mohamed Saleh, S., Studies on mechanical and biodegradability properties of PVA/lignin blend films. *International journal of environmental studies* **2016,** *73* (1), 18-24.

104. Yang, W.; Qi, G.; Ding, H.; Xu, P.; Dong, W.; Zhu, X.; Zheng, T.; Ma, P., Biodegradable poly (lactic acid)-poly (ε-caprolactone)-nanolignin composite films with excellent flexibility and UV barrier performance. *Composites communications* **2020,** *22*, 100497.

105. Ashton, J. H.; Mertz, J. A. M.; Harper, J. L.; Slepian, M. J.; Mills, J. L.; McGrath, D. V.; Vande Geest, J. P., Polymeric endoaortic paving: Mechanical, thermoforming, and degradation properties of polycaprolactone/polyurethane blends for cardiovascular applications. *Acta biomaterialia* **2011,** *7* (1), 287-294.

106. Wu, H.; Wu, L.; Lu, S.; Lin, X.; Xiao, H.; Ouyang, X.; Cao, S.; Chen, L.; Huang, L., Robust superhydrophobic and superoleophilic filter paper via atom transfer radical polymerization for oil/water separation. *Carbohydrate polymers* **2018,** *181*, 419-425.

107. Schuerch, C., The Solvent Properties of Liquids and Their Relation to the Solubility, Swelling, Isolation and Fractionation of Lignin. *Journal of the American Chemical Society* **1952,** *74* (20), 5061-5067.

108. Ebrahimi Majdar, R.; Ghasemian, A.; Resalati, H.; Saraeian, A.; Crestini, C.; Lange, H., Case Study in Kraft Lignin Fractionation: "Structurally Purified" Lignin Fractions The Role of Solvent H-Bonding Affinity. *ACS sustainable chemistry & engineering* **2020,** *8* (45), 16803-16813.

109. Rohde, V.; Böringer, S.; Tübke, B.; Adam, C.; Dahmen, N.; Schmiedl, D., Fractionation of three different lignins by thermal separation techniques—A comparative study. **2019,** *11* (1), 206-217.

110. Sadeghifar, H.; Ragauskas, A., Perspective on Technical Lignin Fractionation. *ACS sustainable chemistry & engineering* **2020,** *8* (22), 8086-8101.

111. Najarro, M. C. c.; Nikolic, M.; Iruthayaraj, J.; Johannsen, I., Tuning the Lignin-Caprolactone Copolymer for Coating Metal Surfaces. *ACS applied polymer materials* **2020,** *2* (12), 5767-5778.

112. Antonino, L. D.; Gouveia, J. R.; de Sousa Júnior, R. R.; Garcia, G. E. S.; Gobbo, L. C.; Tavares, L. B.; Dos Santos, D. J., Reactivity of Aliphatic and Phenolic Hydroxyl Groups in Kraft Lignin towards 4,4' MDI. *Molecules (Basel, Switzerland)* **2021,** *26* (8), 2131.

113. Kuroda, K.; Kunimura, H.; Fukaya, Y.; Nakamura, N.; Ohno, H., 1H NMR Evaluation of Polar and Nondeuterated Ionic Liquids for Selective Extraction of Cellulose and Xylan from Wheat Bran. *ACS sustainable chemistry & engineering* **2014,** *2* (9), 2204-2210.

114. Shi, Z.; Xu, G.; Deng, J.; Dong, M.; Murugadoss, V.; Liu, C.; Shao, Q.; Wu, S.; Guo, Z., Structural characterization of lignin from D. sinicus by FTIR and NMR techniques. *Green chemistry letters and reviews* **2019,** *12* (3), 235-243.

115. Hirose, S.; Hatakeyama, T.; Izuta, Y.; Hatakeyama, TG-FTIR studies on lignin-based polycaprolactones : Speciality Polymers. *Journal of thermal analysis and calorimetry* **2002,** *70* (3), 853-860.

116. Argyropoulos, D. S.; Sadeghifar, H.; Cui, C.; Sen, S., Synthesis and Characterization of Poly(arylene ether sulfone) Kraft Lignin Heat Stable Copolymers. *ACS sustainable chemistry & engineering* **2014,** *2* (2), 264-271.

117. Liu, X.; Wang, J.; Li, S.; Zhuang, X.; Xu, Y.; Wang, C.; Chu, F., Preparation and properties of UV-absorbent lignin graft copolymer films from lignocellulosic butanol residue. *Industrial crops and products* **2014,** *52*, 633-641.

118. Evtuguin, D. V.; Andreolety, J. P.; Gandini, A., Polyurethanes based on oxygen-organosolv lignin. *European Polymer Journal* **1998,** *34* (8), 1163-1169.

119. Mohamad Aini, N. A.; Othman, N.; Hussin, M. H.; Sahakaro, K.; Hayeemasae, N., Effect of extraction methods on the molecular structure and thermal stability of kenaf (Hibiscus cannabinus core) biomass as an alternative bio-filler for rubber composites. *International Journal of Biological Macromolecules* **2020,** *154*, 1255-1264.

120. Das, S. C.; Stewart, P. J., Characterising surface energy of pharmaceutical powders by inverse gas chromatography at finite dilution. *Journal of Pharmacy and Pharmacology* **2012,** *64* (9), 1337-1348.

121. Legras, A.; Kondor, A.; Alcock, M.; Heitzmann, M. T.; Truss, R. W., Inverse gas chromatography for natural fibre characterisation: dispersive and acid-base distribution profiles of the surface energy. *Cellulose (London)* **2017,** *24* (11), 4691-4700.

122. Niu, C.; Xia, W.; Peng, Y., Analysis of coal wettability by inverse gas chromatography and its guidance for coal flotation. *Fuel (Guildford)* **2018,** *228*, 290-296.

123. Gamelas, J. A. F.; Duarte, G. V.; Ferreira, P. J., Inverse gas chromatography and XPS of extracted kraft pulps. *International journal of the sociology of language* **2012,** (218).

124. Michael, I., ACCESSIBILITY AND CRYSTALLINITY OF CELLULOSE. *Bioresources* **2009,** *4* (3), 1168-1177.

125. Hamada, T.; Hasegawa, S.; Fukasawa, H.; Sawada, S.-i.; Koshikawa, H.; Miyashita, A.; Maekawa, Y., Poly(ether ether ketone) (PEEK)-based graft-type polymer electrolyte membranes having high crystallinity for high conducting and mechanical properties under various humidified conditions. *Journal of materials chemistry. A, Materials for energy and sustainability* **2015,** *3* (42), 20983-20991.

126. Lin, M.; Yang, L.; Zhang, H.; Xia, Y.; He, Y.; Lan, W.; Ren, J.; Yue, F.; Lu, F., Revealing the structure-activity relationship between lignin and anti-UV radiation. *Industrial crops and products* **2021,** *174*, 114212.

127. Klapiszewski, Ł.; Podkościelna, B.; Goliszek, M.; Kubiak, A.; Młynarczyk, K.; Jesionowski, T., Synthesis, characterization and aging tests of functional rigid polymeric biocomposites with kraft lignin. *International journal of biological macromolecules* **2021,** *178*, 344-353.

128. Parit, M.; Du, H.; Zhang, X.; Jiang, Z., Flexible, Transparent, UV-Protecting, Water-Resistant Nanocomposite Films Based on Polyvinyl Alcohol and Kraft Lignin-Grafted Cellulose Nanofibers. *ACS applied polymer materials* **2022,** *4* (5), 3587-3597.

129. Federle, T. W.; Barlaz, M. A.; Pettigrew, C. A.; Kerr, K. M.; Kemper, J. J.; Nuck, B. A.; Schechtman, L. A., Anaerobic Biodegradation of Aliphatic Polyesters: Poly(3-hydroxybutyrate-c o-3-hydroxyoctanoate) and Poly(ε-caprolactone). *Biomacromolecules* **2002,** *3* (4), 813-822.

130. Ben Abdallah, A.; Kallel, A.; Gamaoun, F.; Tcharkhtchi, A., Enzymatic Hydrolysis of Poly (Caprolactone) and its Blend with Styrene–Butadiene–Styrene (40% PCL/60% SBS). *Journal of polymers and the environment* **2019,** *27* (11), 2341-2351.

131. Liu, Q.; Wang, H.; Chen, L.; Li, W.; Zong, Y.; Sun, Y.; Li, Z., Enzymatic degradation of fluorinated Poly(ε-caprolactone) (PCL) block copolymer films with improved hydrophobicity. *Polymer degradation and stability* **2019,** *165*, 27-34.

132. Jia, Y.; Yang, C.; Shen, B.; Ling, Z.; Huang, C.; Li, X.; Lai, C.; Yong, Q., Comparative study on enzymatic digestibility of acid-pretreated poplar and larch based on a comprehensive analysis of the lignin-derived recalcitrance. *Bioresource technology* **2021,** *319*, 124225-124225.

133. Tian, D.; Guo, Y.; Huang, M.; Zhao, L.; Deng, S.; Deng, O.; Zhou, W.; Hu, J.; Shen, F., Bacterial cellulose/lignin nanoparticles composite films with retarded biodegradability. *Carbohydrate polymers* **2021,** *274*, 118656-118656.

134. Yoshida, M.; Liu, Y.; Uchida, S.; Kawarada, K.; Ukagami, Y.; Ichinose, H.; Kaneko, S.; Fukuda, K., Effects of cellulose crystallinity, hemicellulose, and lignin on the enzymatic hydrolysis of Miscanthus sinensis to monosaccharides. *Bioscience, biotechnology, and biochemistry* **2008,** *72* (3), 805-810.

135. Sun, H.; Liu, Z.; Liu, K.; Gibril, M. E.; Kong, F.; Wang, S., Lignin-based superhydrophobic melamine resin sponges and their application in oil/water separation. *Industrial crops and products* **2021,** *170*, 113798.

136. Wang, K.; Liu, X.; Tan, Y.; Zhang, W.; Zhang, S.; Li, J., Two-dimensional membrane and three-dimensional bulk aerogel materials via top-down wood nanotechnology for multibehavioral and reusable oil/water separation. *Chemical engineering journal (Lausanne, Switzerland : 1996)* **2019,** *371*, 769-780.

137. Yu, M.; Mishra, D.; Cui, Z.; Wang, X.; Lu, Q., Recycling papermill waste lignin into recyclable and flowerlike composites for effective oil/water separation. *Composites. Part B, Engineering* **2021,** *216*, 108884.

138. Saito, K.; Eisenreich, F.; Türel, T.; Tomović, Ž., Closed-Loop Recycling of Poly(Imine-Carbonate) Derived from Plastic Waste and Bio-based Resources. *Angewandte Chemie International Edition* **2022,** *61* (43), e202211806.

139. Wang, Y.; Xu, A.; Zhang, L.; chen, Z.; Qin, R.; Liu, Y.; Jiang, X.; Ye, D.; Liu, Z., Recyclable Carbon Fiber Reinforced Vanillin-Based Polyimine Vitrimers: Degradation and Mechanical Properties Study. *Macromolecular materials and engineering* **2022,** *307* (7), 2100893-n/a.

140. Häußler, M.; Eck, M.; Rothauer, D.; Mecking, S., Closed-loop recycling of polyethylene-like materials. *Nature (London)* **2021,** *590* (7846), 423-427.

141. Li, C.; Ju, B.; Zhang, S., Twin-screw extrusion molding of a cellulose-based vitrimer containing a crosslinkable macromolecular plasticizer. *International journal of biological macromolecules* **2023,** *225*, 1487-1493.

142. Chong, K. L.; Lai, J. C.; Rahman, R. A.; Adrus, N.; Al-Saffar, Z. H.; Hassan, A.; Lim, T. H.; Wahit, M. U., A review on recent approaches to sustainable bio-based epoxy vitrimer from epoxidized vegetable oils. *Industrial crops and products* **2022,** *189*, 115857.

143. Xie, D.; Pu, Y.; Meng, X.; Bryant, N. D.; Zhang, K.; Wang, W.; Ragauskas, A. J.; Li, M., Effect of the Lignin Structure on the Physicochemical Properties of Lignin-Grafted-Poly(ε-caprolactone) and Its Application for Water/Oil Separation. *ACS Sustainable Chemistry & Engineering* **2022**.

144. Meister, J. J., Review of the Synthesis, Characterization, and Testing of Graft Copolymers of Lignin. Springer US: Boston, MA, pp 305-322.

145. de Baynast, H.; Tribot, A.; Niez, B.; Audonnet, F.; Badel, E.; Cesar, G.; Dussap, C.-G.; Gastaldi, E.; Massacrier, L.; Michaud, P.; Delattre, C., Effects of Kraft lignin and corn cob agro-residue on the properties of injected-moulded biocomposites. *Industrial crops and products* **2022,** *177*, 114421.

146. Huang, J.; Liu, W.; Qiu, X., High Performance Thermoplastic Elastomers with Biomass Lignin as Plastic Phase. *ACS Sustainable Chemistry & Engineering* **2019,** *7* (7), 6550-6560.

147. Mourdikoudis, S.; Liz-Marzán, L. M., Oleylamine in Nanoparticle Synthesis. *Chemistry of Materials* **2013,** *25* (9), 1465-1476.

148. Bui, R.; Brook, M. A., Thermoplastic silicone elastomers from divanillin crosslinkers in a catalyst-free process. *Green chemistry : an international journal and green chemistry resource : GC* **2021,** *23* (15), 56-568.

149. Chen, X.; Guo, T.; Mo, X.; Zhang, L.; Wang, R.; Xue, Y.; Fan, X.; Sun, S., Reduced nutrient release and greenhouse gas emissions of lignin-based coated urea by synergy of carbon black and polysiloxane. *International Journal of Biological Macromolecules* **2023,** *231*, 123334.

150. Xie, D.; Pu, Y.; Meng, X.; Bryant, N. D.; Zhang, K.; Wang, W.; Ragauskas, A. J.; Li, M., Effect of the Lignin Structure on the Physicochemical Properties of Lignin-Grafted-Poly(ε-caprolactone) and Its Application for Water/Oil Separation. *ACS sustainable chemistry & engineering* **2022,** *10* (50), 16882-16895.

151. Wang, S.; Ma, S.; Li, Q.; Xu, X.; Wang, B.; Huang, K.; liu, Y.; Zhu, J., Facile Preparation of Polyimine Vitrimers with Enhanced Creep Resistance and Thermal and Mechanical Properties via Metal Coordination. *Macromolecules* **2020,** *53* (8), 2919-2931.

152. Zhou, B.; Li, J.; Liu, W.; Jiang, H.; Li, S.; Tan, L.; Dong, L.; She, L.; Wei, Z., Functional-Group Modification of Kraft Lignin for Enhanced Supercapacitors. *ChemSusChem* **2020,** *13* (10), 2628-2633.

153. Song, C.; Gao, C.; Fatehi, P.; Wang, S.; Jiang, C.; Kong, F., Influence of structure and functional group of modified kraft lignin on adsorption behavior of dye. *International journal of biological macromolecules* **2023,** *240*, 124368-124368.

154. Shorey, R.; Mekonnen, T. H., Esterification of lignin with long chain fatty acids for the stabilization of oil-in-water Pickering emulsions. *International journal of biological macromolecules* **2023,** *230*, 123143.

155. Guo, H.; Zhu, L.; Dang, C.; Zhao, J.; Dick, B., Synthesis and photophysical properties of ruthenium(ii) polyimine complexes decorated with flavin. *Physical Chemistry Chemical Physics* **2018,** *20* (25), 17504-17516.

156. Hong, N.; Yu, W.; Xue, Y.; Zeng, W.; Huang, J.; Xie, W.; Qiu, X.; Li, Y., A novel and highly efficient polymerization of sulfomethylated alkaline lignins via alkyl chain cross-linking method. *Holzforschung* **2016,** *70* (4), 297-304.

157. Chao, A.; Negulescu, I.; Zhang, D., Dynamic Covalent Polymer Networks Based on Degenerative Imine Bond Exchange: Tuning the Malleability and Self-Healing Properties by Solvent. *Macromolecules* **2016,** *49* (17), 6277-6284.

158. Chen, X.; Li, Z.; Zhang, L.; Wang, H.; Qiu, C.; Fan, X.; Sun, S., Preparation of a novel lignin-based film with high solid content and its physicochemical characteristics. *Industrial Crops and Products* **2021,** *164*, 113396.

159. Tanadchangsaeng, N.; Yu, J., Thermal stability and degradation of biological terpolyesters over a broad temperature range. *Journal of applied polymer science* **2015,** *132* (13), np-n/a.

160. Sbrescia, S.; Engels, T.; Van Ruymbeke, E.; Seitz, M., Molecular weight effects on the stress-relaxation behavior of soft thermoplastic elastomer by means of temperature scanning stress relaxation (TSSR). *Journal of rheology (New York : 1978)* **2022,** *66* (6), 1321-1330.

161. Jones, B. H.; Wheeler, D. R.; Black, H. T.; Stavig, M. E.; Sawyer, P. S.; Giron, N. H.; Celina, M. C.; Lambert, T. N.; Alam, T. M., Stress Relaxation in Epoxy Thermosets via a Ferrocene-Based Amine Curing Agent. *Macromolecules* **2017,** *50* (13), 5014-5024.

162. Scheutz, G. M.; Lessard, J. J.; Sims, M. B.; Sumerlin, B. S., Adaptable Crosslinks in Polymeric Materials: Resolving the Intersection of Thermoplastics and Thermosets. *Journal of the American Chemical Society* **2019,** *141* (41), 16181-16196.

163. Grassia, L.; D'Amore, A., Deconvolution of the segmental and chain modes in amorphous polymers: Do the short-chain modes affect the bulk relaxation? *Polymer* **2021,** *225*, 123801.

164. Elling, B. R.; Dichtel, W. R., Reprocessable Cross-Linked Polymer Networks: Are Associative Exchange Mechanisms Desirable? *ACS central science* **2020,** *6* (9), 1488-1496.

165. Taynton, P.; Zhu, C.; Loob, S.; Shoemaker, R.; Pritchard, J.; Jin, Y.; Zhang, W., Re-healable polyimine thermosets: Polymer composition and moisture sensitivity. *Polymer chemistry* **2016,** *7* (46), 7052-7056.

166. Scarica, C.; Suriano, R.; Levi, M.; Turri, S.; Griffini, G., Lignin Functionalized with Succinic Anhydride as Building Block for Biobased Thermosetting Polyester Coatings. *ACS sustainable chemistry & engineering* **2018,** *6* (3), 3392-3401.

167. Griffini, G.; Passoni, V.; Suriano, R.; Levi, M.; Turri, S., Polyurethane Coatings Based on Chemically Unmodified Fractionated Lignin. *ACS sustainable chemistry & engineering* **2015,** *3* (6), 1145-1154.

168. Xia, Q.; Chen, C.; Yao, Y.; He, S.; Wang, X.; Li, J.; Gao, J.; Gan, W.; Jiang, B.; Cui, M.; Hu, L., In Situ Lignin Modification toward Photonic Wood. *Advanced materials (Weinheim)* **2021,** *33* (8), e2001588-n/a.

169. Sayem, A. S. M.; Simorangkir, R. B. V. B.; Esselle, K. P.; Hashmi, R. M.; Liu, H., A Method to Develop Flexible Robust Optically Transparent Unidirectional Antennas Utilizing Pure Water, PDMS, and Transparent Conductive Mesh. *IEEE transactions on antennas and propagation* **2020,** *68* (10), 6943-6952.

170. Zheng, X.; Yang, H.; Sun, Y.; Zhang, Y.; Guo, Y., A molecular dynamics simulation on self-healing behavior based on disulfide bond exchange reactions. *Polymer (Guilford)* **2021,** *212*, 123111.

171. Urzúa-Leiva, R.; Denis-Alpizar, O., Study of the CN(X2Σ+) + N(4S) Reaction at High Temperatures: Potential Energy Surface and Thermal Rate Coefficients. *The journal of physical chemistry. A, Molecules, spectroscopy, kinetics, environment, & general theory* **2021,** *125* (37), 8168-8174.

172. Kuchma, A. E.; Shchekin, A. K., Regularities of non-stationary diffusion growth of overcritical gas bubbles and kinetics of bubble distribution in presence of capillary and viscous forces. *The Journal of chemical physics* **2021,** *154* (14), 144101-144101.

173. Lin, L. H.; Lee, H. P.; Yeh, M. L., Characterization of a Sandwich PLGA-Gallic Acid-PLGA Coating on Mg Alloy ZK60 for Bioresorbable Coronary Artery Stents. *Materials (Basel, Switzerland)* **2020,** *13* (23).

174. Yang, Y.; Shan, L.; Shen, H.; Qiu, J., Manufacturing of robust superhydrophobic Wood surfaces based on PEG–Functionalized SiO2/PVA/PAA/Fluoropolymer hybrid transparent coating. *Progress in organic coatings* **2021,** *154*, 106186.

175. Łukawski, D.; Lekawa-Raus, A.; Lisiecki, F.; Koziol, K.; Dudkowiak, A., Towards the development of superhydrophobic carbon nanomaterial coatings on wood. *Progress in Organic Coatings* **2018,** *125*, 23-31.

176. Wang, X.; Liu, F.; Li, Y.; Zhang, W.; Bai, S.; Zheng, X.; Huan, J.; Cao, G.; Yang, T.; Wang, M.; Jiang, Z.; Wang, C.; Ho, S.-H., Development of a facile and bi-functional superhydrophobic suspension and its applications in superhydrophobic coatings and aerogels in high-efficiency oil-water separation. *Green chemistry : an international journal and green chemistry resource : GC* **2020,** *22* (21), 7424-7434.

177. Raeisi, M.; Kazerouni, Y.; Mohammadi, A.; Hashemi, M.; Hejazi, I.; Seyfi, J.; Khonakdar, H. A.; Davachi, S. M., Superhydrophobic cotton fabrics coated by chitosan and titanium dioxide nanoparticles with enhanced antibacterial and UV-protecting properties. *International journal of biological macromolecules* **2021,** *171*, 158-165.

178. Song, X.; Tang, S.; Chi, X.; Han, G.; Bai, L.; Shi, S. Q.; Zhu, Z.; Cheng, W., Valorization of Lignin from Biorefinery: Colloidal Lignin Micro-Nanospheres as Multifunctional Bio-Based Fillers for Waterborne Wood Coating Enhancement. *ACS Sustainable Chemistry & Engineering* **2022,** *10* (35), 11655-11665.

179. Wang, G.; Pang, T.; Chen, S.; Sui, W.; Si, C.; Ni, Y., Fabrication of lignin nanospheres by emulsification in a binary γ-valerolactone/glycerol system and their application as a bifunctional reducer and carrier for Pd nanoparticles with enhanced catalytic activity. *Green Chemistry* **2020,** *22* (24), 8594-8603.

180. Liu, Q.; Wang, B.; Jiang, H.; Lu, Q.; Wang, L.; Yang, Y.; Cheng, R.; Gao, Q.; Yang, L.; Du, G.; Gao, W., Optimization of durable superhydrophobic wood with

superstrong ultraviolet resistance and chemical stability. *Chemical engineering journal (Lausanne, Switzerland : 1996)* **2024,** *480*, 148164.

181. Wang, D.; Sun, Q.; Hokkanen, M. J.; Zhang, C.; Lin, F. Y.; Liu, Q.; Zhu, S. P.; Zhou, T.; Chang, Q.; He, B.; Zhou, Q.; Chen, L.; Wang, Z.; Ras, R. H. A.; Deng, X., Design of robust superhydrophobic surfaces. *Nature* **2020,** *582* (7810), 55-59.

182. Standard test method for tensile properties of thin plastic sheeting. *West Conshohocken* **2010**, PA 19428-2959, United States.

183. Wan, W.; Yang, Z.; Tan, T.; Li, Y.; Zhang, Z.; Zhang, P.; He, F., Three-dimensional hydrophobic melamine@methyl trichlorosilane/polydimethylsiloxane sponge for consecutive and long-term oil/water separation. *Chemical engineering journal (Lausanne, Switzerland : 1996)* **2023,** *476*, 146824.

184. Wang, J.; Zhang, W.; Lv, D., A super-hydrophobic composite coating with near-infrared low reflection and low emissivity of 8∼14 μm. *Optik (Stuttgart)* **2021,** *241*, 166379.

185. Cheng, T.; He, R.; Zhang, Q.; Zhan, X.; Chen, F., Magnetic particle-based super-hydrophobic coatings with excellent anti-icing and thermoresponsive deicing performance. *Journal of materials chemistry. A, Materials for energy and sustainability* **2015,** *3* (43), 21637-21646.

186. Chen, L.; Luo, S.-M.; Huo, C.-M.; Shi, Y.-F.; Feng, J.; Zhu, J.-Y.; Xue, W.; Qiu, X., New insight into lignin aggregation guiding efficient synthesis and functionalization of a lignin nanosphere with excellent performance. *Green chemistry : an international journal and green chemistry resource : GC* **2022,** *24* (1), 285-294.

187. Wang, Y.; Zhang, X.; Kan, L.; Shen, F.; Ling, H.; Wang, X., All-biomass-based eco-friendly waterproof coating for paper-based green packaging. *Green chemistry : an international journal and green chemistry resource : GC* **2022,** *24* (18), 739-748.

188. Lv, D.; Shao, H.; Gao, X.; Lu, K.; Lu, H.; Ma, H., Fabrication and corrosion resistance properties of super-hydrophobic coatings on iron and steel substrates by creating micro-/nano-structures and modifying rough surfaces. *RSC advances* **2016,** *6* (96), 93419-93427.

189. Wu, G.; Liu, D.; Chen, J.; Liu, G.; Kong, Z., Preparation and properties of super hydrophobic films from siloxane-modified two-component waterborne polyurethane and hydrophobic nano SiO2. *Progress in organic coatings* **2019,** *127*, 80-87.

190. Wang, F.; Feng, L.; Li, G.; Zhai, Z.; Ma, H.; Deng, B.; Zhang, S., Fabrication and properties of superhydrophobic waterborne polyurethane composites with micro-rough surface structure using electrostatic spraying. *Polymers* **2019,** *11* (11), 1748.

191. Kang, Z.; Lai, X.; Sang, J.; Li, Y., Fabrication of hydrophobic/super-hydrophobic nanofilms on magnesium alloys by polymer plating. *Thin solid films* **2011,** *520* (2), 800-806.

192. Suryaprabha, T.; Sethuraman, M. G., A Facile Approach for Fabrication Superhydrophobic and UV-blocking Cotton Fabrics with Self-cleaning Properties. *Fibers and Polymers* **2021,** *22* (4), 1033-1040.

193. Sandberg, D.; Söderström, O., Crack formation due to weathering of radial and tangential sections of pine and spruce. *Wood material science and engineering* **2006,** *1* (1), 12-20.

194. Yang, B.; Niu, K.; Haag, F.; Cao, N.; Zhang, J.; Zhang, H.; Li, Q.; Allegretti, F.; Björk, J.; Barth, J. V.; Chi, L., Abiotic Formation of an Amide Bond via Surface-Supported Direct Carboxyl–Amine Coupling. *Angewandte Chemie (International ed.)* **2022,** *61* (5), e202113590-n/a.

195. Wu, X.; Li, S., Synthesis of polylactide/poly(ethylene glycol) diblock copolymers with functional endgroups. *Polymer international* **2013,** *62* (7), 1014-1021.

196. Tranvan, L.; Legrand, V.; Jacquemin, F., Thermal decomposition kinetics of balsa wood: Kinetics and degradation mechanisms comparison between dry and moisturized materials. *Polymer degradation and stability* **2014,** *110*, 208-215.

197. Kim, C. H.; Joo, C.-K.; Chun, H. J.; Yoo, B. R.; Noh, D. I.; Shim, Y. B., Instrumental studies on silicone oil adsorption to the surface of intraocular lenses. *Applied surface science* **2012,** *262*, 146-152.

APPENDIX

Appendix A – Supporting information for Chapter II Effect of Lignin Structure on the Physicochemical Properties of Lignin-grafted-poly(ε-caprolactone) and its Application for Water/Oil Separation

Table 7-1 Young's modulus, tensile strength and impact strength of neat PCL and lignin-*g*-PCL films

Samples	Young's modulus (MPa)	Tensile strength (MPa)	Impact strength (MPa)
Neat PCL	49.81±1.13	0.25±0.009	30.00±2.46
KL-PCL	59.69±1.93	0.17±0.012	19.38±1.38
F_{ins}-PCL	68.67±1.01	0.06±0.004	9.63±1.00
F2-PCL	57.10±1.96	0.34±0.014	40.92±3.61
F3-PCL	47.70±1.04	0.16±0.008	11.13±1.89
F4-PCL	69.19±2.68	0.09±0.008	3.33±0.93

Note: The data are in a form of mean ± standard deviation

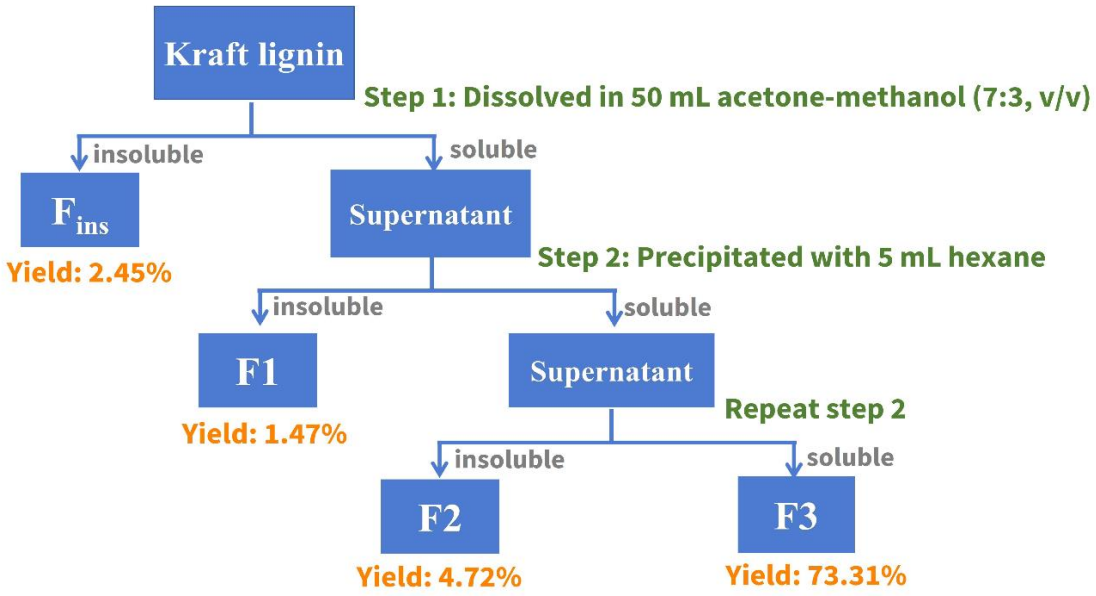


Figure 7-1 Fractionation procedure of kraft lignin

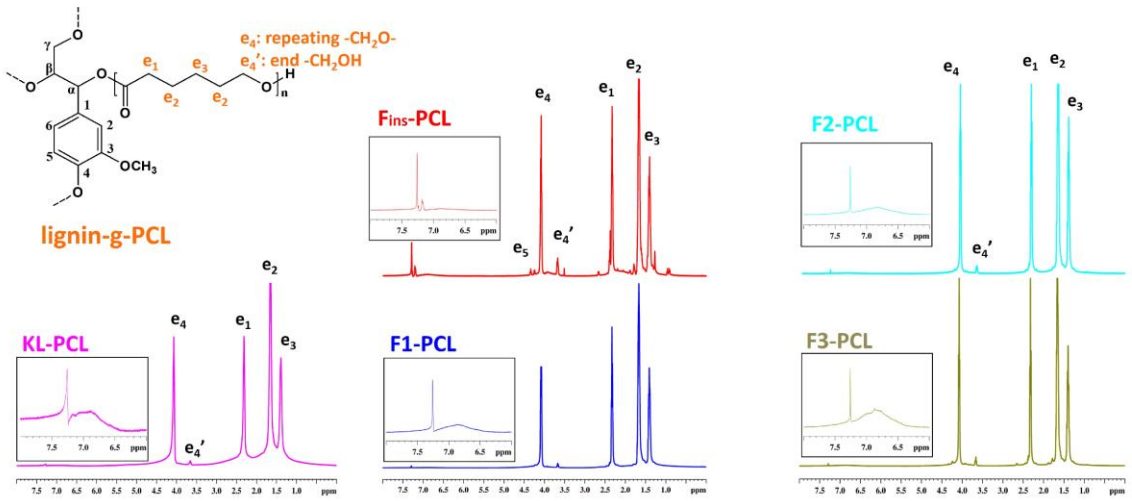


Figure 7-2 ^{1}H NMR spectra of lignin-*g*-PCLs. Signal assignment is displayed as top left image referred by literature[91]; e_1 (2.30 ppm), e_2 (1.64 ppm) and e_3 (1.38 ppm) represent -CH_2- in different positions of PCL chains, e_4 (4.05 ppm) represents repeating -CH_2O- units in PCL chains, and e_4' (3.65 ppm) represents end -CH_2OH-group in PCL chains

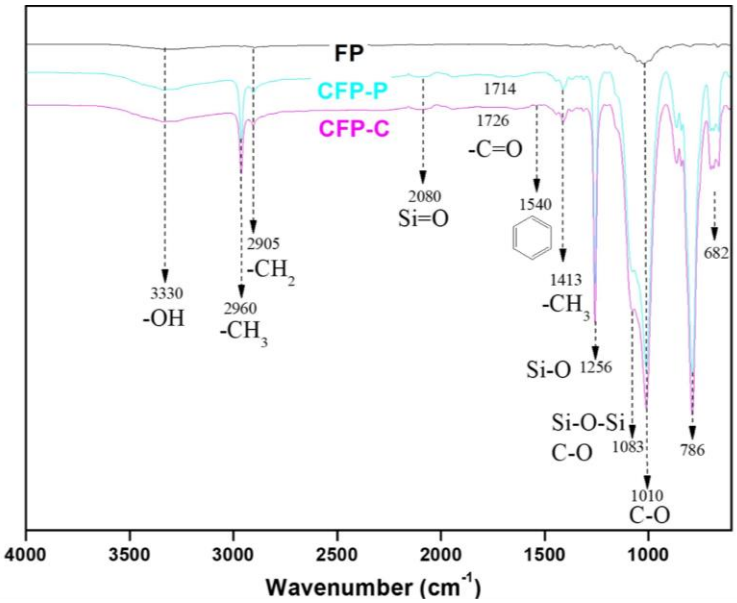


Figure 7-3 FTIR spectra of FP, CFP-P and CFP-C. Signals assignments are referred by literatures.[45, 197]

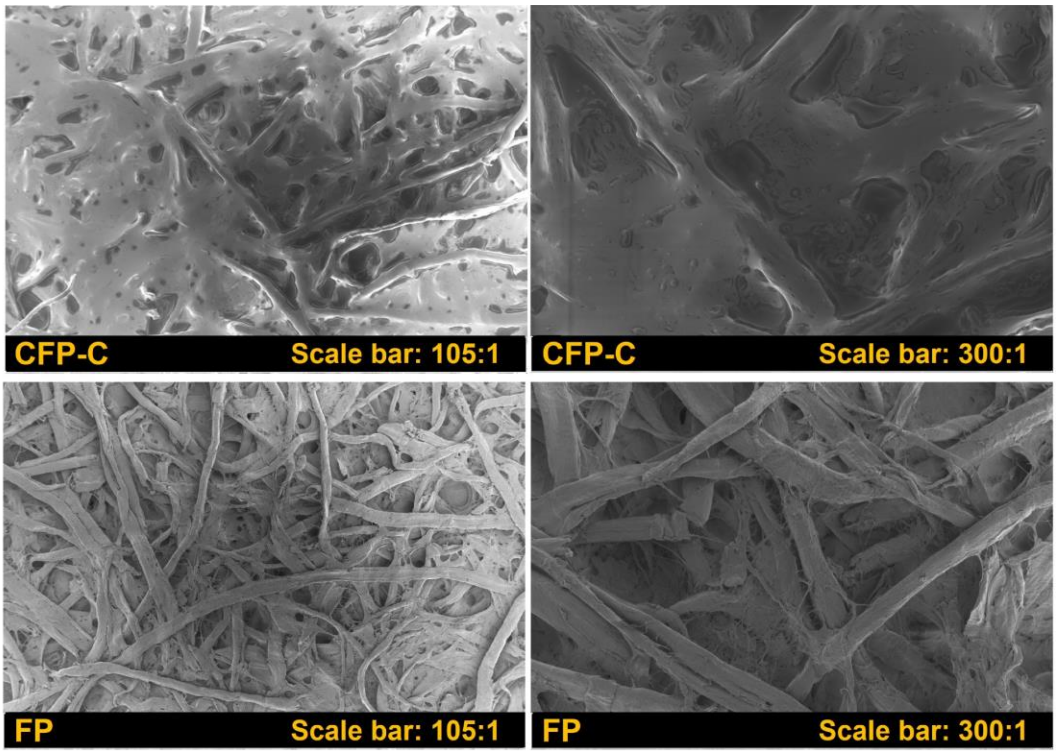


Figure 7-4 SEM images of FP (bottom) and CFP-C (upper) under scale bars of 105 (left) and 300 (right).

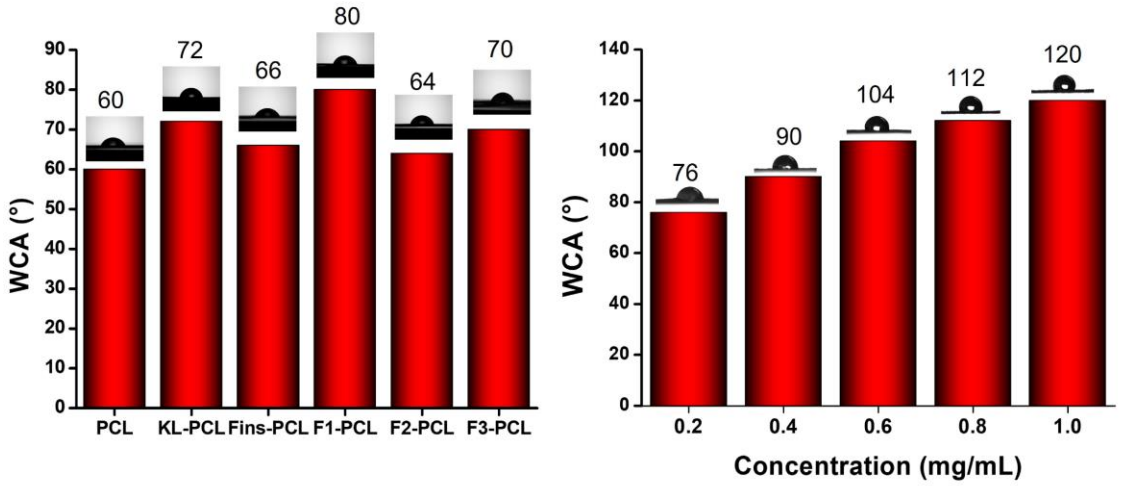


Figure 7-5 WCA of neat PCL, lignin-*g*-PCL films (A), CFP-C coated by different concentrations (0.2, 0.4, 0.6, 0.8 and 1.0 mg/mL) of F1-PCL/acetone solutions (B)

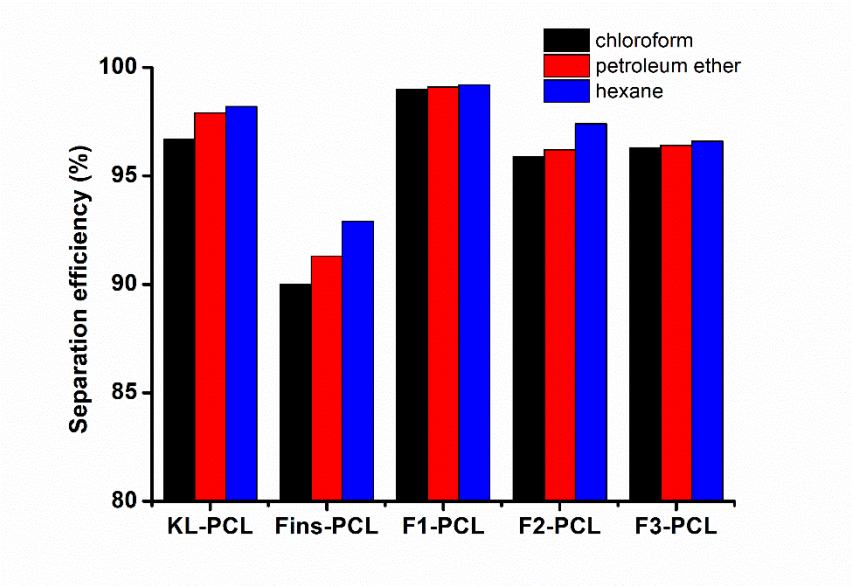


Figure 7-6 Separation efficiencies of FP coated with KL-PCL, F_{ins}-PCL, F1-PCL, F2-PCL, and F3-PCL for separating chloroform-, petroleum ether- and hexane-water mixtures under the first cycle

Appendix B – Supporting information for Chapter III Synthesis of Bio-based Repairable Polyimines with Tailed Properties by Lignin Fractionation

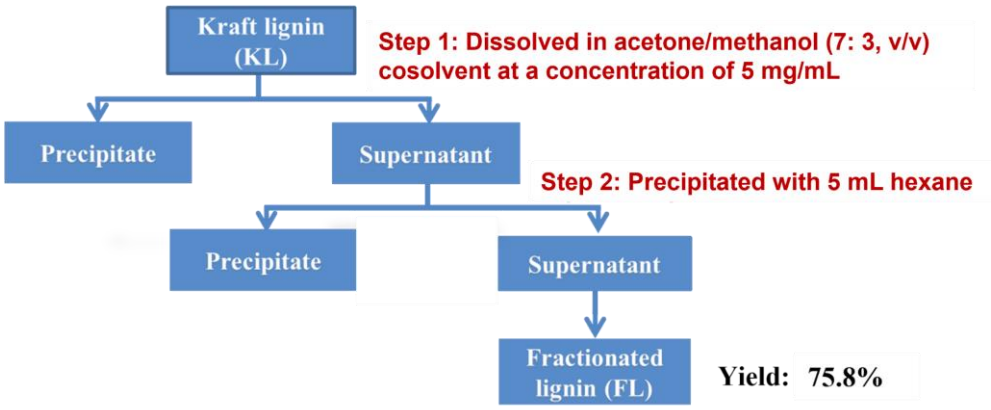


Figure 8-1 Solvent fractionation of KL into FL

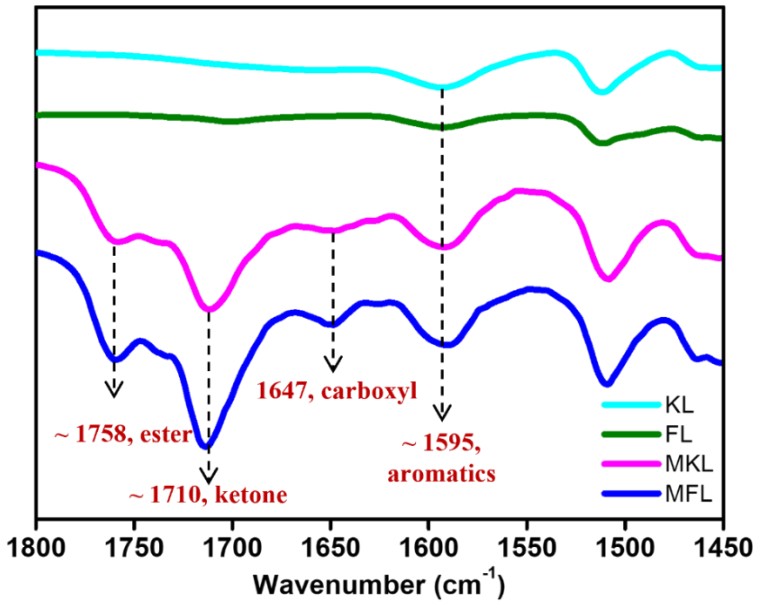


Figure 8-2 FTIR spectra of lignin and modified lignin

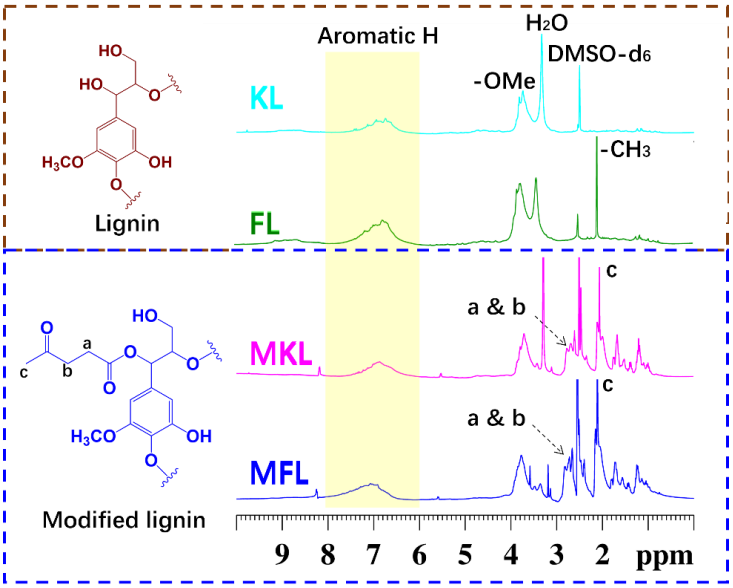


Figure 8-3 ^{1}H NMR spectra of lignin and modified lignin

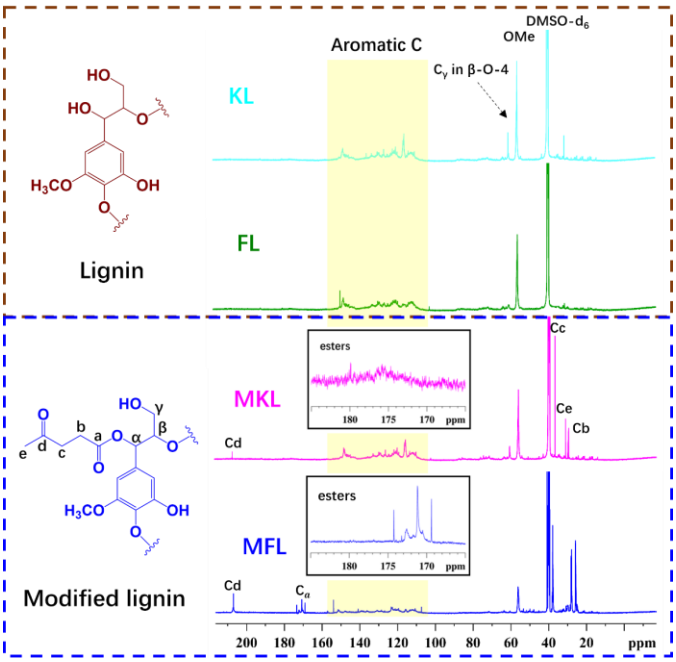


Figure 8-4 ^{13}C NMR spectra of lignin and modified lignin

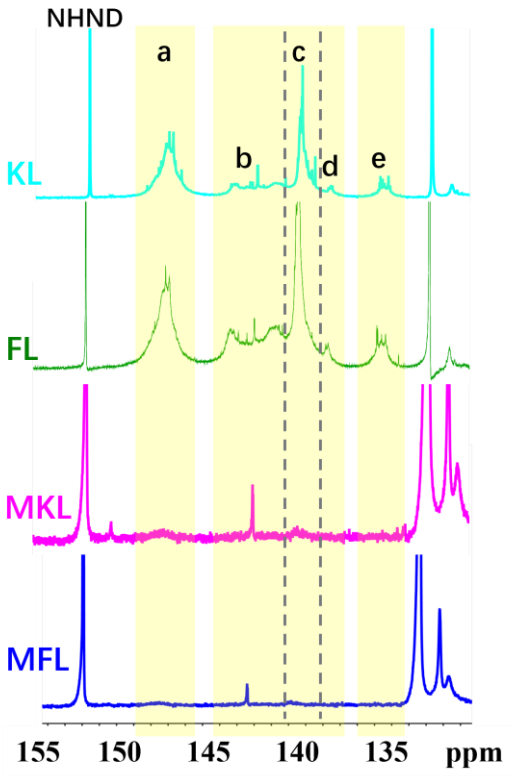


Figure 8-5 ^{31}P NMR spectra of lignin and modified lignin. (a) aliphatic OH, (b) C5-substituted OH, (c) guaiacyl OH, (d) p-hydroxyphenyl OH, and (e) carboxylic OH.

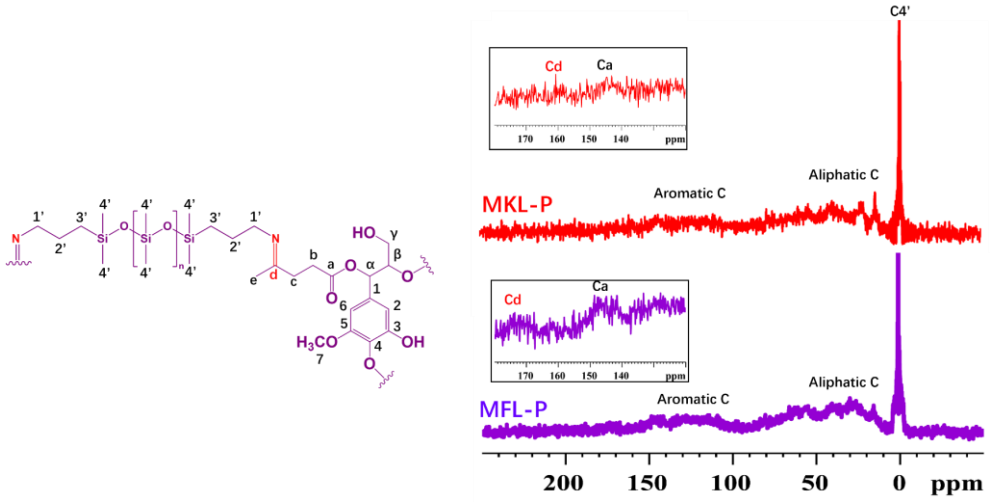


Figure 8-6 Solid-state NMR spectra of MKL-P and MFL-P

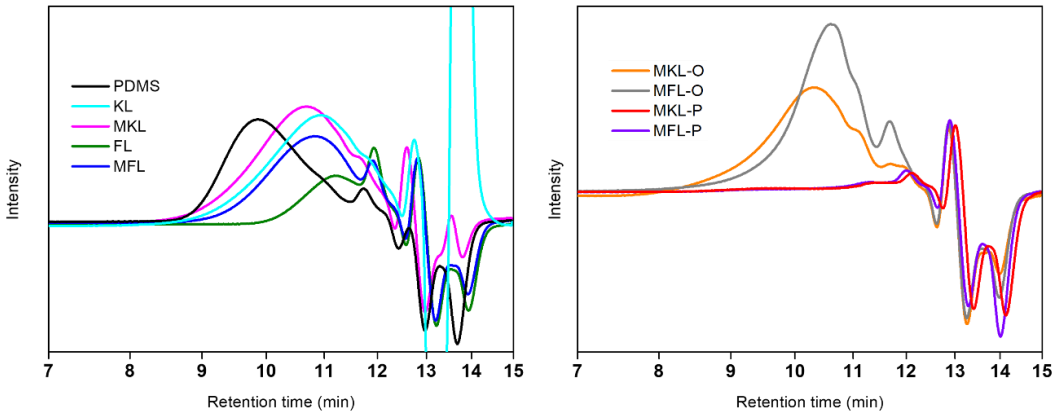


Figure 8-7 GPC curves of PDMS, lignin, modified lignin (left) and polyimines (right)

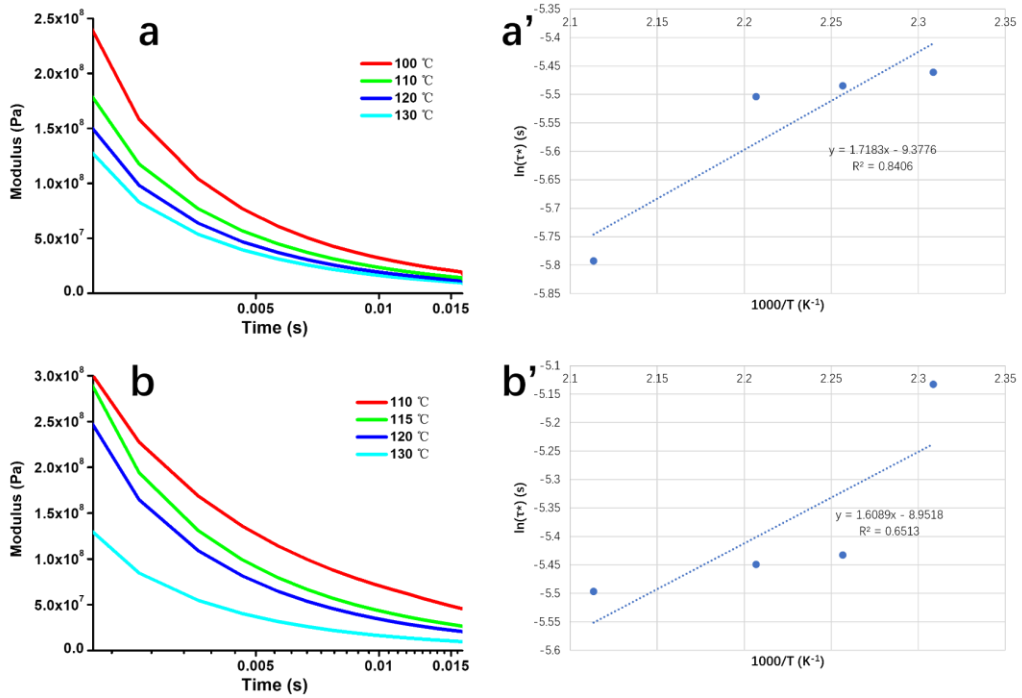


Figure 8-8 Stress-relaxation curves and the Arrhenius equation plots of MKL (a and a') and MFL (b and b')

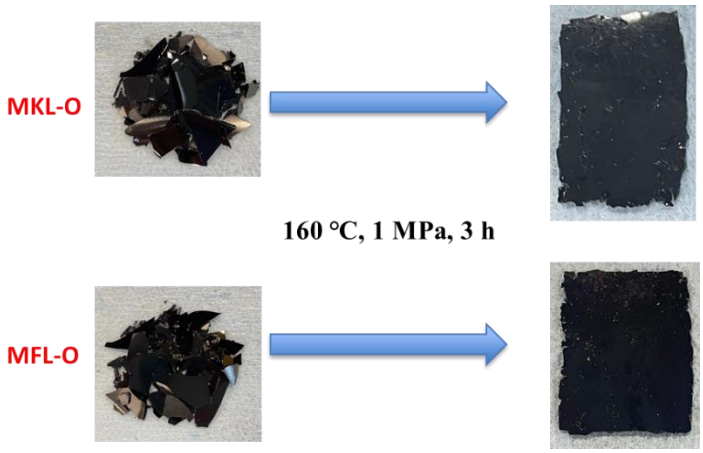


Figure 8-9 Reprocess ability test for lignin-OAm polyimine films

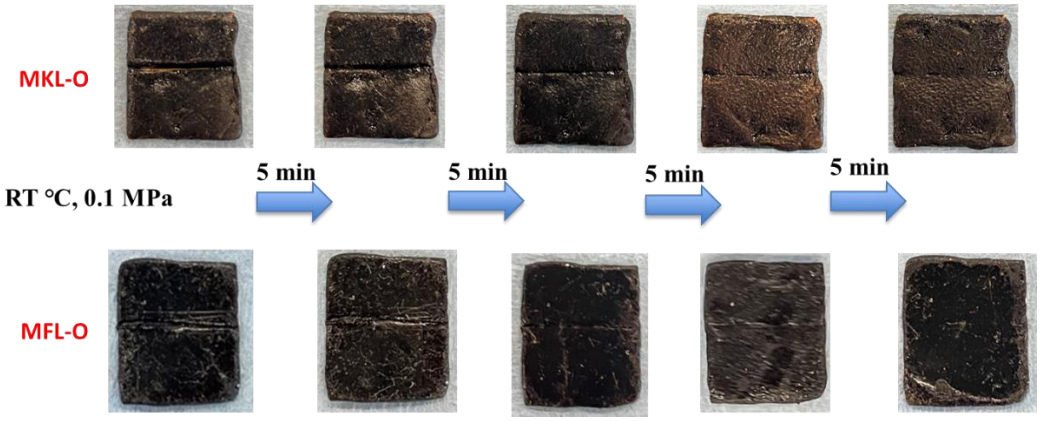


Figure 8-10 Self-healing ability test for lignin-OAm polyimine films

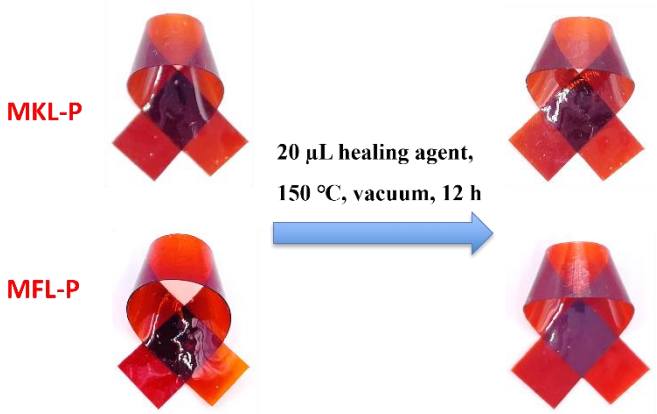


Figure 8-11 Images of lignin-PDMS polyimine films before (left) and after (right) repair

Table 8-1 Quantification of hydroxyl groups in lignin and modified lignin determined by ^{31}P NMR

	KL (mmol/g)	MKL (mmol/g)	FL (mmol/g)	MFL (mmol/g)
Aliphatic OH	2.24	0.59	1.83	0.32
C_5 subsituted OH	1.11	0.24	1.89	0.21
Guaiacyl OH	1.79	0.40	1.77	0.27
p-hydroxyphenyl	0.10	0.02	0.22	0.03
Carboxylic OH	0.32	0.08	0.46	0.09
Total Phenol OH	3.00	0.66	3.88	0.62
Total OH	5.56	1.33	6.17	1.03

Appendix C – Supporting information for Chapter V Robust Superhydrophobic Coatings with Polyimine Crosslinking Network and Lignin Micro-nanospheres

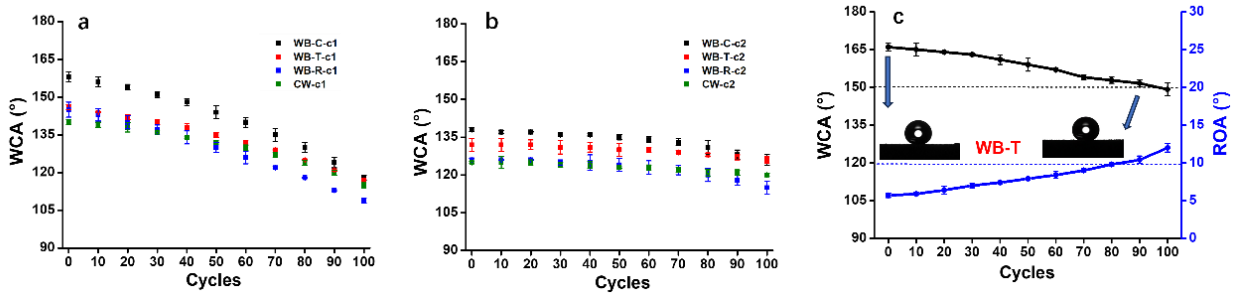


Figure 9-1 Tape-peeling test of control 1 (a), control 2 (b), and WB-T (c)

Figure 9-2 Waterdrop impact test of control 1 (a), control 2 (b), and WB-T (c)

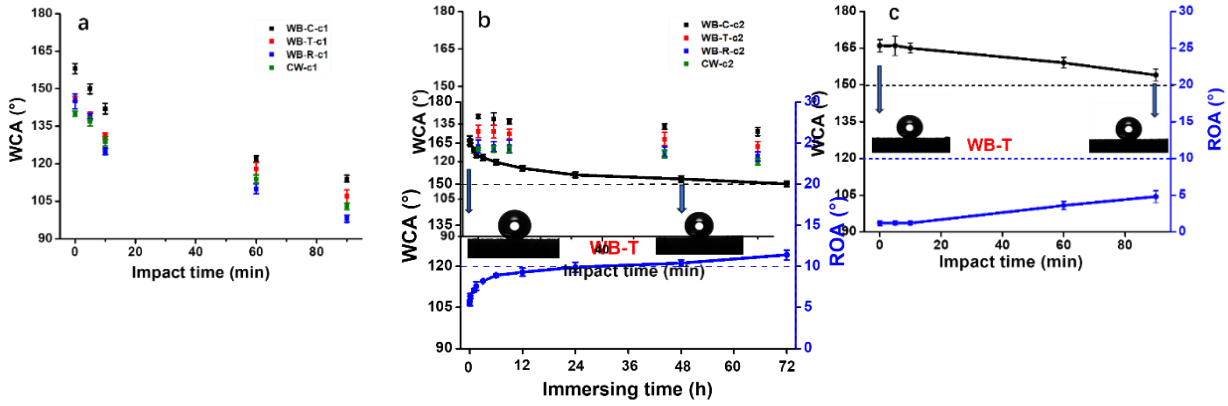


Figure 9-3 WCA of WB-T after being immersed under water for different time

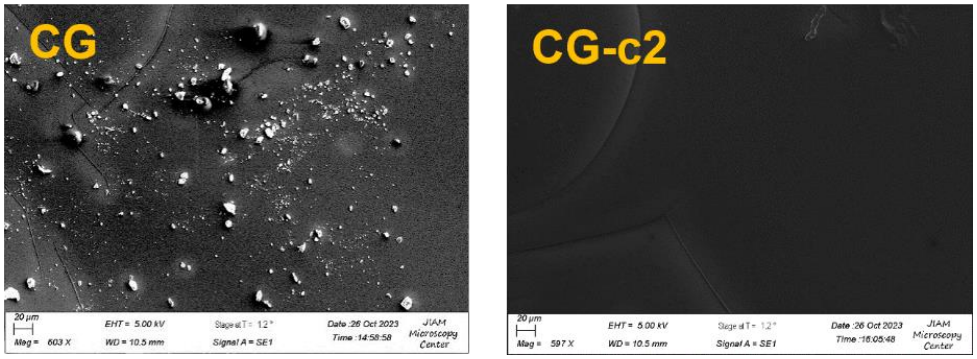


Figure 9-4 SEM images of CG and CG-c2; CG: coated glass product, CG-c2: coated glass control 2

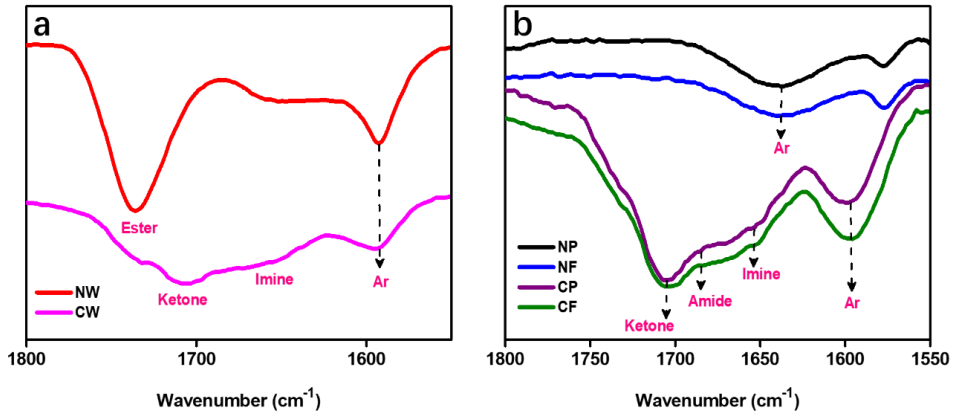


Figure 9-5 FTIR spectra of NW and CW (a), NP, NF, CP, and CF (b)

Table 9-1 ANOVA analysis of WCA of different coating products and their controls 1

Difference sources	Sum Square	Degree of freedom	Mean Square	F	P-value	F crit
Lignin-PDMS crosslinking	457.14	1	457.14	24.30	0.0026	5.99
Substrate type	3707.71	6	617.95	32.85	0.0002	4.28
Error	112.86	6	18.81			
Sum						

Table 9-2 ANOVA analysis of WCA of different coating products and their controls 2

Difference sources	Sum Square	Degree of freedom	Mean Square	F	P-value	F crit
LMNS deposition	2366	1	2366	54.39	0.0003	5.99
Substrate type	2770.43	6	461.74	10.61	0.0056	4.28
Error	261	6	43.5			
Sum						

Table 9-3 ANOVA analysis of WCA of different coated wood block section products and their controls

Difference sources	Sum Square	Degree of freedom	Mean Square	F	P-value	F crit
Wood block section	1392.667	2	696.3333	30.05755	0.003892	6.944272
Coating process	416.6667	2	208.3333	8.992806	0.033101	6.944272
Error	92.66667	4	23.16667			
Sum	1902	8				

Table 9-4 ANOVA analysis of WCA of different coated 2D products and their controls

Difference sources	Sum Square	Degree of freedom	Mean Square	F	P-value	F crit
Substrate type	1037.167	2	518.5833	17.72934	0.003031	5.143253
Coating process	1583	3	527.6667	18.03989	0.002091	4.757063
Error	175.5	6	29.25			
Sum	2795.667	11				

Table 9-5 ANOVA analysis of WCA of different coated wood block sections before and after knife scratch

Difference sources	Sum Square	Degree of freedom	Mean Square	F	P-value	F crit
Wood block section	1207	3	402.3333	27.1236	0.01126	9.276628
Knife scratch	60.5	1	60.5	4.078652	0.136713	10.12796
Error	44.5	3	14.83333			
Sum	1312	7				

Table 9-6 ANOVA analysis of WCA of different coated 2D substrates before and after knife scratch

Difference sources	Sum Square	Degree of freedom	Mean Square	F	P-value	F crit
Substrate type	1994.5	3	664.8333	117.3235	0.001316	9.276628
Knife scratch	200	1	200	35.29412	0.009535	10.12796
Error	17	3	5.666667			
Sum	2211.5	7				

Table 9-7 The minimum, median and maximum values of γ_d and γ_{sp} as well as hydrophilicity index ($\gamma_{sp}/(\gamma_{sp}+\gamma_d)$) and specific surface area of KL and LMNS

Samples	γ_d (mJ/m^2)			γ_{sp} (mJ/m^2)			$\gamma_{sp}/(\gamma_{sp}+\gamma_d)$	Specific surface area (m^2/g)
	minimum	median	maximum	minimum	median	maximum		
KL	46.13	55.34	95.01	2.96	3.73	7.08	0.06	1.63
LMNS	43.67	47.34	63.30	2.88	4.71	9.43	0.10	3.75

VITA

Di Xie is from Jiangsu province, China. She obtained her B.S. and M.S. degrees in Pulp & Paper Engineering at Nanjing Forestry University, China in 2018 and 2020, respectively. She has been a student research assistant at Nanjing Forestry University since she was a sophomore. Her research topic was isolation, characterization, and antioxidant activities of lignin-carbohydrate complex from wheat straw. During her Master program, she worked as a part-time academic editor in the editor office of Journal of Bioresources and Bioproducts at Nanjing Forestry University. She also worked as a senior medical editor in Shanghai QeeJen Bio-Tech Co., Ltd. in 2021. In 2021 August, she came to The University of Tennessee, Knoxville to pursue her PhD degree under the advisement of Dr. Mi Li. Her doctoral research mainly focuses on designing and developing lignin-based recyclable copolymers for hydrophobic coatings.